2014-07-29

# High-Performance Polymer Monoliths for Capillary Liquid Chromatography

Pankaj Aggarwal
*Brigham Young University - Provo*

# High Performance Polymer Monoliths for Capillary Liquid Chromatography

Pankaj Aggarwal

A dissertation submitted to the faculty of
Brigham Young University
in partial fulfillment of the requirements for the degree of

Doctor of Philosophy

Milton L. Lee, Chair
H. Dennis Tolley
Adam T. Woolley
Mathew R. Linford
Merritt B. Andrus

Department of Chemistry and Biochemistry

Brigham Young University

August 2014

ABSTRACT

High Performance Polymer Monoliths for Capillary Liquid Chromatography

Pankaj Aggarwal
Department of Chemistry and Biochemistry, BYU
Doctor of Philosophy

This dissertation focuses on improving the chromatographic efficiency of polymeric organic monoliths by characterizing and optimizing the bed morphology. In-situ characterization techniques such as capillary flow porometry (CFP), 3-dimensional scanning electron microscopy (3D SEM) and conductivity measurements were developed and implemented to quantitatively characterize the morphology of poly(ethylene glycol) diacrylate (PEGDA) monoliths. The CFP measurements for monoliths prepared by the same procedure in capillaries with different diameters (i.e., 75, 150, and 250 μm) clearly showed a change in average through-pore size with capillary diameter, thus, certifying the need for in-situ measurement techniques. Serial sectioning and imaging of PEGDA monoliths using 3D SEM gave quantitative information about the average pore size, porosity, radial heterogeneity and tortuosity of the monolith. Chromatographic efficiency was better for a monolith with smaller average pore size (i.e., 5.23 μm), porosity (i.e., 0.49), radial heterogeneity (i.e., 0.20) and tortuosity (i.e., 1.50) compared to another monolith with values of 5.90 μm, 0.59, 0.50 and 2.34, respectively. Other than providing information about monolith morphology, these techniques also aided in identifying factors governing morphological changes, such as capillary diameter, polymerization method, physical/chemical properties of the pre-polymer constituents and weight proportion of the same. A statistical model was developed for optimizing the weight proportion of pre-polymer constituents from their physical/chemical properties for improved chromatographic efficiency.

Fabricated PEGDA columns were used for liquid chromatography of small molecules such as phenols, hydroxyl benzoic acids, and alkyl parabens. The chromatographic retention mechanism was determined to be principally reversed-phase (RP) with additional hydrogen bonding between the polar groups of the analytes and the ethylene oxide groups embedded in the monolith structure. The chromatographic efficiency measured for a non-retained compound (uracil) was 186,000 plates/m when corrected for injector dead volume. High resolution gradient separations of selected pharmaceutical compounds and phenylurea herbicides were achieved in less than 18 min. Column preparation was highly reproducible, with relative standard deviation (RSD) values less than 2.1%, based on retention times of the phenol standards (3 different columns). A further improvement in chromatographic performance was achieved for monoliths fabricated using a different polymerization method, i.e., living free-radical polymerization (LFRP). The columns gave an unprecedented column performance of 238, 000 plates/m for a non-retained compound under RP conditions.

Keywords: Column efficiency, Liquid chromatography, Organic monolith, Morphology characterization, Porogen selection, Poly(ethylene glycol) diacrylate

ACKNOWLEDGEMENTS

First and foremost, I gratefully acknowledge my mentor, Dr. Milton L. Lee, for providing me an opportunity to study and perform research in his group. He has been a constant source of guidance, encouragement and support during my educational experience at Brigham Young University. He not only provided me a model of what a successful scientist should be but also taught me how to be successful in life, with his sense of humor and love for life. I am also thankful to him for his help and advice with my career path. I am honored to have my name listed as a student of a great and experienced scientist. The experience which I have learned during my stay is invaluable for me and my career.

I would like to thank professors in the chemistry department for teaching me the theoretical and experimental skills in analytical chemistry. I especially thank Dr. H. Dennis Tolley, for his encouragement and advice in my research work. My graduate committee members, Dr. Adam T. Woolley, Dr. Mathew R. Linford, and Dr. Merritt B. Andrus have provided critical evaluation and useful suggestions in my progress reports during my five-year PhD program. I also thank Dr. John S. Lawson, for his suggestions and help during my research.

Current and past group members of the Lee group are gratefully acknowledged for their useful suggestions and friendship. Each member in this group contributes immensely to the scientific discoveries in a complementary way. I would like to thank Dr. Yuanyuan Li and Dr. Xin Chen for teaching me about polymer monoliths and practical liquid chromatography techniques. I also thank Dr. Kun Liu for her collaboration, scientific discussions and friendship. Dr. Dan Li, Dr. Jie Xuan, Xiaofeng Xie, Anzi Wang, and Sonika Sharma are greatly acknowledged for their friendship and help at Brigham Young University.

I would like to thank people in the department instrument shop and computer support office for their help with the technical issues in the research work. The help from Michael Standing in the Microscopy department at Brigham Young University is acknowledged. I also appreciate the opportunity and financial support offered by the Department of Chemistry and Biochemistry at Brigham Young University. The financial support from the Analytical Chemistry Division of the American Chemical Society is also gratefully acknowledged.

Last but not least, I want to extend my deep gratitude to my parents, Satbir Aggarwal and Saroj Aggarwal, for their constant love, strength and faith in me. I would like to dedicate this dissertation to my parents. I also owe many thanks to my dear friends and relatives, who are always there to lend a helping hand. Your love and support means a lot to me.

Pankaj Aggarwal

TABLE OF CONTENTS

LIST OF ABBREVIATIONS

| | |
|---|---|
| 2-HB | 2-Hydroxybenzoic acid |
| 2,4-DHB | 2,4-Dihydroxybenzoic acid |
| 2-Me-1,8-ODDMA | 2-Methyl-1,8-octanediol dimethacrylate |
| 3-HB | 3-Hydroxybenzoic acid |
| 3,4-DHB | 3,4-Dihydroxybenzoic acid |
| 3,4,5-THB | 3,4,5-Trihydroxybenzoic acid |
| 3D SEM | 3-Dimensional scanning electron microscopy |
| AC | Alternating current |
| ACN | Acetonitrile |
| ADC | Antibody drug conjugate |
| AIBN | 2,2'-Azobisisobutyronitrile |
| ATRP | Atom transfer free-radical polymerization |
| AUFS | Absorbance units full scale |
| BA | Benzoic acid |
| BADMA | Poly(bisphenol A dimethacrylate) |
| BAEDA | Bisphenol A ethoxylate diacrylate |
| BSA | Bovine serum albumin |
| BTEE | Ethyl-2-methyl-2-butyltellanyl propionate |
| $C^4D$ | Capacitively-coupled contactless conductivity detection |
| CFP | Capillary flow porometry |
| CFRP | Conventional free-radical polymerization |
| CLD | Chord length distribution |
| CLSM | Confocal laser scanning microscopy |
| DB FIB | Dual beam focused ion beam |

| | |
|---|---|
| DMF | *N, N*-Dimethyformammide |
| DMPA | 2,2-Dimethoxy-2-phenyl-acetophenone |
| DVB | Divinylbenzene |
| EDMA | Ethylene dimethacrylate |
| EGDMA | Ethylene glycol dimethacrylate |
| GC | Gas chromatography |
| GDMA | Glycerol dimethacrylate |
| GMA-EDMA | Poly(glycidyl methacrylate-co-ethylene dimethacrylate) |
| HEMA | 2-Hydroxyethyl methacrylate |
| HIC | Hydrophobic interaction chromatography |
| HIPE | High internal phase emulsion polymerization |
| HPAA | Polyacrylic acid |
| HPLC | High performance liquid chromatography |
| i.d. | Internal diameter |
| ISEC | Inverse size exclusion chromatography |
| LC | Liquid chromatography |
| LEM | Linear extrapolation method |
| LFRP | Living free-radical polymerization |
| MIP | Mercury intrusion porosimetry |
| MMA | Methyl methacrylate |
| NaCl | Sodium chloride |
| NaPSS | Sodium styrene sulfonate |
| NMP | Nitroxide-mediated living radical polymerization |
| NSAID's | Non-steroidal anti-inflammatory drugs |
| PDAM | Pentaerythritol diacrylate monostearate |

| | |
|---|---|
| PAHEMA | Phosphoric acid 2-hydroxyethyl methacrylate |
| PEG | Poly(ethylene glycol) |
| PEGDA | Poly(ethylene glycol) diacrylate |
| PEGDMA | Poly(ethylene glycol) dimethacrylate |
| PEGMEMA | Poly(ethylene glycol) methyl ether methacrylate |
| PEO | Polyethylene oxide |
| PEO-PPO-PEO | Poly(ethylene oxide)-poly(propylene oxide)-poly(ethylene oxide) |
| PETA | Pentaerythritol triacrylate |
| PNM | Parallel network model |
| PPM | Parallel pore model |
| PS | Polystyrene |
| PSD | Particle size distribution |
| RAFT | Reversible addition-fragmentation chain transfer polymerization |
| RP | Reversed phase |
| RPLC | Reversed phase liquid chromatography |
| RSD | Relative standard deviation |
| SDS | Sodium dodecyl sulfate |
| SEC | Size exclusion chromatography |
| SPMA | 3-Sulfopropyl methacrylate |
| TEM | Transmission electron microscopy |
| TEOS | Tetraethyl orthosilicate |
| TERP | Tellurium mediated living radical polymerization |
| THF | Tetrahydrofuran |
| TMOS | Tetramethyl orthosilicate |
| TPB | Total pore blocking |

| | |
|---|---|
| TPM | 3-(Trimethoxysilyl)propyl methacrylate |
| TRIM | Trimethylolpropane trimethacrylate |
| SEM | Scanning electron microscopy |
| STY | Styrene |
| UV | Ultra violet |

LIST OF TABLES

LIST OF FIGURES

# CHAPTER 1 BACKGROUND AND SIGNIFICANCE*

## 1.1 Introduction

Liquid chromatography (LC) is a separation technique based on differential distribution of solute molecules between a stationary phase and mobile phase. The properties of these two phases, more importantly the stationary phase, govern the column performance and separation efficiency. The stationary phase bed structure generally has both small mesopores as well as large through-pores, making them suitable for small as well as large molecule separations, although the separation of large molecules does not necessarily require small pores. The small mesopores give rise to large surface area required for retention of solutes and, hence, resolution. On the other hand, the distribution and size of large pores (i.e., through-pores) control column efficiency and hydraulic impedance, as they allow the mobile phase to flow through the bed. A large through-pore size and wide distribution offer high column permeability, however, at the expense of efficiency, since a wide through-pore size distribution results in an increase in eddy diffusion contribution in the van Deemter equation. Thus, optimization of the bed structure to optimize the chromatography, i.e., good efficiency and high permeability, requires compromise, as both of these characteristics are inversely related. Therefore, the bed structure must be extensively investigated to achieve the best efficiency, keeping in mind the compromise between performance and practical constraints.

Stationary phases most commonly used today are particulate or monolithic in nature. Particle packed columns have long been used as stationary phases, starting from Tswett's [1] work with column beds packed with fine particles. Since then, there has been significant progress in column performance with the advent of small particles (5 μm and less) and small dimension

* This chapter was largely reproduced from: Aggarwal, P.; Tolley, H. D.; Lee, M.L. *J. Chromatogr. A* **2012, *1219***, 1-14.

columns, such as capillary columns and microfluidic devices [2-3]. However, these advancements have all resulted in an increase in hydraulic resistance of the column, thereby increasing the analysis time and/or necessitating the use of high pressure pumps. This tradeoff between efficient separation and analysis time was clearly demonstrated by Knox and Saleem [4], which (along with some technical problems associated with capillary column packing) has dampened some enthusiasm for these columns as particle size approaches 1 μm. There are no real possibilities of increasing the permeability of these packed beds, as any increase in permeability eventually leads to imperfections and, hence, poor performance. Therefore, there has been a need for new stationary phases capable of permitting efficient separation with good permeability.

Recent improvements in monolithic columns and core-shell particles represent major developments in the design of liquid chromatographic columns. These two stationary phase types offer the potential for satisfying the requirement of columns having good efficiency and high permeability [5]. Core-shell particles have a solid core surrounded by a porous outer layer, enabling the mobile phase to penetrate only the shell and not the core. Since larger particles are used, core-shell particles lead to reduced backpressure of the column in comparison to columns packed with porous particles. In contrast, monoliths are integrated, continuous porous separation media with no inter-particular voids and an open macropore structure. The porous layer structure and larger diameter of core-shell particles and the open macropore structure of monolithic columns permit rapid separation of analytes at reasonable back pressure, while retaining good separation efficiency.

As discussed above, the properties of these stationary phases are influenced by their bed structures, either in terms of efficiency or resistance to flow. It is the bed structures of these

different types of stationary phases, particle packed (fully porous or core-shell) and monolithic (polymeric or silica), that make them so different. The cross-sectional area of a monolithic skeleton is also typically less than that of particles in packed columns. This reduced dimension of the stationary phase facilitates mass transfer from the stationary phase to the mobile phase, thereby potentially improving column efficiency. Also, the voids (through-pores) in particle packed columns result from the inter-particle space, which in turn is a function of the particle size. In polymer monoliths, they arise due to the presence of porogens. The through-pores are more tortuous and constricted in packed bed structures as compared to monolithic structures, thereby adding to decreased permeability compared to monolithic beds [6]. In particle packed columns, the through-pores are simply a function of particle size and cannot be optimized independently. In comparison to monolith bed structure, the homogeneity and, hence, the performance of a particle packed bed structure is controlled by the particle size, particle size distribution and packing method.

The bed structure of these two stationary phase types is also different along the column walls, apart from that in the bulk. The particles along the walls in the particle packed column may be loosely or more tightly packed, depending on the packing procedure. On the other hand, polymeric monoliths fabricated in capillary columns are firmly attached to the capillary wall, thereby eliminating the column heterogeneity arising due to column packing. Although some radial heterogeneity occurs in monolithic columns as a consequence of different polymerization rates or porogen compositions at different locations along the column radius, it is much less than that in a particle packed column. This heterogeneity in the column greatly degrades the column performance whether it is a particle packed column or a monolithic column.

In addition to these differences between particle packed and monolithic columns, the morphologies of the monoliths vary among themselves. The skeleton of a monolith may be a globular or fused mass with no distinct microglobules, depending on the monomer and porogen compositions. The morphology also differs between inorganic silica monoliths and organic polymeric monoliths. Inorganic silica monoliths have a significant fraction of small mesopores in the skeleton formed as a consequence of treatment with ammonia or urea as a second step in the synthesis. Organic polymeric monoliths typically lack a significant fraction of mesopores [7]. However, recently there have been a number of publications reporting use of special procedures and/or reagents during synthesis to generate mesopores in the organic polymeric skeleton such as use of surfactants as template molecules [8], early termination of the polymerization reaction [9] and hyper-crosslinking of the monolith using Friedel Crafts reaction as the second step in monolith development [10].

Overall, there are many advantages of monoliths, with a major one being the independent optimization of the size of the through-pores and microglobules. Apart from these structural differences, monoliths have many advantages in terms of production time and equipment requirements. In situ polymerization of the monolithic stationary phase is especially useful for fabrication of capillary columns in contrast to packing of particles, which requires high pressure pumps. Since monoliths are bonded to the wall, there is no need for frits at the ends of the capillary column. Moreover, their ease of surface modification along with high stability make them an attractive alternative to conventional particle packed columns for capillary column chromatography. However, monolithic columns are still in their infancy, and require much more research to optimize their design and preparation for improved performance.

This chapter describes the general fabrication processes and bed structures of organic monoliths in comparison to structures of silica monoliths and particle beds. The first section describes packed column bed structure with emphasis on bed heterogeneity in the bulk and at the walls, as well as mobile phase flow through the bed. Because particle packed columns have long been studied, their bed structures can provide beneficial insights in understanding the dependence of column performance on bed structure. The second section emphasizes general monolith technology, followed by descriptions of silica and organic polymeric monolith bed structures, with greater emphasis on polymeric monoliths. These polymeric monoliths have different morphologies and pore structures, depending on the conditions of polymerization and the monomers themselves. The last section describes future efforts needed to improve efficiency and to increase the applicability of monolithic columns, laying the foundation for this PhD work.

**1.2 Particle packed columns**

The most common stationary phases used for liquid chromatography have been spherical particles. Columns packed with particles are available in a variety of lengths and diameters, starting with conventional (4.6 and 2 mm i.d) to microbore (1 mm i.d.) and capillary (< 0.5 mm i.d.) columns. The packed bed structure, governed by the size, shape, and orientation of the constituent particles, along with column geometry and size have been regarded as prime factors influencing chromatographic performance [11-12]. The bed structure of particulate columns has been characterized by a variety of statistical models and experimental techniques to provide information on external porosity, permeability, and uniformity. Recently, Tallarek et al. [13-14] reported the analysis of bed structure and its correlation with column performance for both particle packed and monolithic columns using confocal laser scanning electron microscopy (CLSM). The influence of stationary phase particle shape and column packing pressure on local

radial distribution of flow rate and resultant column efficiency was studied by Lottes et al. [15] using X-ray computed tomography. These studies along with optimization of the column technology, particle morphology and operating parameters have greatly improved chromatographic performance, especially separation efficiency, of these particulate columns.

### 1.2.1 Particle packed column structure

A close packed arrangement, as shown in Figure 1.1, should ideally be formed in columns packed with uniform size particles. A substantial improvement in separation performance with perfectly uniform packed columns was reported by Billen et al. [16] and Knox [17]. However, this ideal structure cannot be obtained in reality because of imperfections in the packing procedure. The structures of packed beds are typically found to be non-homogenous, both radially and axially [18], which has been attributed to packing instability, causing channeling in the packed bed structure, as well as the "wall effect" [17,19].

*Effect of particle morphology on bed structure.* The morphological features of the particles, such as size and shape, are known to influence bed uniformity and have been extensively studied to improve chromatographic performance. Reports have claimed more uniform bed structure with small particles as compared to large particles. The reason was ascribed by Lottes et al. [15] to be the extra packing force required to move larger particles to favorable positions, since they tend to block the paths of each other. However, the high back pressure associated with use of these small particles (sub-2 μm) limits further reduction in their size. In contrast, the uniformity of the column decreases with an increase in column permeability, since there is a proportional increase in defects in the packed bed [20]. Therefore, there is a tradeoff between chromatographic efficiency and column back pressure.

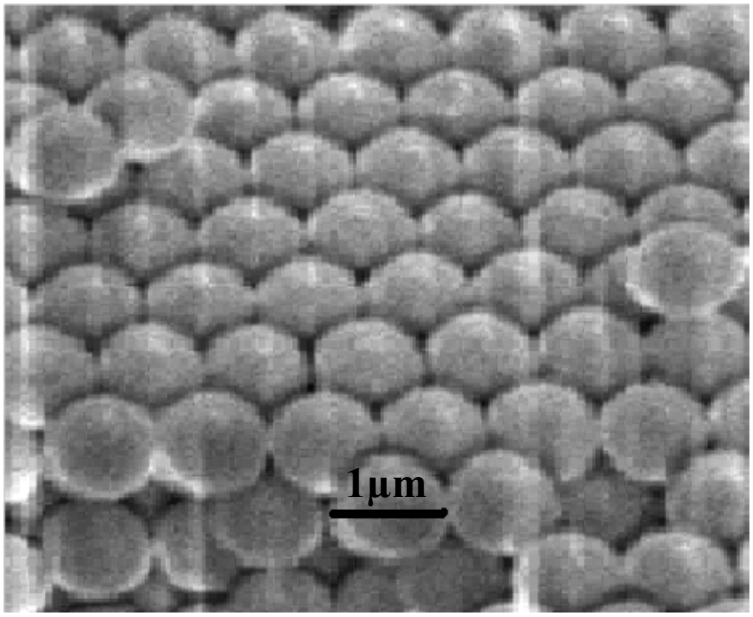


**Figure 2.1.** SEM image of a capillary column packed with 1 µm particles.

This compromise has led to discovery of alternate routes for improvement in column performance, such as the use of core-shell particles [21]. For such particles, the axial diffusion path within the stagnant mobile phase is greatly reduced since the material is only superficially porous. The decreased diffusion path should, in principle, decrease the C-term contribution to plate height in the van Deemter model [22]. This improved mass transfer also occurs in nonporous particles; however, increased efficiency occurs at the expense of sample loading capacity [5]. Thus, the porosity of the particle also contributes to column performance as it determines the bed structure at the microscopic scale.

In addition to small particle size, narrow particle size distribution (PSD) is also considered to be an important factor for improving column homogeneity and performance [23-25]. The narrow PSD associated with core-shell particles has been reported to be a major reason for their improved performance over conventional particle packed columns [21]. In contrast, others have reported column homogeneity to be better with broad PSD than with narrow size distribution [26-27]. The effect of PSD on plate height (H) and permeability was reported by Halasz and Naefe [28] to be negligible, until the PSD was less than 40 % around the mean. Billen et al. [29] also supported this claim based on the relationship between particle size distribution and kinetic performance of packed columns. The presence of fines was reported to influence the column performance more than the PSD, since they filled the voids between the larger particles.

Particle shape has also been considered to be an important characteristic influencing packed column performance. Spherical particles have been reported by Lottes et al. [15] to give more homogenous bed structures than irregular ones. In contrast, De Smet et al. [30] reported

better efficiency with diamond shaped pillars than with cylindrical or ellipsoidal ones for his pillar array columns. Moreover, the reduced plate height (h) was shown to be 2 times smaller for a perfectly ordered array of porous cylindrical pillars than for the best spherical particle packed columns via mathematical calculations [31]. However, there is one significant difference between particle packed and pillar array columns, i.e., the packing elements contact each other in particulate columns. Nevertheless, the influence of particle shape on column performance is clearly demonstrated by these studies. Surface roughness of the particle seems to be one more factor that influences column performance, as bed structure has been reported to be less dense with rough particles than with smooth particles [32].

*Effect of column wall on bed structure.* The column wall has been shown to be an important factor that contributes to column performance. The wall causes a radial variation of packing density, disturbing the particle packing close to the wall, termed the "wall effect" [33-35]. Two different wall effects have been reported by Shalliker et al. [36]. One is due to the rigid wall of the column which makes it impossible to pack the particles tightly against the wall. The second effect is due to friction between the bed and column wall, which makes it difficult to obtain a homogenous packing radially across the column. Recently, Tallarek et al. [13] confirmed and visualized these geometrical and friction-based wall effects in capillary columns by empirically analyzing the porosity profile of statistically derived packed beds.

Some authors have reported the thickness of the wall region to be a function of the column diameter [15], while others report it to be approximately several tens of particle diameters [37], irrespective of column dimensions. In capillary columns, heterogeneity near the wall has been found to be minimum with aspect ratios less than 10 (ratio of column to particle diameter), as the core region disappears and the packing structure is composed of only a wall

region, i.e., the packing structure becomes effectively more homogenous and ordered, thereby leading to excellent performance in terms of H. The reduced plate height was reported by Jorgenson et al. [2] to decrease with a decrease in column diameter. However, these changes in column efficiency could be attributed more to the change in particle diameter rather than column diameter, emphasizing packing density more than the wall effect [12,38].

Apart from particle and column dimensions, the column packing technique was found to contribute to bed density, causing differences in radial heterogeneity. In a dry-packed column, the permeability was reported to increase from the center to the wall, while for slurry packed columns, the permeability decreases from the center to the wall [17,39-41]. Farkas et al. [33] reported the presence of a homogenous core at the column center surrounded by a thick heterogeneous packing layer along the column wall, with no defined boundary in between. In contrast, Jorgenson et al. [42] reported the exact opposite, as they found particles to be more densely packed around the walls than in the center for capillary diameters greater than 75 μm.

### 1.2.2 Influence of bed structure on fluid flow through packed columns

There occurs a radial and axial variation in local mobile phase velocities as a consequence of the above stated radial and axial heterogeneities in the bed structures of chromatographic columns. Moreover, depending on the particle packing density near the walls, the velocity along the column wall may be slower or faster than in the core. Billen et al. [16] proved this via computational fluid dynamics simulations in a simplified two-dimensional mimic of particle packed columns, which was in agreement with results presented by Schure and Maier [20], indicating an increase in permeability with increased defects in the column packing. The latter study experimentally proved the mathematical predictions of Gzil and coworkers [43] regarding increased flow through the preferential flow path in the bed structure. The maximum

velocity of the mobile phase in uniformly packed columns was found to be lower than that of non-uniformly packed columns. The solute traveled with a higher velocity through the preferential path, thereby traveling a greater distance than through the constricted bed area. Hence, the solute, introduced initially as a plug, became distributed in these different flow regions, which resulted in band broadening. Tallarek et al. [44] further verified this variation in porosity along the column length and related it to the transcolumn velocity gradients reported by Giddings. This study provided valuable insight into structure-transport relationships.

### 1.2.3 Performance of particle packed columns

The efficiency of chromatographic columns is expressed mathematically in terms of theoretical plates (N) or plate height (H), with lower plate height and higher theoretical plate count corresponding to better column performance. The performance of chromatographic columns is related to their bed structures. Therefore, the factors influencing bed structure also govern column performance. Assuming the use of spherical particles, the two major factors affecting the column efficiency are column and particle diameters.

*Effect of column diameter.* The efficiency of particle packed columns has been improved progressively over time with column miniaturization. Kennedy and Jorgenson [45] compared the efficiencies of packed capillary columns (28 and 50 μm i.d.) with conventional columns (9.4 mm i.d.). The 50 μm i.d. capillary column (30.1 cm long) gave 21,700 total theoretical plates (72,093 plates/m) compared to 8,900 (35,600 plates/m) from a 25 cm long conventional column for bovine serum albumin (BSA). Although there was a difference in column length, it could not account for the difference in plate count. This improved performance for capillary columns has been attributed to reduced column heterogeneity with decrease in column diameter and, thereby, reduced A and C terms in the van Deemter equation [2].

Jorgensen et al. [2] observed the same with different capillary diameters (50 to 21 μm) packed with 5 μm porous octylsilane modified silica particles. The reduced plate height decreased from 1.4 to 1.0 (non-retained analyte) with a corresponding decrease in column diameter. For a retained analyte, the value for the minimum h decreased from 2.4 to 1.5. This difference in h value resulted from greater longitudinal diffusion of the retained analytes. The column was operated under isocratic conditions with 10 % acetonitrile and 90 % sodium phosphate solution with $10^{-3}$ M EDTA (pH =7.0) as mobile phase.

In an another study, McGuffin and Novotny [3] reported a statistically significant reduction in plate height (0.160 to 0.120 mm) or increase in theoretical plate count ($1.65 \times 10^5$ to $2.20 \times 10^5$, or 6,250 to 8,333 plates/m) for a decrease in column diameter from 100 to 60 μm (26.4 m columns). The results reported were obtained using toluene as analyte (k = 0.01) with 0.3 % methanol in hexane as mobile phase.

*Effect of particle diameter.* In the same study, McGuffin and Novotny [3] showed the improved performance of capillary columns with decreasing particle size. An increase in the total plate count from $1.96 \times 10^5$ to $3.10 \times 10^5$ (7,424 to 11,742 plates/m) with a decrease in particle size from 30 to 10 μm for a 26.4 m x 75 μm i.d. capillary column was reported. This difference in column performance was attributed to lower eddy diffusion in columns packed with smaller particles. Hirata and Jinno [46] proved the same by reporting 110,000 and 50,000 theoretical plates/m for 1 m x 0.2 mm i.d. glass columns packed with 3 and 10 μm particles, respectively. The columns were operated in the reversed phase mode for the separation of benzene derivatives, employing methanol as mobile phase. This improved performance with reduction in particle size was further supported in a study by Lie et al. [47]. A total plate count of 27,000 plates (180,000

plates/m) was reported for a 15 cm x 75 μm i.d. capillary column packed with 1.7 μm particles, in contrast to a plate count of 15,000 (100,000 plates/m) for 3 μm size particles in reversed phase chromatography.

Overall, the performance of packed capillary columns has been improved by packing more uniform bed structures, miniaturizing the column, optimizing the packing procedure and, most importantly, controlling the particle shape and morphology. Since there are some practical constraints, e.g,. high back pressure associated with small particles and reduced column diameter, the use of core shell particles and monoliths have been proposed as alternative stationary phases to overcome these limitations.

**1.3 Monolithic columns**

Monoliths were first developed and successfully used for LC in the early 1990's with the work of Hjerten [48] and Nakanishi and Soga [49]. They have been regarded as a substitute for particle packed columns, offering high permeability with good separation efficiency. Monoliths can be divided into two general categories: silica-based monolithic columns (prepared using sol-gel technology) and organic polymer based monoliths (prepared by chain polymerization reaction). Monoliths can be prepared by in-situ polymerization of a pre-polymer solution and bonded chemically to the walls or cladded by tubing. This eliminates the need for retaining frits in capillary columns and also eliminates effort otherwise required for packing the column with particles.

As the performance of particle packed columns is determined by their bed structures, similarly the performance of monoliths (silica or organic) is governed by their morphology and pore structure which are affected by factors involved in their synthesis, such as nature of monomer and porogen along with polymerization conditions. The work of Tallerek et al. [14,44]

using CLSM characterization has provided important insight in this regard. Therefore, monolith morphology (silica and polymeric) and the factors affecting their morphologies will be discussed in subsequent sections.

### 1.4 Silica monoliths

Silica monoliths have been successfully applied to the separation of both small and large molecules over the last 15 years [6]. Silica monoliths possess a spongy structure characterized by round pores [50] and a network skeletal structure as shown in Figure 1.2 [51]. They have a surface chemistry similar to particle packed columns, but have been reported to have large through-pore/skeleton size ratio (1.2-2.5) as compared to 0.25-0.4 for particle packed columns [52-53]. As a consequence, they have 65% external porosity as compared to 25% for particle packed columns [54], thereby providing shorter diffusion path length in the stationary phase and lower flow resistance, simultaneously. These silica macroporous structures have also been reported to have a bimodal pore size distribution, with a significant fraction of mesopores. This section briefly explains the factors affecting the morphologies of silica monoliths and, thereby, performance.

#### 1.4.1 Preparation of silica monoliths

The preparation of silica monoliths consists of hydrolyzing a mixture of silane compounds in the presence of an inert compound, the porogen. There occurs spinodal decomposition (sol preparation and hydrolysis), giving rise to periodic domains (silica-rich and solvent-rich). These network structures are then frozen by gelation (washing and aging of the gel), yielding the final polymeric skeleton with through-pores and mesopores [55]. Unreacted monomer and porogens present after polymerization are removed from the column by washing

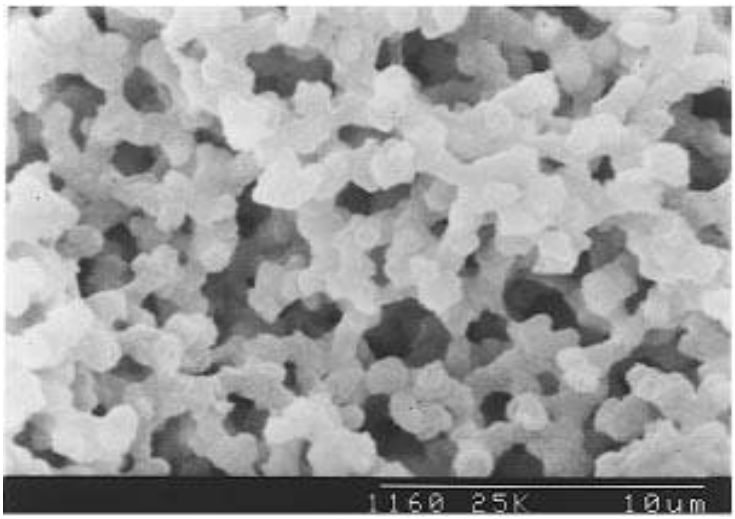


**Figure 1.2.** SEM image of a silica monolith [51].

with an appropriate solvent. Finally, the fabricated monolith may be modified with one or more reagents to provide the desired surface chemistry. Thermal initiation has been the most popular method for fabrication of these sol-gel monoliths in capillaries as well as in conventional column formats. However, Zare et al. [56] successfully fabricated sol-gel monoliths using photo initiation in capillary columns and used them for capillary electrochromatography. Initially, silica monoliths shrank during polycondensation, leaving a wide gap along the column walls. Therefore, they were enclosed with thermally shrinkable peek tubing after synthesis. This problem was eliminated with reduction in the column diameter (i.e., fabrication in capillary columns) and with improvements in the polymerization recipe [57]. The structural domains (particulate or monolithic mass) can be tailored by modifying the composition of the starting polymerization mixture of monomer, porogen and catalyst; varying the time of polymerization; and changing the temperature.

**1.4.2 Silica monolith structure**

The skeletal structure of silica monoliths has been described as agglomerated silica particles with varying size and through-pore distributions governed by the above mentioned factors. The bed permeability is inversely related to the domain size, similar to that in particle packed columns; however, the overall permeability is higher for monolithic columns. Nakanishi and Soga [49] prepared their first monoliths by reacting solutions of TEOS and TMOS containing poly(sodium styrene sulfonate) (NaPSS) of different molecular weights. They reported interconnected morphology with well-defined periodicity in the silica monolithic structure using NaPSS5 with a molecular weight of 10 kDa. The use of other molecular weight NaPSS gave gels with isolated domains or interconnected pores. Also, an increasing concentration of NaPSS at 40 °C caused a shift in morphology from isolated domains to

interconnected pores. There have been many reports on the effect of various polymerization factors on the morphologies of silica monoliths [58]. The same authors used different porogenic reagents, such as HPAA (polyacrylic acid) and PEO (polyethylene oxide). The size distribution of the through pores was found to be considerably narrower with PEO, and varied in mean size with changing PEO concentration [59]. The range of porogen concentration resulting in a monolith was found to decrease with an increase in molecular weight of the porogen used. Apart from this, the average domain size (i.e., through-pore plus skeleton size) was found to be larger with an increase in time difference between phase separation and sol-gel decomposition [60].

The mesopore fraction in the silica monolith skeleton can be tailored by aging and drying (solvent exchange). The rates of formation of the pore network and the pore size distribution were found to vary with temperature [59]. The distribution was found to be broadened with an increase in temperature, but with a concomitant decrease in intrinsic porosity of the monolith. The same study also showed that the pH of the wash liquid also influenced the mesopore size distribution, with a basic pH solvent having the maximum effect. Therefore, varying these parameters would alter the morphology of the monolith.

The composition of the pre-polymer solution and the temperature of polymerization govern the homogeneity of the monolith. Since most monolith synthesis reactions are exothermic, heat transfer must take place radially across the column and through the mold wall in which the monolith is made. Therefore, the center of the bed tends to be hotter than the region near the wall. Nakanishi and Soga [58] showed that the local porogen concentration governing the through-pore size distribution in the monolith is determined by the temperature of that region. Also, shrinking of the monolith after polymerization causes mechanical stress at the monolith-to-column wall boundary. This might result in a gap at the wall, creating a preferential

flow path for the mobile phase. Therefore, these factors must be reduced for better chromatographic efficiency.

1.4.3 Performance of silica monoliths

Smaller domain size, high phase ratio (volume of mobile phase to stationary phase), and good bed homogeneity have long been emphasized for improving the separation efficiencies of monolithic structures [61]. Kobayashi et al. [62] found that monolithic and particle packed columns had similar minimum plate height values; however, the efficiencies of silica monolithic columns were found to decrease much less rapidly than packed columns with increasing mobile phase velocity. This was attributed to larger A coefficients and smaller C coefficients in the van Deemter equation for monolithic columns compared to particle packed columns. Recently, a kinetic plot analysis of silica monoliths and particle packed columns by Morisato et al. [63] revealed that monolithic columns with macropore diameter and skeleton thicknesses of 1 μm performed equivalent to a 3 μm particle column. In an another study by Minakuchi et al. [54], silica monoliths with smaller size skeletons resulted in van Deemter plots (for amylbenzene and insulin) with minimum plate heights at higher linear mobile phase velocities than for particle packed columns. The slope of the curve was found to decrease with a decrease in the skeleton size. This was attributed to the short diffusion path length associated with the smaller skeleton size, which had less contribution to the plate height C term. The same authors studied the effect of domain size in the monolithic structure, and found that the plate height was reduced with a reduction in domain size [64]. Also, a smaller effect of mobile phase linear velocity on plate height for amylbenzenes was reported. The tendency was more pronounced for large molecules, such as insulin, since diffusion in the mesopores is slower for large molecules, which has a greater influence in the C term of the van Deemter equation.

In the same study, the authors estimated the optimum domain size for best performance, but found that the performance actually achieved was lower than that predicted [64]. The van Deemter plots indicated that the A coefficient increased and the C coefficient decreased with a decrease in domain size, suggesting that the mobile phase mass transfer was slower, although the small domain size facilitated faster mass transfer in the stationary phase [65]. Monoliths with small skeleton size were found to have greater irregularity in structure and wider through-pore size distribution, resulting in worse performance than expected [66]. Also, these silica monoliths were reported to have smaller phase ratio, resulting in poor resolution [67]. Desmet et al. [66] also showed theoretically that the performance of silica monoliths with small domain size can be greatly improved by increasing the homogeneity of the skeleton and through-pores, along with increasing the phase ratio. Hara et al. [61] synthesized silica monoliths with high phase ratio, small domain size and homogenous skeleton. They reported a plate height of 4.8 μm for a silica monolith with 2.2 μm domain size in a 15 cm x 100 μm i.d. column, which was better than that of a 3 μm particle packed column.

In addition to modification of the stationary phase bed structure, optimization of the chromatographic parameters can also improve column performance. Leinweber et al. [68] showed a decrease in plate height for insulin with an increase in temperature and assigned the reason to lower contribution of the A and C terms to the plate height in the van Deemter equation. This occurs because an increase in temperature increases both the lateral mass transfer and the intra-skeleton mass transfer.

Desmet et al. [69] showed that silica monolith performance could be better than particle packed column performance using kinetic plots. They also showed the existence of a desirable, but forbidden, region where no existing stationary phase support seems to operate, and indicated

that synthetic methods are required to greatly improve the bed structure homogeneity and decrease the domain size for monoliths.

### 1.5 Organic monoliths

Organic monoliths were successfully developed and used for the first time in the 1989 when Hjertén [48] prepared a highly swollen crosslinked gel of *N,N*-methylenebisacrylamide and acrylic acid in the presence of a salt in an aqueous medium. Since then, organic monoliths have been greatly improved, showing better performance for large molecule separations than silica monoliths because of their biocompatibility and large domain size (cauliflower-like) morphology, as can be seen in Figure 1.3 [70-71]. However, the performance of polymeric monoliths in the isocratic separation of low-molecular-weight organic compounds is relatively poor [9]. These differences in performance might be attributed to lack of mesopores or presence of micropores in the bed structures of the monoliths, and structural inhomogeneity leading to flow dispersion [6,72]. Also, Nischang et al. [9] attributed this poor performance to heterogeneous gel porosity in the globular structure of the monolith, stemming from radial distribution of the crosslinker density in the globule. As a consequence, increased band dispersion for retained analytes slowly deteriorates the separation, and results in a totally unsuitable material for small molecule separation. There are many reviews in the literature that report organic monolith synthesis routes and performance, but with little emphasis on bed structure [70,73-74].

#### 1.5.1 Preparation of organic monoliths

Capillary surface modification and initiation of polymerization in pre-polymer solution are two important steps involved in preparation of organic monoliths in capillary columns. First,

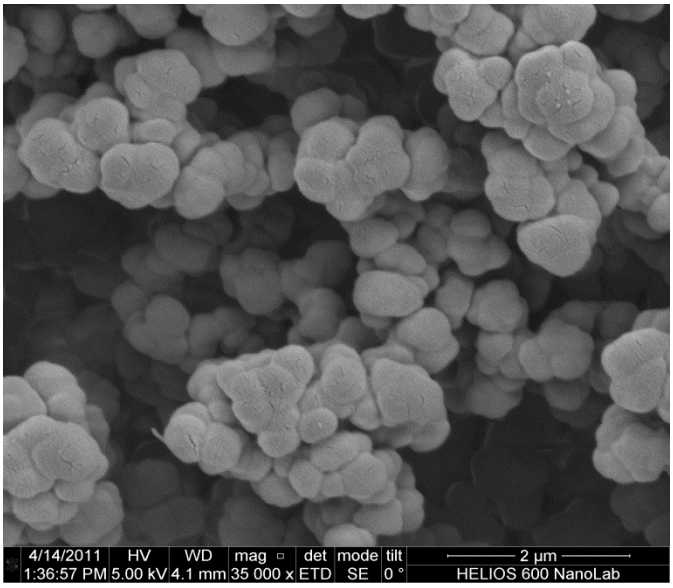


**Figure 1.3.** SEM image of an organic monolith.

the inner wall of the capillary is functionalized with a bi-functional reagent through a silanization reaction. Second, the capillary is filled with a pre-polymer mixture comprised of initiator, monomer(s) and porogen(s), and sealed at both ends with rubber plugs, followed by thermal or photo-initiated polymerization. During polymerization, monoliths are covalently bonded to the capillary surface, ensuring that the monolith can withstand relatively high pressures without being extruded from the capillary.

*Modification of the capillary surface.* The capillary surface is usually modified with a bi-functional silanizing reagent such as vinyl silane, acrylate silane or methacrylate silane. The most common reagent used is 3-(trimethoxysilyl)propyl methacrylate (TPM) [75]. Generally, capillary surface modification involves capillary pretreatment, silanization and drying steps.

There have been many reports in the literature for optimizing the pretreatment and silanization procedures involved in surface modification. For example, Courtois et al. [75] compared 3 pretreatments and 11 silanization procedures by varying the parameters involved in them. The study showed that the etching step (using base) increased the roughness of the inner capillary surface along with silanol group concentration, both of which contributed to better adhesion of the monolith to the capillary wall. Vidic et al. [76] also showed pretreatment to be a critical step in surface modification, and found that 15% TPM in dry toluene solution worked best for silanization.

The above mentioned two procedures involved either etching or leaching of the surface in the pretreatment step. However, Cifuentes et al. [77] proved that etching of columns with NaOH followed by leaching with HCl gave more reproducible surface treatment. Therefore, the optimized capillary surface modification procedure included both etching and leaching steps.

*Monolith synthesis.* After surface treatment, the treated capillary is filled with a pre-polymer solution and exposed to UV light or heat. The monomers may consist of a functional monomer along with a crosslinker, or simply a single functionalized crosslinking monomer. Porogens can be low or high molecular weight inert chemicals responsible for generating pores in the monolith. There occurs differential phase separation in the homogenous precursor solution during polymerization, which is induced by porogenic solvents with different thermodynamic properties. The monomers and porogens, as well as the initiation method, greatly influence the polymerization mechanism and phase separation, thereby affecting monolith morphology, pore size distribution, and separation performance.

### 1.5.2 Organic monolith structure

Similar to particle packed columns and silica monoliths, the performance of organic monoliths is also determined by their bed structure morphology and porosity. Monoliths should have both large surface area and good permeability. A large surface area provides more active sites for effective interactions, and good permeability allows faster analysis and moderate back-pressure. Porosity is the most important morphology characteristic, as it reflects the size and organization of both microglobules and clusters. Therefore, the morphologies of these monolithic structures, along with factors that influence the morphology, should be evaluated in order to optimize their performance.

*Effect of initiation method*. The initiation method and various parameters related to it such as temperature, light intensity, etc., govern the rate of polymerization reaction, which ultimately determines the monolith morphology. This section focuses on the initiation method, which may be radiation polymerization [78], living polymerization [79], high internal phase emulsion polymerization (HIPE) [80] and polycondensation [81]. Svec [82] recently published

an excellent review describing the various approaches used for monolith synthesis. The different initiation methods give rise to different monolith morphologies; for example, HIPE [80] gives an open pore monolith while thermal or photo initiation gives globular or fused morphology contingent upon other factors. Among these different initiation methods, thermal and photo initiation are more commonly used and will be discussed in detail.

Thermal initiation is one of the earliest methods used for organic monolith synthesis. For example, Svec and Frechet [83] successfully fabricated a porous poly(glycidyl methacrylate-co-ethylene dimethacrylate) monolith using 1% 2,2'-azobisisobutyronitrile (AIBN) as the thermal initiator. They also documented the effects of polymerization temperature, polymerization time, and type and concentration of thermal initiator on the morphology of the monoliths [84]. Viklund et al. [85] further showed that the pore size distribution of monoliths shifted toward smaller values with increased polymerization temperature and subsequent increase in surface area. They assigned the cause to higher decomposition rate of initiator and, subsequently, polymerization rate. An increase in temperature also resulted in an increase in solubility of the monomer, thereby resulting in late phase separation and large pore size; however, this effect had less influence than decomposition rate.

The polymerization time also changes the porosity of the fabricated monolith. As was observed by Svec et al. [86], the large pores disappeared upon prolonged polymerization, which were otherwise characteristic of the monolith in the early stages of polymerization. However, Trojer et al. [87] showed that the mesopore fraction increased significantly with a decrease in polymerization time, as BET measurements revealed a surface area increase from 26.8 $m^2/g$ to 77.2 $m^2/g$ on reduction of the polymerization time from 24 h to 45 min. This could be due to less crosslinking with shorter polymerization time. These results were also supported by Nischang et

al. [9] who reported a decrease in column performance with increase in polymerization time. They attributed this to increased importance of resistance to mass transfer originating from stagnant mass transfer zones in the porous structures. However, polymerization time is not widely used to tailor the pore size distribution, since maximum rigidity requires sufficient polymerization time.

Initiator type and concentration also affect monolith morphology and porosity. A higher concentration of initiator was found to produce smaller microglobules as a consequence of a large number of free radicals [88]. The selection of a free radical initiator is governed, to some extent, by its decomposition temperature.

Photo polymerization provides a number of advantages over thermal initiation. This initiation method significantly reduces the polymerization time from hours to minutes and also increases the range of solvents that can be used as porogens. Volatile organic solvents, such as ethyl ether, methanol and hexanes, can be used as porogens [89]. This broad range of porogen selectivity provides better control over the morphology and porosity of the monolith as compared to thermal initiation. Moreover, during thermal polymerization, there exists a thermal gradient along the radial direction of the capillary, as the polymerization reaction is exothermic and not all of the heat generated is dissipated uniformly throughout. Therefore, monoliths fabricated by photo initiation are more uniform compared to those made by thermal polymerization.

The factors governing photo polymerization are intensity and wavelength of the light source, as well as nature and concentration of the initiator. The former two remain constant with a particular lamp, while the latter two must be optimized for a good monolith. Some commonly used photo initiators are 2-methoxy-2-phenylacetophenone, 2,2-dimethoxy-2-phenylacetophenone (DMPA) and AIBN. Khimich et al. [90] studied the effect of initiator

concentration and found that an increase from 0.2 to 1% led to an increase in polymer density and formation of uniform pore structure. In another study, Viklund et al. [91] found that a concentration of approximately 3-4% led to cracks in the continuous polymer structure. Although the type and concentration of initiator can be varied, they are not usually preferred. The influence of temperature on photo polymerization has been documented in the literature [92], but has been found to be less significant. Although photo initiation has many significant advantages over thermal initiation, both are still equally used for monolith synthesis, and both affect the monolith morphology.

*Effect of porogens*. The porosity of the monolithic bed can be tailored by altering the natures of the porogenic solvents and/or their ratios without affecting the chemical composition of the final polymer. The porogens influence the pore properties of the monolith by controlling the solubility of the growing polymer chains in the polymerizing mixture and inducing differential phase separation in the homogenous precursor solution during polymerization [93]. Porogens can be classified as macro-porogens (those that create through pores) or meso-porogens (those that create mesopores), depending on the size of pores they create in the polymer skeleton. Generally, a poor solvent will generate larger through pores by facilitating early onset of phase separation. The new phase swells with the monomers because they are thermodynamically better solvents for the polymer than the porogen. As a consequence, large globules are formed with larger voids between them. In contrast, a good solvent generates smaller pores by delaying the onset of phase separation and competing for the monomer in solvating the nuclei.

The effect of porogen nature on porosity has been well documented in the literature. Viklund et al. [85] showed the effect of addition of a poor solvent on the pore size distribution in

a poly(glycidyl methacrylate-co-ethylenedimethacrylate) monolith (GMA-EDMA). They reported an increase in the mode (pore diameter at the highest peak) of the pore size distribution curve from 150 nm to 2,570 nm with an increase in percentage of dodecanol (poor solvent) from 0% to 15%. On the other hand, addition of even a relatively small percentage of toluene (good solvent) resulted in a dramatic decrease in pore sizes for a poly(styrene-co-divinylbenzene) monolith.

The influence of porogen nature on monolith morphology and surface area was well documented in a study by Santora et al. [94]. In a non-polar divinylbenzene-styrene (DVB/STY) monomer system, the non-polar porogen, *n*-hexane, effectively generated high surface area, while the polar porogen, methanol, gave smaller surface area. They found that the solvent roles were reversed in a more polar ethylene dimethacrylate-methyl methacrylate (EDMA/MMA) monomer system, with hexane and methanol giving low and high surface area materials, respectively. SEM images showed that the monolith with high surface area had fused or very small micro-globule morphology as compared to monoliths with low surface area and large globular morphology. Although these polymers had surface areas as large as 820 $m^2/g$, it is unlikely that they would be permeable to flow since the pores were rather small. In another study, Premstaller et al. [95] found that a porogen mixture of decanol and THF gave a poly(styrene/divinylbenzene) monolith with large through-pores and morphology similar to nonporous particles that have no micropores (termed micropellicular). These monolithic columns allowed rapid separation of oligonucleotides with high resolution.

Apart from the nature of the porogens, the ratio of porogens used can also influence the monolith morphology. Li et al. [96] successfully fabricated poly(bisphenol A dimethacrylate) (BADMA) monolithic columns with toluene and decanol as porogens, but found the porosity of

these structures to be very sensitive to ratio of toluene and decanol. They also found that the monolith shrank and detached from the wall, which led to replacement of toluene with THF as a good solvent. They also reported that monoliths with low back pressure had larger microglobules and microglobule clusters, while monoliths with high back pressure were composed of microglobules that were much smaller in size.

In addition to common organic solvents as porogens, solutions of a polymer in a solvent can also work as porogens. In a thorough study of the effects of poly(ethyleneglycol) (PEG) dissolved in 2-methoxyethanol on the pore properties of glycidyl methacrylate-co-trimethylolpropane trimethacrylate-co-triethylene glycol dimethacrylate) monoliths, Courtois et al. [97] found that the larger the molecular weight of the PEG, the larger the pores produced. Our group used PPG-PEG-PPG triblock copolymers and diethyl ether as porogens to prepare monolithic poly(ethylene glycol methyl ether acrylate-co-polyethylene glycol diacrylate) capillary columns [8]. These columns were found to have a considerable fraction of mesopores in the polymeric skeleton. In another study, a combination of high molecular mass polystyrene (PS) and chlorobenzene was used for the preparation of poly(glycerol dimethacrylate) (poly-GDMA) monoliths with an interesting morphology [98]. The structure of a poly-GDMA monolith prepared in situ with toluene as a poor porogenic solvent showed a typical agglomerated globular structure, whereas the morphology of a poly-GDMA monolith prepared in situ with the PS porogen was transformed from an aggregated globule form to a continuous skeletal structure. Along with this morphological transformation or change, the pore size distribution showed a sharp bimodal distribution, with one peak being located around 4 nm in the mesopore range (2-50 nm) and the other peak located around 1-2 μm in the macropore range (>50 nm), respectively.

Another atypical porogen is supercritical carbon dioxide. Using EDMA and TRIM as monomers, monoliths with a broad range of through-pore diameters (20 nm - 8 µm) have been prepared [99-100]. The authors found a direct dependence of properties such as pore size, pore volume, and surface area on $CO_2$ pressure. However, special equipment was required for the application of high pressures in the range of 15-30 MPa for the synthesis, and no applications of the resultant chromatographic column technology have been reported.

Porogen selection still remains more of an art rather than a science and is primarily accomplished by experimentation. Researchers still prefer to look for appropriate porogenic solvents based on their experience and the published work of others. The above described monoliths demonstrated different performance for small and large molecule separations (discussed in Section 1.5.3).

*Effect of monomers*. A change in chemical properties of a monomer or amount of a monomer in the polymerization process not only changes the morphology and porosity of the bed structure, but it also changes the chemical composition of the monolith. The amount of crosslinker effects the globule size and morphology, as a higher concentration induces early phase separation, analogous to a poor solvent. Since crosslinking restricts the swelling of the globules, the pore size distribution shifts towards a smaller domain. A single monomer can also alter the polymerization kinetics and, thereby, the monolith morphology. It can also alter the surface chemistry and separation selectivity.

Smirnov et al. [101] showed a dramatic decrease in the size of the globules and, consequently, the size of the interstices between these globules with an increase in weight fraction of 2-hydroxyethyl methacrylate (HEMA) from 4% to 8% in the polymerization mixture. The authors attributed this to improved polymer-porogen interactions with an increase in the

number of hydroxyl groups. Similar effects have also been shown for monomer mixtures such as GMA/EDMA and PS/DVB [85,102]. Santora et al. [94] also reported a decrease in surface area with a decrease in crosslinker ratio in the polymerization mixture. Xu et al. [103] investigated the effects of varying length and branching ratio of the crosslinker on column performance, keeping the molar ratio of the crosslinker and the monomer constant. They found that the volume of small mesopores increased with an increase in the length of the crosslinker, hence, leading to better separation efficiency for small molecules. These highly interconnected mesopores provided increased surface area and fast transfer kinetics for small alkylbenzenes. Thus, the effective thickness of the diffusion layer was significantly decreased.

The use of a single crosslinking monomer effectively increases the surface area and the concentration of desirable mesopores in the monolith, which has been demonstrated in several reports. Our group synthesized several monoliths from single crosslinking monomers, including bisphenol A dimethacrylate, bisphenol A ethoxylate diacrylate (BAEDA, EO/phenol = 2 or 4) and pentaerythritol diacrylate monostearate (PDAM) [96]. Among these monoliths, the morphology differed from one monomer to another. BAEDA-4 monoliths had a different morphology than BAEDA-2 monoliths. Distinct microglobules were not observed; instead, the monolith resembled a fused skeletal structure. Due to enhanced surface area resulting from the highly crosslinked structure, high resolution separations of alkyl benzenes and alkyl parabens were demonstrated using these columns.

Urban et al. [104] reported the use of a hypercrosslinking technique for extending the applicability of polymeric monoliths for small molecule separation. They used a mixture of styrene, vinylbenzyl chloride, and divinylbenzene monomers to prepare the monolith, followed by crosslinking of the functional groups on the surface using Friedel-Crafts alkylation. The

surface area of the monolith and the fraction of mesopores were significantly increased following hypercrosslinking.

*Effect of monomer to porogen ratio*. The effect of monomer concentration on the properties of the final polymer was recently demonstrated by Trojer et al. [87,105] for poly[p-methylstyrene-co-1,2-(p-vinylphenyl)ethane] monoliths. The macropore distribution shifted from 8.78 to 0.09 μm when the total monomer to porogen ratio was increased from 35% to 45% (v/v). This can be explained by a larger number of nuclei formed via irradiation of more concentrated monomers. When high density nuclei compete for the monomer, their sizes grow much slower before they touch each other. Smaller voids are consequently formed between the microglobules in clusters in the final monolithic polymer, resulting in smaller macropores. Thus, to guarantee a reasonable solvent flow with the operating pressure limits of LC instrumentation, the monomer to porogen ratio should not be high (< 50% in most cases). At the same time, although a decrease in the initial monomer concentration produces larger macropores, it decreases the density and rigidity of the monolith as well. Actually, it was observed that monolithic polymers were not formed with low monomer concentration (< 0.5 g/mL) for synthesis of trimethylolpropane trimethacrylate (TRIM), but resulted in a powder [100]. Decreased rigidity due to lower initial monomer concentration was also demonstrated in our synthesis of poly(triethylene glycol dimethacrylate) monoliths [106]. Monoliths prepared from a monomer concentration of 32.2 wt% could be stored dry. When the monomer concentration decreased to 20.2 wt%, the monolith exhibited lower back pressure and was not able to be regenerated after drying. Smirnov et al. [101] also showed a decrease in column permeability with an increase in monomer content in the polymerization mixture. Eeltink et al. [107] reported on low density methacrylate monoliths having a broad porosity profile, which were prepared using a total monomer content of 20%.

Only column efficiency was measured to compare low-density monoliths with high-density monoliths.

### 1.5.3 Performance of organic monoliths

The major chromatographic performance characteristics (i.e., efficiency, resolution and permeability) of organic monolithic columns arise from the pore-size distribution and skeletal size, similar to that of any other stationary phase. Organic monoliths have been primarily used for large biomolecule separations (unlike silica monoliths, which have been used for both small and large molecules) and their morphologies have been reported to be globular in nature [108]. Recently, however, there have been reports of successful separations of small molecules using organic monoliths [9,106].

*Effect of initiation method*. The nature, time and condition of polymerization has been known to affect monolith morphology. The studies of Trojer et al. [87] and Nischang et al. [9] have shown shorter polymerization time to be favorable for small molecule separation as a consequence of increased mesopore volume fraction. In thermal polymerization, the column performance has been reported to increase with an increase in polymerization temperature, as there occurs a decrease in though-pore size, thereby reducing the resistance to mass transfer and eddy term contributions in the van Deemter equation.

*Effect of porogens*. As described in Section 1.5.2, the porogens control the porosity of the monoliths, including pore-size and their distribution. Altering the type or the quantity of porogen determines whether the monolith can be used for small or large molecule separations and, also, the column performance for a particular separation. Premstaller et al. [95] demonstrated the performance of a monolithic column (with micropellicular morphology) for oligodexoynucleotide separations to be 40% better than particle packed columns. This was

attributed to a reduction in intraparticle dispersion due to the complete absence of small pores in the monolithic skeleton, allowing only convective flow through the bed structure.

On the other hand, poly(BADMA) monolithic columns with small microglobules or fused morphologies were reported to be suitable for separation of small molecules such as alkylbenzenes and alkylparabens [96]. They gave efficiency measurements between 20,000 and 30,000 plates/m for uracil at 0.1 μL/min (i.e., 0.38 mm/s). The plate count was as high as 61,432 plates/m for retained compounds. The performance was attributed to small domain size and high surface area. In a study by Aoki et al. [98], the column efficiency was found to be 34,075 plates/m ($H$ = 29.3 μm) when the monolith was prepared in situ with high molecular weight polystyrene as coporogen. This was much higher than 5,650 plates/m ($H$ = 177.0 μm), and 1,335 plates/m ($H$ = 749.3 μm) obtained from capillaries prepared in situ with low molecular weight standard PS or with toluene as porogens. These observations indicate that the high molecular weight PS porogenic solution delayed phase separation because of visco-elasticity. Li et al. [8,111] also reported size exclusion chromatography using organic monoliths prepared using poly(ethylene oxide)-poly(propylene oxide)-poly(ethylene oxide) (PEO-PPO-PEO) or PPO-PEO-PPO and Brij 58P as mesoporogens. The separations indicated the presence of mesopores in the skeletal structure.

*Effect of monomers.* In a study by Smirnov et al. [101], the column efficiency showed a significant increase (i.e., plate height decreased from 188 to 51 μm for an non-retained compound) with an increase in HEMA content from 4% to 8% in the polymerization mixture. They attributed this to reduced globule size in the monolithic skeleton. Xu et al. [103] reported an increase in number of theoretical plates/m from 11,000 to 83,000 for thiourea with a change in crosslinker from ethylene dimethacrylate (EDMA) to 2-methyl-1,8-octanediol dimethacrylate (2-

Me-1,8-ODDMA). The increase was attributed to an increase in fraction of mesopores and, thus, reduced C term in the van Deemter equation. Urban et al. [104] reported an H value of 39 μm for benzene on their hypercrosslinked columns. They used the same column for rapid isocratic separation of peptides and gradient elution of 7 small molecules. They also demonstrated the use of this column for size exclusion of polystyrene standards using an organic mobile phase.

*Effect of monomer to porogen ratio.* Eeltink et al. [107] experienced an increase in separation efficiency for a small molecule by a factor of ~5, which they ascribed to broadening of the porosity curve when reducing the amount of monomers from 40 to 20%. In an another study, Trojer et al. [105] found the retention times for biomolecules to be unaffected by an increase in monomer content while the resolution increased. However, for oligonucleotides, both the retention time and resolution were altered with change in monomer to porogen ratio, indicating a change in both mesopore volume and through-pore size. This also indicates that small molecule separations require broad pore distribution, as an increase in surface area increases small molecule interaction with the stationary phase.

Overall, the structures of polymeric monolithic columns determine their applicability. They have been effectively used for biomolecule separations with few applications for small molecules. Organic monoliths provided faster and more efficient separations than conventional HPLC columns (packed with 5 μm particles) for peptides in a kinetic plot study by Guillarme et al. [110], which they ascribed to improved mass transfer kinetics. However, with the advent of small particle sizes the performance of organic monolithic columns lags behind that of particulate columns.

### 1.6. Dissertation Overview

Monolithic column technology is still in its infancy, and discoveries in the field are expected to give rise to novel materials with unique properties. Monolith technology has been greatly improved over the past decade, and has been employed for both large and small molecule separations [111-112]. The performance of monolithic columns has been shown to be comparable to particle packed columns (using the kinetic plot method) in some cases with silica monoliths [61]; however, it can still be significantly improved for polymeric monoliths, as is evident from Table 1.1. The published literature clearly indicates a dependence of column performance on stationary phase bed structure [113]. Also, the applicability of globular organic polymer monoliths to large molecule separations and their poor performance for small molecules have been ascribed to the structure of the monoliths [9]. Therefore, efforts should be directed toward better understanding of the relationship of monolith bed structure and performance, and control of through-pore structure and morphology.

My research was focused on improving the chromatographic efficiency of PEGDA organic monoliths by characterizing the monolith morphology, correlating it to its chromatographic efficiency and optimizing the morphology for improved performance. Chapter 2 reports use of capillary flow porometry for characterizing the effect of fabrication conditions such as capillary diameter, pre-polymer composition on monolith morphology and performance. Chapter 3 describes the development and implementation of 3D SEM as a technique for providing quantitative descriptors of monolith morphology such as pore size, radial heterogeneity, and bed tortuosity. The morphological parameters were correlated with the chromatographic performance of PEGDA monoliths. These characterization studies aided in identifying the factors governing monolith morphology and its performance. Chapter 4 lists the

**Table 1.1.** Representative performance data for a variety of packed and monolithic columns.

| Stationary Phase | Performance | | K | Back pressure | Column dimensions | Reference |
|---|---|---|---|---|---|---|
| | N (plates/m) | H (µm) | | | | |
| | | | Particle packed columns | | | |
| *Particle Diameter* | | | | | | |
| 5 µm | 83,000 | 12.0 | 2.7 | 899 psi at 0.088 cm/s | 33 cm x 50 µm i.d. | [2] |
| 3 µm | 110,000 | 9.1 | 0.9 | Constant pressure of 200 kg/cm$^2$ | 100 cm x 200 µm i.d. | [46] |
| 1.5 µm | 209,000 | 2.4 | 0.2 | 23,000 psi at 0.145 cm/s | 49.3 cm x 30 µm i.d. | [115] |
| 1 µm | 521,000 | 2.0 | 2.0 | 40,000 psi at 0.15 cm/s | 46 cm x 30 µm i.d. | [116] |
| | | | Silica monoliths | | | |
| *Domain size* | | | | | | |
| 3.1 µm | 186,000 | 5.4 | 1.4 | 377 psi at 2.0 mm/s | 14.5 cm x 100 µm i.d. | [61] |
| 2.6 µm | 200,000 | 5.0 | 1.4 | 537 psi at 2.0 mm/s | 15 cm x 100 µm i.d. | [61] |
| 2.2 µm | 210,000 | 4.8 | 1.4 | 653 at psi 2.0 mm/s | 15 cm x 100 µm i.d. | [61] |
| | | | Organic monoliths | | | |
| *Domain Size* | | | | | | |
| N.A. | 48,000 | 20.5 | 11.5 (estimated from chromatogram) | 1740 psi at 6.4 mm/s | 8 cm x 200 µm i.d. | [117] |
| N.A. | 60,000 | 16.6 | 7.9 | 700 psi at 1.1 mm/s | 16 cm x 75 µm i.d. | [96] |
| N.A. | 83,200 | 12.0 | 0.04 | 3770 psi at 0.1 µL/min | 13 cm x 100 µm i.d. | [94] |

corrections needed in calculating column efficiency because of the extra-column dead volume associated with the capillary liquid chromatograph. The liquid chromatograph used in all of the studies was found to have a dead volume of ~35 nL. The measured column performance was found to be 60% of actual chromatographic performance. In Chapter 5, PEGDA monoliths were fabricated by optimizing the factors governing monolith performance using statistical principles with column efficiency as the guiding parameter. The monolithic columns were used for RPLC of small molecules, exhibiting column efficiencies of 186,000 plates/m (corrected for extra-column dead volume) for a non-retained compound. High resolution gradient separations of selected pharmaceutical compounds and phenylurea herbicides were achieved in less than 18 min on the fabricated PEGDA monoliths. Chapter 6 describes fabrication of PEGDA monoliths using organotellurium-mediated living radical polymerization (TERP) for reducing the inherent structural heterogeneity associated with conventional free-radical polymerization. The fabricated columns gave an unprecedented column performance of 238,000 plates/m (corrected for dead volume) for a non-retained compound. Chapter 7 presents some proposed future directions in using the developed characterization and fabrication techniques for other monomer systems, which could be used for other modes of chromatography.

**1.7 References**


[1] Tswett, M.S.; Varshav, T.P. *Obshch. Estestvoistpyt.* **1905**, *14*, 20.

[2] Kennedy, R.T.; Jorgenson, J.W. *Anal. Chem.* **1989**, *61*, 1128-1135.

[3] McGuffin, V.L.; Novotný, M. *J. Chromatogr. A* **1983**, *255*, 381-393.

[4] Knox, J.H.; Saleem, M. *J. Chromatogr. Sci.* **1969**, *7*, 614-622.

[5] Carr, P.W.; Stoll, D.R., Wang, X. *Anal. Chem.* **2011**, *83*, 1890-1900.

[6] Guiochon, G. *J. Chromatogr. A* **2007**, *1168*, 101-168.

[7] Liao, J.L.; Zhang, R.; Hjerten, S. *J. Chromatogr.* **1991**, *586*, 21-26.

[8] Li, Y.; Tolley, H.D.; Lee, M.L. *Anal. Chem.* **2009**, *81*, 4406-4413.

[9] Nischang, I.; Brüggemann, O. *J. Chromatogr. A* **2010**, *1217*, 5389-5397.

[10] Urban, J.; Svec, F.; Fréchet, J.M.J. *J. Chromatogr. A* **2010**, *1217*, 8212-8221.

[11] Afandizadeh, S.; Foumeny, E.A. *Appl. Therm. Eng.* **2001**, *21*, 669-682.

[12] Halasz, I.; Heine, E. *Nature* **1962**, *194*, 971-973.

[13] Bruns, S.; Hara, T.; Smarsly, B.M.; Tallarek, U. *J. Chromatogr. A* **2011**, *1218*, 5187-5194.

[14] Leinweber, F.C.; Tallarek, U. *J. Chromatogr. A* **2003**, *1006*, 207-228.

[15] Lottes, F.; Arlt, W.; Minceva, M.; Stenby, E.H. *J. Chromatogr. A* **2006**, *1216*, 5687-5595.

[16] Billen, J.; Gzil, P.; Vervoort, N.; Baron, G.V.; Desmet, G. *J. Chromatogr. A* **2005**, *1073*, 53-61.

[17] Knox, J.H. *J. Chromatogr. A* **2002**, *960*, 7-18.

[18] Yuan, Q.S.; Rosenfeld, A.; Root, T.W.; Klingenberg, D.J.; Lightfoot, E.N. *J. Chromatogr. A* **1999**, *831*, 149-165.

[19] Porsch, B. *J. Chromatogr. A* **1994**, *658*, 179-194.

[20] Schure, M.R.; Maier, R.S. in, San Francisco, CA, June 17-22, **2006**, p. paper L.

[21] Kirkland, J.J.; Langlois, T.J.; Destefano, J.J. *Am. Lab* **2007**, *39*, 18-21.

[22] Atia, N.N.; York, P.; Clark, B.J. *J. Sep. Sci.* **2009**, *32*, 2732-2736.

[23] Majors, R.E.; Barth, H.G.; Lochmuller, C.H. *Anal. Chem.***1982**, *54*, 323-363.

[24] Endele, R.; Halasz, I.N.; Unger, K. *J. Chromatogr. A* **1974**, *99*, 377-393.

[25] Dewaele, C.; Verzele, M. *J. Chromatogr. A* **1983**, *260*, 13-21.

[26] Ohmacht, R.; Halász, I. *Chromatographia* **1981**, 14, 155-162.

[27] Kulin, L.-I.; Flodin, P.; Ellingsen, T.; Ugelstad, J. *J. Chromatogr. A* **1990**, *514*, 1-9.

[28] Halasz, I.; Naefe, M. *Anal. Chem.* **1972**, *44*, 76-84.

[29] Billen, J.; Guillarme, D.; Rudaz, S.; Veuthey, J.-L.; Ritchie, H.; Grady, B.; Desmet, G. *J. Chromatogr. A* **2007**, *1161*, 224-233.

[30] De Smet, J.; Gzil, P.; Vervoort, N.; Verelst, H.; Baron, G.V.; Desmet, G. *J. Chromatogr. A* **2005**, *1073*, 43-51.

[31] De Smet, J.; Gzil, P.; Vervoort, N.; Verelst, H.; Baron, G.V.; Desmet, G. *Anal. Chem.* **2004**, *76*, 3716-3726.

[32] Leva, M.; Weinfraub, M.; Rummer, M.; Pollchik, M.; Sforch, H.H. Fluid Flow Through Packed And Fludized Systems.

[33] Farkas, T.; Guiochon, G. *Anal. Chem.* **1997**, *69*, 4592-4600.

[34] Knox, J.H.; Laird, G.R.; Raven, P.A. *J. Chromatogr. A* **1976**, *122*, 129-145.

[35] Baur, J.E.; Wightman, R.M. *J. Chromatogr. A* **1989**, *482*, 65-73.

[36] Shalliker, R.A.; Broyles, B.S.; Guiochon, G. *J. Chromatogr. A* **2000**, *888*, 1-12.

[37] Guiochon, G.; Drumm, E.; Cherrak, D. *J. Chromatogr. A* **1999**, *835*, 41-58.

[38] Eeltink, S.; Rozing, G.P.; Schoenmakers, P.J.; Kok, W.T. *J. Chromatogr. A* **2004**, *1044*, 311-316.

[39] Lee, M.L. Fundamentals of Analytical Separations, Brigham Young University, provo, Utah, **2010**.

[40] Eon, C.H. *J. Chromatogr. A* **1978**, *149*, 29-42.

[41] Frakas, T.; Sepaniak, M.J.; Guiochon, G. *AICHE J.* **1997**, *43*, 1964-1974.

[42] Patel, K.D.; Jerkovich, A.D.; Link, J.C.; Jorgenson, J.W. *Anal. Chem.* **2004**, *76*, 5777-5786.

[43] Gzil, P.; Vervoort, N.; Baron, G.V.; Desmet, G. *J. Sep. Sci.* **2004**, *27*, 887-896.

[44] Bruns, S.; Tallarek, U. *J. Chromatogr. A* **2011**, *1218*, 1849-1860.

[45] Kennedy, R.T.; Jorgensen, W.; *J. Microcol. Sep.* **1990**, *2*, 120-126.

[46] Hirata, Y.; Jinno, K. *J. High Resolut. Chromatogr.* **1983**, *6*, 196-199.

[47] Liu, H.; Finch, J.W.; Lavallee, M.J.; Collamati, R.A.; Benevides, C.C.; Gebler, J.C. *J. Chromatogr. A* **2007**, *1147*, 30-36.

[48] Hjerten, S.; Liao, J.L.; Zhang, R. *J. Chromatogr.* **1989**, *473*, 273-275.

[49] Nakanishi, K.; Soga, N. *J. Am. Ceramic Soc.* **1991**, *74*, 2518-2530.

[50] Unger, K.K. *Porous Silica; Elsevier: Amsterdam* **1979**, Chapter 2

[51] Minakuchi, H.; Nakanishi, K.; Soga, N.; Ishizuka, N.; Tanaka, N. *Anal. Chem.* **1996**, *68*, 3498-3501.

[52] Unger, K.K.; *Porous Silica, Elsevier, Amsterdam* **1979**, Chapter 5.

[53] Knox, J.H.; Scott, H.P. *J. Chromatogr. A* **1984,** *316*, 311-332.

[54] Minakuchi, H.; Nakanishi, K.; Soga, N.; Ishizuka, N.; Tanaka, N. *J. Chromatogr. A* **1997**, *762*, 135-146.

[55] Tanaka, N.; Kobayashi, H.; Ishizuka, N.; Minakuchi, H.; Nakanishi, K.; Hosoya, K.; Ikegami, T. *J. Chromatogr. A* **2002**, *965*, 35-49.

[56] Kato, M.; Sakai-Kato, K.; Toyo'oka, T.; Dulay, M.T.; Quirino, J.P.; Bennett, B.D.; Zare, R.N. *J. Chromatogr. A* **2002**, *961*, 45-51.

[57] Ishizuka, N.; Minakuchi, H.; Nakanishi, K.; Soga, N.; Hosoya, K.; Tanaka, N. *J. High Resolut. Chromatogr.* **1998**, *21*, 477-479.

[58] Nakanishi, K.; Soga, N. *J. Non-Cryst. Solids* **1992**, 14-24.

[59] Nakanishi, K.; Minakuchi, H.; Soga, N.; Tanaka, N. *J. Sol-Gel Sci.Technol.* **1998**, *13*, 163-169.

[60] Nakanishi, K. *J. Porous Mater.* **1997**, *4*, 67-112.

[61] Hara, T.; Kobayashi, H.; Ikegami, T.; Nakanishi, K.; Tanaka, N. *Anal. Chem.* **2006**, *78*, 7632-7642.

[62] Kobayashi, H.; Tokuda, D.; Ichimaru, J.; Ikegami, T.; Miyabe, K.; Tanaka, N. *J. Chromatogr. A* **2006,** *1109*, 2-9.

[63] Morisato, K.; Miyazaki, S.; Ohira, M.; Furuno, M.; Nyudo, M.; Terashima, H.; Nakanishi, K. *J. Chromatogr. A* **2009**, *1216*, 7384-7387.

[64] Minakuchi, H.; Nakanishi, K.; Soga, N.; Ishizuka, N.; Tanaka, N. *J. Chromatogr. A* **1998**, *797*, 121-131.

[65] Ishizuka, N.; Kobayashi, H.; Minakuchi, H.; Nakanishi, K.; Hirao, K.; Hosoya, K.; Ikegami, T.; Tanaka, N. *J. Chromatogr. A* **2002**, *960*, 85-96.

[66] Gzil, P.; Vervoort, N.; Baron, G.V.; Desmet, G. *Anal. Chem.* **2004**, *76*, 6707-6718.

[67] Ishizuka, N.; Minakuchi, H.; Nakanishi, K.; Soga, N.; Nagayama, H.; Hosoya, K.; Tanaka, N. *Anal. Chem.* **2000**, *72*, 1275-1280.

[68] Leinweber, F.C.; Lubda, D.; Cabrera, K.; Tallarek, U. *Anal. Chem.* **2002**, *74*, 2470-2477.

[69] Gzil, P.; De Smet, J.; Desmet, G. *J. Sep. Sci.* **2006**, *29*, 1675-1685.

[70] Vlakh, E.G.; Tennikova, T.B. *J. Chromatogr. A* **2009**, *1216*, 2637-2650.

[71] Smith, N.W.; Jiang, Z. *J. Chromatogr. A* **2008**, *1184*, 416-440.

[72] Svec, F. *J. Chromatogr. A* **2010**, *1217*, 902-924.

[73] Svec, F. *J. Chromatogr. B* **2006**, *841*, 52-64.

[74] Svec, F.; Kurganov, A.A. *J. Chromatogr. A* **2008**, *1184*, 281-295.

[75] Courtois, J.; Szumski, M.; Bystrom, E.; Iwasiewicz, A.; Shchukarev, A.; Irgum, K. *J. Sep. Sci.* K. **2006**, *29*, 325.

[76] Vidic, J.; Podgornik, A.; Strancar, A. *J Chromatogr A* **2005**, *1065*, 51-58.

[77] Cifuentes, A.; Canalejas, P.; Ortega, A.; Diez-Masa, J.C. *J. Chromatogr. A* **1998**, *823* 561-571.,

[78] Vizioli, N.M.; Rusell, M.L.; Carbajal, M.L.; Carducci, C.N.; Grasselli, M. *Electrophoresis* **2005**, *26*, 2942-2948.

[79] Kanamori, K.; Nakanishi, K.; Hanada, T. *Adv. Mater.* **2006**, *18*, 2407-2411.

[80] Yao, C.; Qi, L.; Yang, G.; Wang, F. *J. Sep. Sci.* **2010**, *33*, 475-483.

[81] Peskoller, C.; Niessner, R.; Seidel, M. *J. Chromatogr. A* **2009**, *1216*, 3794-3801.

[82] Svec, F. *J. Chromatogr. A* **2010**, *1217*, 902-924.

[83] Svec, F.; Frechet, J.M.J. *Anal. Chem.* **1992**, *64*, 820-822.

[84] Svec, F.; Frechet, J.M.J. *Macromolecules* **1995,** *28*, 7580-7582.

[85] Viklund, C.; Svec, F.; Frechet, J.M.J.; Irgum, K. *Chem. Mater.* **1996**, *8*, 744-750.

[86] Svec, F.; Frechet, J.M.J. *Chem. Mater.* **1995,** *7*, 707-715.

[87] Trojer, L.; Bisjak, C.P.; Wieder, W.; Bonn, G.K. *J. Chromatogr. A* **2009**, *1216*, 6303-6309.

[88] Lubbad, S.H.; Buchmeiser, M.R. *J. Sep. Sci.* **2009**, *32*, 2521-2529.

[89] Throckmorton, D.J.; Shepodd, T.J.; Singh, A.K. *Anal. Chem.* **2002**, *74*, 784-789.

[90] Khimich, G.N.; Tennikova, T.B. *Russ J Appl Chem* **2005**, *78*, 623-627.

[91] Viklund, C.; Ponten, E.; Glad, B.; Irgum, K.; Horstedt, P.; Svec, F. *Chem. Mater.* **1997**, *9*, 463-471.

[92] Szumski, M.; Buszewski, B. *J. Sep. Sci.* **2009**, *32*, 2574-2581.

[93] Peters, E.C.; Svec, F.; Fréchet, J.M.J.; Viklund, C. ; Irgum, K. *Macromolecules* **1999**, *32*, 6377-6379.

[94] Santora, B.P.; Gagne, M.R.; Moloy, K.G.; Radu, N.S. *Macromolecules* **2001**, *34*, 658-661.

[95] Premstaller, A.; Oberacher, H.; Huber, C.G. *Anal. Chem.***2000**, *72*, 4386-4393.

[96] Li, Y.; Tolley, H.D.; Lee, M.L. *J. Chromatogr. A* **2011**, *1218*, 1399-1408.

[97] Courtois, J.; Bystrom, E.; Irgum, K. *Polymer* **2006**, *47*, 2603-2611.

[98] Aoki, H.; Kubo, T.; Ikegami, T.; Tanaka, N.; Hosoya, K.; Tokuda, D.; Ishizuka, N. *J. Chromatogr. A* **2006**, *1119*, 66-79.

[99] Cooper, A.I.; Holmes, A.B. *Adv. Mater.* **1999**, *11*, 1270-1274.

[100] Hebb, A.K.; Senoo, K.; Cooper, A.I. *Compos Sci Technol* **2003**, *63*, 2379-2387.

[101] Smirnov, K.N.; Dyatchkov, I.A.; Telnov, M.V.; Pirogov, A.V.; Shpigun, O.A. *J. Chromatogr. A* **2011**, *1218*, 5010-5019.

[102] Tennikova, T.B.; Belenkii, B.G.; Svec, F. *J Liq Chromatogr* **1990**, *13*, 63-70.

[103] Xu, Z.; Yang, L.; Wang, Q. *J. Chromatogr. A* **2009**, *1216*, 3098-3106.

[104] Urban, J.; Svec, F.; Fréchet, J.M.J. *J. Chromatogr. A* **2010,** *1217*, 8212-8221.

[105] Trojer, L.; Lubbad, S.H.; Bisjak, C.P.; Bonn, G.K. *J. Chromatogr. A* **2006**, *1117*, 56-66.

[106] Li, Y.; Tolley, H. D.; Lee, M.L. *J Chromatogr A* **2010**, *1217*, 4934-4945.

[107] Eeltink, S.; Herrero-Martinez, J.M.; Rozing, G.P.; Schoenmakers, P.J.; Kok, W.T. *Anal. Chem.* **2005**, *77*, 7342-7347.

[108] Svec, F. *J. Sep. Sci.* **2004**, *27*, 1419-1430.

[109] Li, Y.; Tolley, H.D.; Lee, M.L. *J. Chromatogr. A* **2010**, *1217*, 8181-8185.

[110] Guillarme, D.; Ruta, J.; Rudaz, S.; Veuthey, J.-L. *Anal. Bioanal. Chem.* **2010**, *397*, 1069-1082.

[111] Bakry, R. ; Huck, C.W.; Bonn, G.K. *J Chromatogr. Sci.* **2009**, *47*, 418-431.

[112] Canto-Mirapeix, A.; Herrero-Martinez, J.M.; Mongay-Fernandez, C.; Simo-Alfonso, E.F. *Electrophoresis* **2008,** *29*, 4399-4406.

[113] Vervoort, N.; Gzil, P.; Baron, G.V.; Desmet, G. *J. Chromatogr.* **2004**, *1030*, 177-186.

[115] Mellors, J. S. ; Jorgenson, J. W. *Anal. Chem.* **2004**, *76*, 5441-5450.

[116] Macnair, J.E.; Patel, K.D.; Jorgenson, J.W. *Anal. Chem.* **1999**, *71*, 700-708.

[117] Greiderer, A.; Trojer, L.; Huck, C.W.; Bonn, G.K. *J. Chromatogr. A* **2009**, *1216* 7747-7754.

# CHAPTER 2 CHARACTERIZING ORGANIC MONOLITHIC COLUMNS USING CAPILLARY FLOW POROMETRY AND SCANNING ELECTRON MICROSCOPY*

## 2.1 Introduction

The bed structure, including morphology and pore size distribution, of any chromatographic column (particle packed or monolithic) has an important influence on column efficiency apart from chromatographic conditions such as mobile phase composition, flow rate, etc. The porosity of the stationary phase not only determines its performance in terms of mass transfer kinetics (e.g., efficiency) but also affects its hydrodynamic properties (e.g., permeability) [1,2]. Therefore, the bed structure must be extensively investigated and controlled for obtaining the best efficiency, keeping in mind that there must be a compromise between performance and permeability [1-3].

The bed structures of particle packed columns have long been evaluated both microscopically and macroscopically, with the desire to understand the influence of particle shape, size distribution and arrangement in the bed structure on column performance [4,5]. The efficiency of particle packed columns has been greatly improved over time by improving the uniformity of the packed bed, which is facilitated by column miniaturization, small particle size and optimum packing procedure [2,6-8]. However, monolithic column performance has not generally matched that of particle packed columns [9]. This can be attributed to the heterogeneity of monolithic skeletal structures and their wide through-pore size distributions [10]. Therefore, there have been many studies to characterize monoliths in terms of globule size and pore-size distribution to determine the most important factors responsible for their performance [11,12].

Column structural characterization has been accomplished using microscopic techniques such as scanning electron microscopy (SEM) [13], X-ray diffraction analysis [14] and transmission electron microscopy (TEM) [15]. These techniques provide images of the sample,

* This chapter was largely reproduced from: Aggarwal, P.; Tolley, H. D.; Lee, M.L. *Anal.Chem.* **2011,** *84*, 247-254.

but with only limited quantitative information. They provide information about the shape and morphology of the polymeric skeleton along with a rough estimate of the pore-size distribution. These techniques are also quite expensive and time-consuming. Other bulk measurement techniques such as nitrogen adsorption measurements [16] and mercury intrusion porosimetry (MIP) [17], when used together, can provide the macro- and micro- porosities of materials. However, the relevance of these bulk porosity measurements to chromatographic column performance is highly uncertain. Gigova [18] showed the difference between pore-size distribution measurements of the same sample by MIP and capillary flow porometry (CFP) and assigned the reason to different principles of measurement employed by the two techniques. MIP was reported to measure a single pore as two different pores, the wider part of the pore being a large pore while the narrowest part being a small pore. Therefore, other techniques capable of measuring porosity and morphology in the column format are preferred over bulk measurement techniques. Inverse size exclusion chromatography (ISEC) [19] has been one such popular technique used to obtain the three-dimensional porosity of columns. Grimes et al.[20] formulated two models, the parallel pore model (PPM) and parallel network model (PNM), to measure ISEC curves, which expanded the amount of information obtained from ISEC. However, the use of tetrahydrofuran as mobile phase has been reported to destroy certain columns [19]. Newer techniques, such as total pore blocking (TPB) [21] and CLSM [22] have also proved helpful in characterizing stationary phase bed structure in the column format. CLSM provides complete three-dimensional macropore morphology of monoliths based on quantitative physical reconstruction of microscopic images. However, it has only been applicable to silica monoliths because of difficulties involved in matching the refractive index of polymeric monoliths with that of silica tubing.

The research group I worked with previously reported the use of CFP for through-pore size characterization in the column format using a home-built capillary flow porometer [23]. CFP is an extrusion method, which detects the presence of through-pores when gas flow through the bed displaces a wetting liquid from the most constricted part of the pores at a specific pressure. Subsequently, the pore diameter can be calculated from the pressure using [24]

$$P = \frac{4\gamma\cos\theta}{d} \tag{2.1}$$

where P is the inlet gas pressure, $\gamma$ is the surface tension of wetting liquid, $\theta$ is the contact angle between wetting liquid and polymer surface, and d is the through-pore diameter.

Other through-pore characteristics, such as mean through-pore size, through-pore size distribution, and gas permeability can be computed based on measurements of differential pressures and flow rates through wet and dry samples [25]. The through-pores are characterized in their actual forms, making CFP an attractive technique.

In this chapter, use of CFP to characterize different organic monolithic columns to determine the effects of synthesis parameters such as porogen ratio, capillary diameter, capillary length and monomer ratio on the porous properties of the monoliths is introduced. SEM was used to measure the skeletal size and to verify the results obtained from CFP for thorough-pore size distribution. The efficiencies of monolithic columns were analyzed as a function of domain size and pore-size distribution.

## 2.2 Experimental

### 2.2.1 Chemicals and reagents

2,2-Dimethoxy-2-phenyl-acetophenone (DMPA), 3-(trimethoxysilyl)propyl methacrylate (TPM), and poly(ethylene glycol) diacrylate (PEGDA, $M_n$ ~ 258) were purchased from Sigma-Aldrich (St. Louis, MO, USA). Analytical reagent grade methanol (Sigma-Aldrich) and ethyl ether (Mallinckrodt Baker, Phillipsburg, NJ, USA) were used as porogens. Toluene and acetone used for capillary pre-treatment were purchased from Mallinckrodt Baker, while ethanol was bought from Decon Labs (King of Prussia, PA, USA). UV transparent fused-silica capillary tubing was purchased from Polymicro Technologies (Phoenix, AZ, USA).

**2.2.2 Sample preparation**

Monoliths were synthesized inside pre-treated UV transparent capillaries. The surface of the capillary was functionalized by flushing the column first with ethanol and HPLC grade water (Sigma-Aldrich). The inner surface was then etched with 1 M NaOH by heating at 120°C for 3 h followed by leaching with 1 M HCl for 3 h at 110°C. Then it was rinsed with water and ethanol and dried with nitrogen at 110°C overnight in a GC oven. Afterwards, a 15% solution of TPM in dry toluene was placed in the capillary overnight at room temperature. After reaction, the capillary was rinsed with toluene and acetone and dried with nitrogen overnight in a GC oven at room temperature [26].

The pre-polymer solution containing PEGDA, $M_n$ ~ 258, methanol and ethyl ether of variable composition and fixed amount of DMPA (1% w/w of monomer), was introduced into the capillary using helium gas pressure. The capillary was then placed under a PRX 1000-20 UV lamp (TAMARACK Scientific, Corona, CA, USA) for 3 min (390 ± 15 nm). After reaction, the capillary column was flushed with methanol and then HPLC grade water using an HPLC pump.

In this work, the monomer (PEGDA) content in the reagent mixture and the porogen ratio (w/w of methanol/ethyl ether) were varied for fabrication of different monoliths to explore their

influence on monolith morphology. Table 2.1 lists the reagent compositions for these different monolithic columns. Polymeric monoliths with 32% monomer and 1.66 porogen ratio were fabricated in 75, 150 and 250 μm i.d. capillary columns to study the effect of inner diameter on pore structure. Monoliths were prepared in different lengths (1.5 cm, 2 cm, and 3 cm) of 150 μm i.d. capillary tubing to study the effect of capillary length on pore structure.

**2.2.3 Scanning electron microscopy**

The morphologies of polymeric monolithic columns were visualized using a scanning electron microscope (FEI Helios Nanolab 600, Hillsboro, OR, USA) under high vacuum after coating with a thin (~10 nm) conducting layer of gold on a small section (0.5 cm) of each capillary column. The images were captured in high or ultra-high resolution mode and were analyzed using Image J software. The images were used for measuring the globule size (20 measurements for each sample) and through-pore size distribution (50 measurements for each sample) for each monolithic column synthesized.

**2.2.4 Capillary flow porometry**

A home-built flow meter reported earlier [23] was used to measure the microflow rates. The wet up/dry down measurement method was applied in this work, which means a wet curve was determined with nitrogen gas pressure increasing, followed by a dry curve with pressure decreasing for every sample. The wet curve was determined first since polymeric monoliths can be sensitive to drying and, if left for drying overnight, the original pore structures of the monoliths could be altered. HPLC grade water (instead of Galwick used previously) was used as the wetting liquid for determining the wet curve. The dry and wet curves obtained for monoliths

**Table 2.1.** Reagent compositions for different monolithic columns.

| Column number* | Percentage of monomer | Porogen ratio | Capillary diameter (μm) | Capillary length (cm) |
|---|---|---|---|---|
| 1 | 32 | 0.60 | 150 | 1.5 |
| 2 | 32 | 1.00 | 150 | 1.5 |
| 3 | 32 | 1.66 | 150 | 1.5 |
| 4 | 25 | 1.00 | 150 | 1.5 |
| 5 | 32 | 1.00 | 150 | 1.5 |
| 6 | 40 | 1.00 | 150 | 1.5 |
| 7 | 32 | 1.66 | 75 | 1.5 |
| 8 | 32 | 1.66 | 150 | 1.5 |
| 9 | 32 | 1.66 | 250 | 1.5 |
| 10 | 32 | 1.00 | 150 | 1.5 |
| 11 | 32 | 1.00 | 150 | 2.0 |
| 12 | 32 | 1.00 | 150 | 3.0 |

* Columns 2, 5 and 10 are the same column. Similarly, columns 3 and 8 are the same column.

using Galwick as a wetting liquid never met at pressures as high as 130 psi for this PEGDA monolith, which could be due to swelling of the monolith with Galwick. The contact angle between the monolith and wetting liquid was measured using a goniometer, and was found to be 23°.

The time required to obtain a stable flow rate was much greater at low pressure than at high pressure because when the gas flow rate was very low, the number of through-pores opened was less than at higher pressures. The wet and dry curves were repeated three times for every parameter varied (i.e., three columns of the same composition were analyzed) and every data point for the dry and wet curves at each set pressure was measured three times to reduce the error in measurement.

From equation 2.1, the though-pore diameter at a particular pressure can be calculated. The pore size distribution was calculated using the relative flow rates from the dry and wet curve measurements using the following equations:

$$\text{Filter flow \% (FF\%)} = 100 \times \frac{\text{wet flow}}{\text{dry flow}} \tag{2.2}$$

$$\text{Incremental filter flow \% } (\Delta\text{FF\%}) = \text{current FF\%} - \text{previous FF\%} \tag{2.3}$$

$$\text{Incremental pore diameter } (\Delta d) = \text{previous diameter} - \text{current diameter} \tag{2.4}$$

$$\text{Pore size distribution} = \frac{\Delta\text{FF\%}}{\Delta d} \tag{2.5}$$

The gas flow rates measured for dry samples were used to compute the gas permeability[23] using Darcy's law using the following equation:

$$F = k \left(\frac{A}{2\mu l P_s}\right) \left(\frac{T_s}{T}\right) (P_i + P_o) (P_i - P_o) \tag{2.6}$$

where F is the flow rate of the inert gas at inlet pressure $P_i$ and measurement temperature T, k is the permeability, μ is the gas viscosity, A is the cross-sectional area of the porous material, l is

the column length, $P_s$ is the standard atmospheric pressure, $P_o$ is the pressure at the column outlet and $T_s$ is the standard temperature (273.15 K).

The results from the porometric measurements were compared with observations of the monolith structure from SEM. The domain size of the monolith structure was determined using globule size measurement from SEM and through-pore size measurement from CFP.

**2.2.5 Data analysis**

The data obtained from each CFP experiment were smoothed statistically by fitting the dry and wet curves to a fourth power polynomial regression, since measurement at each set pressure value was time-dependent and even a small error in one measurement led to a huge error in the final distribution. Moreover, the flow rate of gas through the pores was reported to be a fourth power function of pore diameter [21], explaining the good fit of curves to a fourth polynomial function.

Apart from this, estimation of the pore size distribution is, of course, subject to uncertainty. There are two sources of uncertainty in the measurements here. The first is the measurement uncertainty in actually obtaining the measurements listed in equation 2.5. This uncertainty is specific to the segment of capillary being measured and is generated by the variability in the equipment and in the measurement process. The second source of uncertainty is the actual variation in pore size distributions created by the pore generation process. This uncertainty is observable when distributions at different locations in the capillary are compared. The uncertainty is relevant to assessing the porosity of the capillary. In this work, I estimated the distribution of pore sizes from three different segments of the capillary. The variation in pore size distribution observed at each observation point contains both sources of uncertainty. Consequently, I determined error bars of the average pore size distribution (average across the

three measurements of a capillary at a particular pore diameter) using the observed standard error. Error bars are shown in Figure 2.2C, but not in other figures, for clarity of the images.

### 2.2.6 Efficiency measurements

The capillary liquid chromatography system used for efficiency measurements was an Ultimate 3000 high pressure gradient LC system (Dionex, Sunnyville, CA, USA) equipped with an FLM-3300 nanoflow manager (1:1000 spilt ratio). Monoliths prepared from different pre-polymer compositions were fabricated in 15 cm long capillary columns, and their chromatographic efficiencies were measured using thiourea (2 mg/mL) as analyte and HPLC grade water as mobile phase at a flow rate of 0.2 µL/min.

## 2.3 Results and Discussion

### 2.3.1 Through-pore size characterization

The wet and dry curves for a monolith can be obtained using CFP, which measures the gas flow rate through the wet and dry monolith at specified pressures. CFP measures the most constricted part of the through-pore, which is called the throat pore diameter. Based on the definition of the dry curve, the half dry curve is half of the gas flow rate through the dry sample as a function of differential pressure. The pressure at which the half dry curve intersects the wet curve gives the mean through-pore diameter. Figure 2.1 shows the representative wet, dry and half dry curves obtained for a PEGDA monolith, with 32% monomer and 0.6 porogen ratio, along with the corresponding pore size measurements. Similar curves were plotted for each organic monolithic column listed in Table 2.1 (i.e., monoliths with different pre-polymer compositions or column diameters).

The porous properties of a monolith and its morphology in the past were mainly considered to be a consequence of porogen ratio, amount of monomer and polymerization

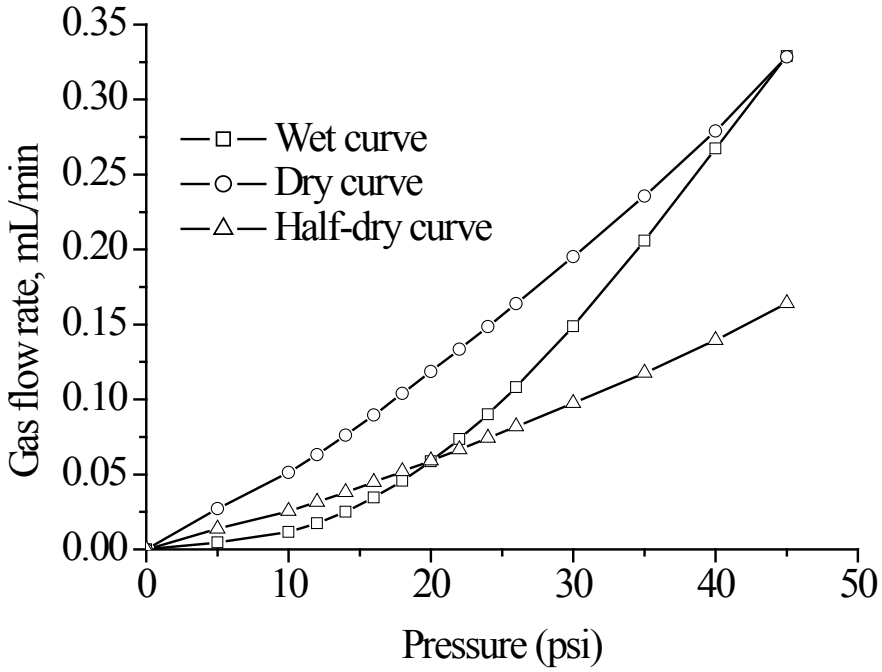


**Figure 2.1.** Wet, dry and half-dry curves for a PEGDA monolith with 32% monomer and 0.6 porogen ratio (Column 1 in Table 2.1).

conditions, while the effect of capillary dimensions (i.e., diameter and length) were not considered to be important. However, the capillary column dimensions for particle packed columns have been reported to have a great influence on column performance [5]. Therefore, they should also have an influence on the morphology and porous properties of monoliths. Therefore, I analyzed the porous properties of PEGDA monolithic columns by CFP for effects of monomer content, porogen ratio and capillary dimensions.

*Effect of Porogen Ratio.* Table 2.2 lists the mean through-pore diameters obtained from CFP of PEGDA monoliths with porogen ratios of 0.60, 1.00 and 1.66. The average values were 1.73, 1.20 and 1.59 μm, respectively. The mean through-pore diameter decreased with increase in porogen ratio (i.e., increase in amount of methanol) from 0.60 to 1.00, but increased thereafter. This indicates that the minimum through-pore size was obtained when equal amounts of methanol and ethyl ether were used as porogen. The permeabilities of the columns also followed the same trend, thereby further verifying this conclusion. Also, the pore size distribution showed a shift toward smaller pore sizes with increase in porogen ratio, as can be seen in Figure 2.2A.

*Effect of Monomer Ratio.* The though-pore diameter and permeability have been reported to decrease with an increase in monomer content as a result of an increase in size of the polymeric skeleton [27]. The increase in monomer concentration leads to more number of nuclei formation on irradiation. When these nuclei compete for monomers, they touch each other before growing to large size. As a result, smaller voids (through-pores) are generated in the microglobular monolithic structure [9]. The same trend was observed from CFP measurements, i.e., the permeability and pore size decreased with increase in percentage of monomer. The cross-over points of the wet and half-dry curves gave mean through-pore diameters of 1.64, 1.20 and

**Table 2.2.** Mean through-pore size diameters and permeabilities determined using CFP for various monoliths.

| Column number | Parameter varied[a] | Mean through-pore diameter (μm)[b] | | | Average | RSD (%) | Permeability (x $10^{-8}$ $m^2$) |
|---|---|---|---|---|---|---|---|
| | | 1 | 2 | 3 | | | |
| | Porogen ratio | | | | | | |
| 1 | 0.60 | 1.62 | 1.62 | 1.94 | 1.73 | 10.86 | 1.24 |
| 2 | 1.00 | 1.11 | 1.11 | 1.39 | 1.20 | 13.43 | 1.19 |
| 3 | 1.66 | 1.79 | 1.49 | 1.49 | 1.59 | 10.68 | 1.20 |
| | Percentage of monomer (%) | | | | | | |
| 4 | 25 | 1.62 | 1.69 | 1.62 | 1.64 | 2.54 | 4.63 |
| 5 | 32 | 1.11 | 1.11 | 1.39 | 1.20 | 13.43 | 1.19 |
| 6 | 40 | 0.79 | 0.83 | 0.79 | 0.80 | 2.78 | 0.04 |
| | Column diameter (μm) | | | | | | |
| 7 | 75 | 3.66 | 3.56 | 3.35 | 3.52 | 4.49 | 1.25 |
| 8 | 150 | 1.79 | 1.49 | 1.49 | 1.59 | 10.68 | 1.20 |
| 9 | 250 | 1.39 | 1.55 | 1.55 | 1.50 | 6.17 | 0.65 |
| | Column length (cm) | | | | | | |
| 10 | 1.5 | 1.11 | 1.11 | 1.39 | 1.20 | 13.43 | - |
| 11 | 2.0 | 1.29 | 1.21 | 1.21 | 1.24 | 3.76 | - |
| 12 | 3.0 | 1.29 | 1.21 | 1.21 | 1.24 | 3.76 | - |

[a] Refer to Table 2.1 for column composition.
[b] Three columns were analyzed for each column listed in Table 2.1.

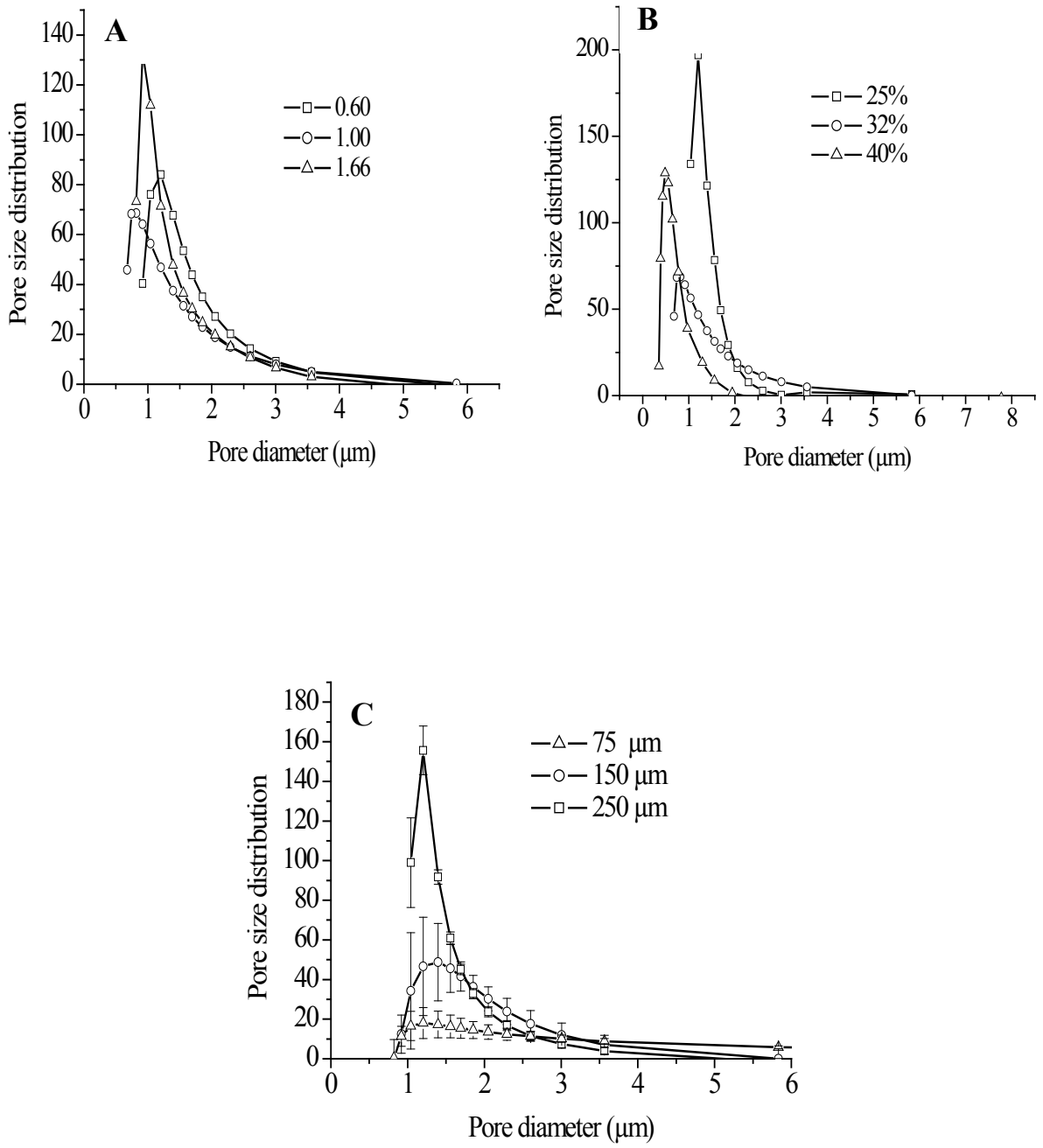


**Figure 2.2.** Through-pore size distributions for organic monolithic capillary columns prepared with (A) different porogen ratios, (B) different percentages of monomer and (C) different capillary diameters.

0.80 for columns listed in Table 2.2. The pore size distribution shifted towards smaller pore diameter with increase in monomer content (Figure 2.2B).

*Effect of Capillary Diameter.* Monolithic columns with inner diameters of 75, 150 and 250 µm exhibited different porous properties and morphologies. CFP measurements showed a decrease in mean through-pore size with increase in capillary diameter (Table 2.2). This could result from chemical reactions occurring in different environments, e.g., different temperature and/or depth of penetration of UV light. In small i.d. columns, light penetrates through the capillary and free radical initiation occurs at a faster rate. Fast initiation increases the overall polymerization rate, promoting early phase separation. As a consequence, the pore size becomes larger [28]. Figure 2.2C shows the through-pore size distributions of columns with different diameters. The monolith prepared in a 250 µm i.d. capillary column had a large number of pores with small diameter, whereas 75 µm i.d. columns had a greater number of larger diameter pores.

*Effect of Length.* The organic monolithic columns had highly interconnected porous structures as verified by the CFP results, which showed the same mean through-pore diameter of 1.24 µm for different lengths of capillary columns (i.e., 1.5, 2.0 and 3.0 cm), as listed in Table 2.2. The through-pore size distribution curves showed similar shape and range, i.e., from 0.64-3.80 µm for all columns. Monoliths were synthesized in different lengths of capillary columns and then the desired lengths were cut from different portions of the columns. Each capillary length was analyzed three times, making certain that replicates were taken from different portions of different capillary columns.

**2.3.2 SEM characterization**

All columns synthesized were also analyzed using SEM for globule size and through-pore size. Several SEM images were captured for the same sample at different points along the

column length and analyzed using Image J software. SEM measurement of through-pore size was accomplished by measuring two orthogonal axes (longest and smallest) of the pore and taking their average as pore diameter. The through-pore size measurements showed the same trends as the CFP measurements for every parameter, i.e., the results of CFP were supported by SEM. The data obtained from SEM images was processed as a histogram and then the histogram was redrawn as a line graph for comparison to CFP measurements. Figure 2.3 shows a comparison of SEM and CFP results for distribution of through-pores for monoliths with porogen ratio of 0.60 and monomer percentage of 32%, prepared in 150 μm i.d. capillary columns (column 1 in Table 2.1). Similar distributions from SEM and CFP measurements also support the uniformity of the pore structure along the column length.

The same SEM images were also used for measuring globule sizes of the monolithic columns. Table 2.3 lists the globule sizes for different monoliths. The domain sizes were calculated using the globule sizes and through-pore size measurements.

**2.3.3 Effect of domain size on efficiency**

The efficiencies (i.e., plate height, H) of monolithic columns have been reported to vary directly with domain size [9]. A decrease in domain size results in a reduced diffusion length for the analyte across the bed structure, thereby decreasing the contribution of the C term in the van Deemter equation, and lowering the H value. A decrease in through-pore size reduces the resistance to mass transfer in the mobile phase, while a decrease in skeleton size decreases the resistance to mass transfer in the stationary phase. Also, narrow through-pore size distribution reduces the eddy diffusion contribution in the van Deemter equation. Therefore, a small domain size and narrow through-pore size distribution should result in an improved efficiency (small H value) of the chromatographic column.

A

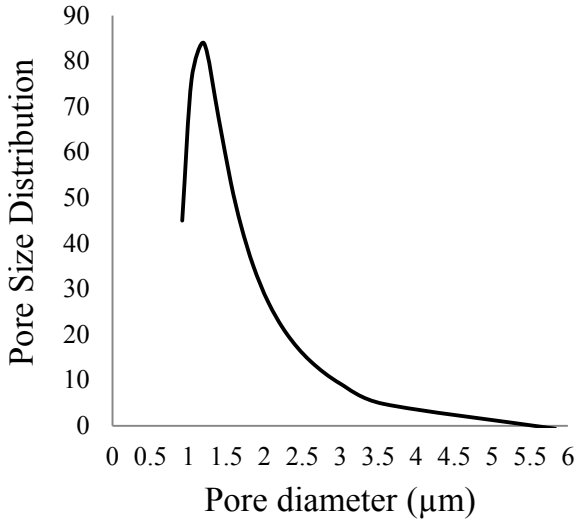


B

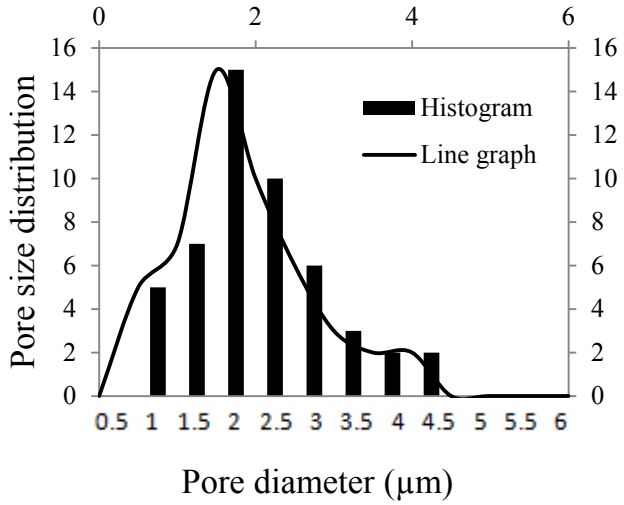


**Figure 2.3.** Pore size distribution for column 1 in Table 2.1 obtained by (A) CFP measurement and (B) SEM measurement in histogram and line graph forms, respectively.

**Table 2.3.** Domain sizes for different monoliths.

| Column number | Parameter varied[a] | Through-pore size (μm) | Globule size (μm)[a] | Domain size (μm)[b] |
|---|---|---|---|---|
| | Porogen ratio | | | |
| 1 | 0.60 | 1.73 | 1.02 | 2.75 |
| 2 | 1.00 | 1.20 | 0.56 | 1.76 |
| 3 | 1.66 | 1.59 | 0.81 | 2.40 |
| | Percentage of monomer (%) | | | |
| 4 | 25 | 1.64 | 0.62 | 2.26 |
| 5 | 32 | 1.20 | 0.56 | 1.76 |
| 6 | 40 | 0.80 | 0.98 | 1.78 |
| | Column diameter (μm) | | | |
| 7 | 75 | 3.52 | 0.69 | 4.21 |
| 8 | 150 | 1.59 | 0.81 | 2.40 |
| 9 | 250 | 1.50 | 0.57 | 2.07 |

[a] Globule size measured from SEM images.
[b] Domain size = globule size + through-pore diameter.

The efficiencies of organic monolithic columns were found to improve (i.e., H value decreased) with an increase in capillary diameter. A 250 μm i.d. column gave a plate height of 88 μm, because the domain size was found to decrease and the through-pore size distribution became narrower with an increase in capillary diameter (Table 2.3). However, the plate height obtained was still high because of the presence of some larger through-pores in this monolithic structure and random distribution of them through the capillary. I believe this plate height can be reduced significantly by decreasing the domain size of the monolithic skeleton and narrowing the through-pore size distribution. Figure 2.4 shows the variation in domain size and efficiency for monoliths prepared in different capillary diameters. The through-pore size decreased with increase in capillary diameter; however, the skeleton size first increased and then decreased. This trend in skeletal size explains the poor performance (i.e., resolution) of PEGDA organic monoliths in 250 μm i.d. columns for size exclusion chromatography [29], due to the reduced number of mesopores in the skeleton.

Figures 2.5 and 2.6 show the variations in domain size and efficiency for monoliths with porogen ratio and percentage of monomer. Among monoliths with different porogen ratio, the monolith with porogen ratio of 1 exhibited the best efficiency (smallest H value), having the smallest mean through-pore size of 1.20 μm and skeletal size of 0.55 μm. Among the monoliths prepared from different amounts of monomers, 25% monomer content gave the best performance and was found to have minimum domain size. The domain size of monoliths with 40% monomer was approximately the same as a monolith with 25% monomer; however, the skeletal size for the former was 0.97 μm compared to 0.55 μm for the latter, thereby leading to an increase in the resistance to mass transfer in the stationary phase for the former. Moreover, with 40% monomer,

A

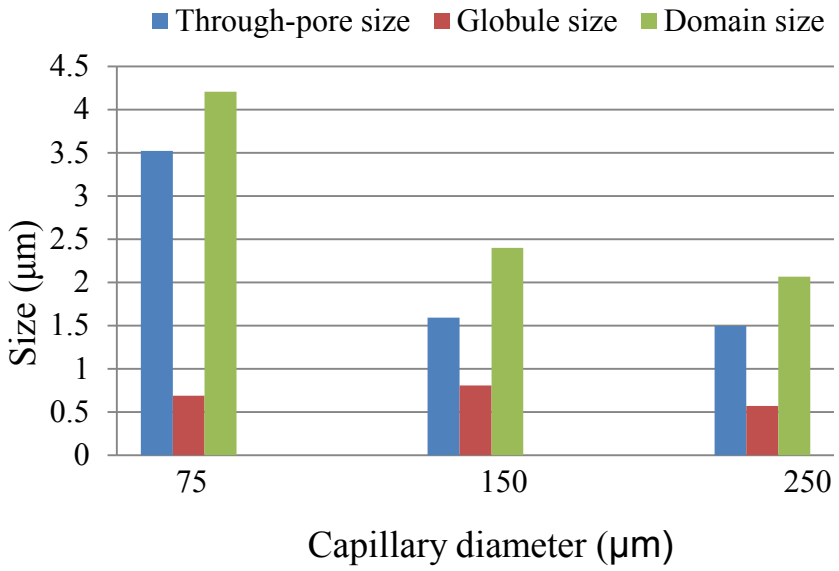


B

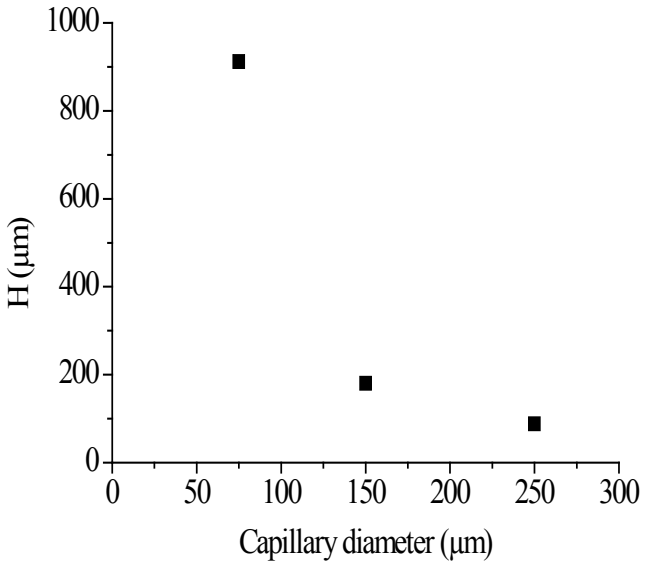


**Figure 2.4.** Effect of capillary diameter on (A) through-pore, globule, and domain sizes and (B) efficiency for monolithic capillary columns.

A

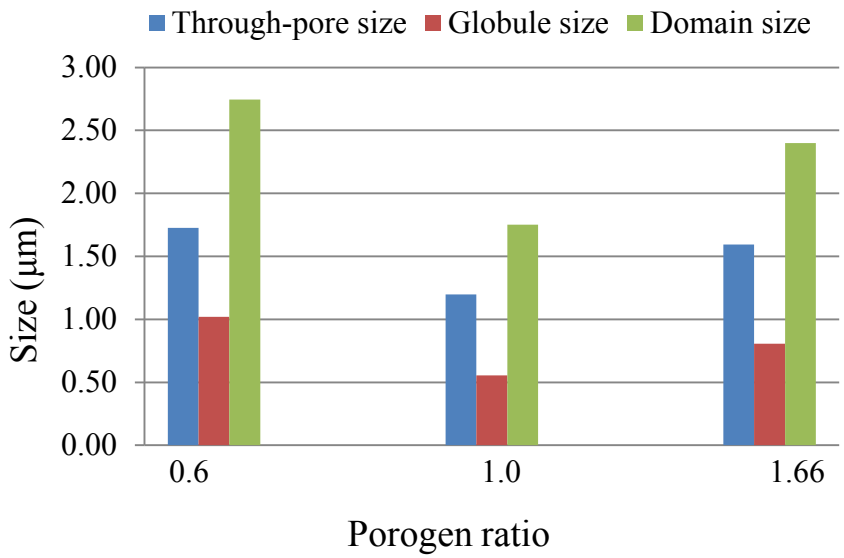


B

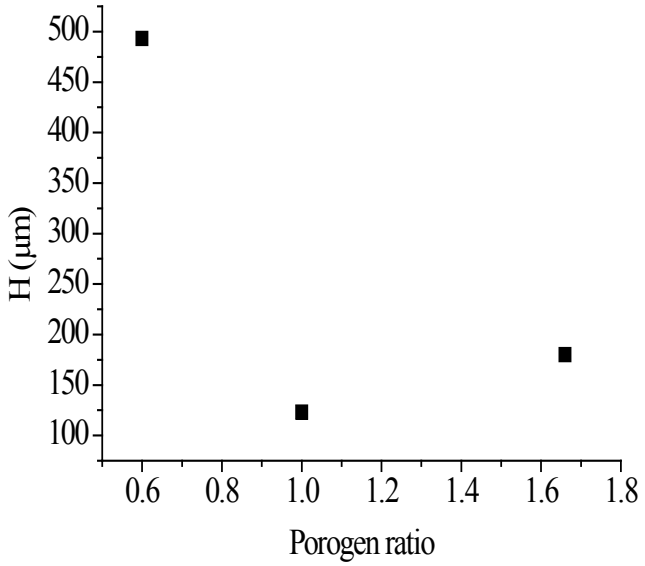


**Figure 2.5.** Effect of porogen ratio on (A) through-pore, globule, and domain sizes and (B) efficiency for monolithic capillary columns.

A

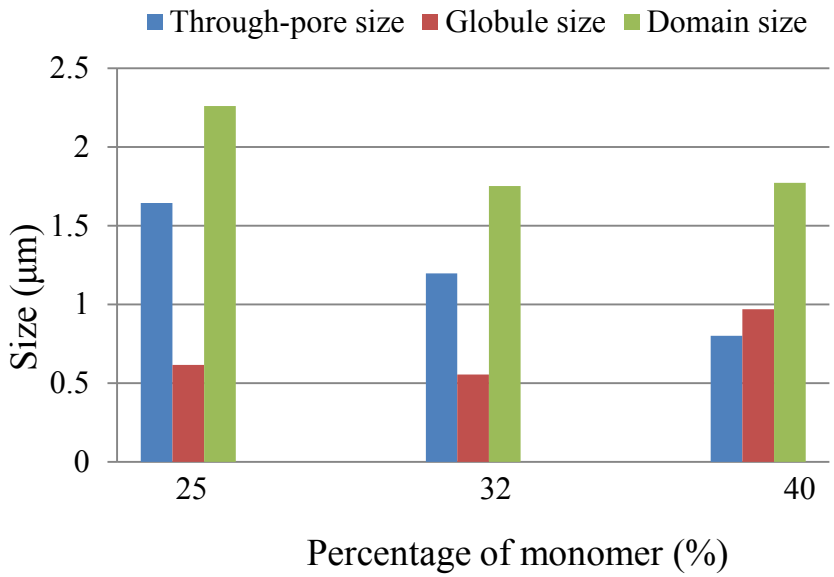


B

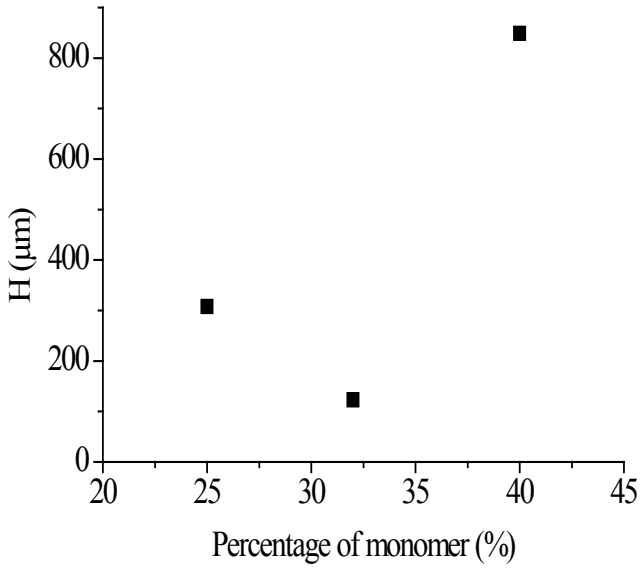


**Figure 2.6.** Effect of percentage of monomer on (A) through-pore, globule, and domain sizes and (B) efficiency for monolithic capillary columns.

the skeletal structure was fused in nature instead of globular (Figure 2.7), further increasing the residence time of solute in the stationary phase and compromising the efficiency.

**2.4 Conclusions**

The effects of capillary diameter, capillary length, porogen ratio and monomer content on morphology and porous properties of PEGDA monoliths were examined using CFP and SEM. Measurements from CFP and SEM were in good agreement for pore size distributions. These results reveal a significant effect of capillary diameter on monolith porosity with through-pore size decreasing from 3.52 to 1.50 μm with an increase in capillary diameter from 75 to 250 μm. The same through-pore size distribution for different lengths of columns verified the presence of highly interconnected through-pores. This emphasizes the need for in-situ characterization techniques for evaluating monolithic capillary columns.

The CFP and SEM analyses provided in-situ measurements, which were used for calculating the domain size and predicting the relative efficiencies of monolithic columns. Columns with narrow through-pore size distribution and small domain size gave the best efficiencies, e.g., a 250 μm i.d column with small domain size gave an H value of 88 μm. These results emphasize the need for narrow through-pore size distribution and small domain size for improving the performance of monolithic columns. In-column characterization techniques can aid in identifying the factors affecting the monolith morphology, which can then be altered to produce a uniform monolithic bed structure with much lower H value (i.e., improved performance).

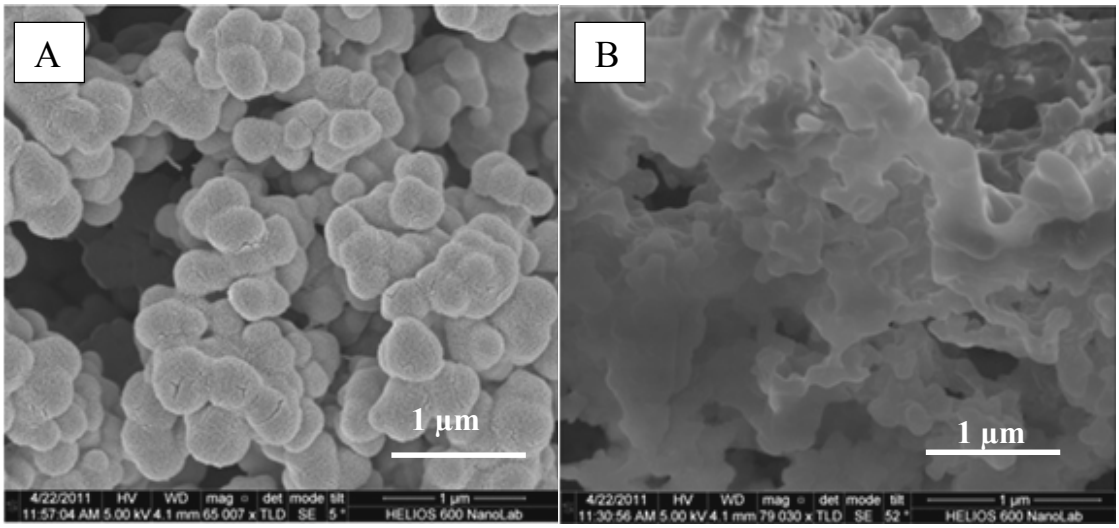


**Figure 2.7.** SEM images for monolithic columns prepared with (A) 25% monomer (B) 40% monomer in the reagent solution.

## 2.5 References


1. Snyder, L. R.; Kirkland, J. J., *Introduction to Modern Liquid Chromatography*. 2nd ed.; John Wiley & Sons: New York, **1979**.
2. McGuffin, V. L.; Novotny, M., *J. Chromatogr. A* **1983,** *255*, 381-393.
3. Knox, J. H.; Saleem, M., *J. Chromatogr. Sci.* **1969,** *7*, 614-622.
4. Caulkin, R.; Jia, X.; Fairweather, M.; Williams, R. A., *Particuology* **2008,** *6*, 404-411.
5. Lottes, F.; Arlt, W.; Minceva, M.; Stenby, E. H., *J. Chromatogr. A* **2009,** *1216*, 5687-5695.
6. Knox, J. H., *J. Chromatogr. A* **2002,** *960*, 7-18.
7. Billen, J.; Gzil, P.; Vervoort, N.; Baron, G. V.; Desmet, G., *J. Chromatogr. A* **2005,** *1073*, 53-61.
8. Kennedy, R. T.; Jorgenson, J. W., *Anal. Chem.* **1989,** *61*, 1128-1135.
9. Li, Y.; Aggarwal, P.; Tolley, H. D.; Lee, M. L., *Advances in Chromatography*. CRC Press: Connecticut, 2012; Vol. 50, Chapter 5.
10. Hlushkou, D.; Bruns, S.; Seidel-Morgenstern, A.; Tallarek, U., *J. Sep. Sci.* **2011,** *34*, 2026-2037.
11. Thommes, M.; Skudas, R.; Unger, K. K.; Lubda, D., *J. Chromatogr. A* **2008,** *1191*, 57-66.
12. Hara, T.; Kobayashi, H.; Ikegami, T.; Nakanishi, K.; Tanaka, N., *Anal. Chem.* **2006,** *78*, 7632-7642.
13. Liang, C.; Dai, S.; Guiochon, G., *Anal. Chem.* **2003,** *75*, 4904-4912.
14. Morgan, A. B.; Gilman, J. W., *J. Appl. Polym. Sci.* **2003,** *87*, 1329-1338.
15. Courtois, J.; Szumski, M.; Georgsson, F.; Irgum, K., *Anal. Chem.* **2006,** *79*, 335-344.

16. Oxelbark, J.; Legido-Quigley, C.; Aureliano, C. S. A.; Titirici, M.-M.; Schillinger, E.; Sellergren, B.; Courtois, J.; Irgum, K.; Dambies, L.; Cormack, P. A. G.; Sherrington, D. C.; De Lorenzi, E., *J. Chromatogr. A* **2007,** *1160*, 215-226.

17. Salmas, C.; Androutsopoulos, G., *J. Colloid Interface Sci.* **2001,** *239*, 178-189.

18. Gigova, A., *J. Power Sources* **2006,** *158*, 1054-1061.

19. Lubda, D.; Lindner, W.; Quaglia, M.; Hohenesche, C. d. F. v.; Unger, K. K., *J. Chromatogr. A* **2005,** *1083*, 14-22.

20. Grimes, B. A.; Skudas, R.; Unger, K. K.; Lubda, D., *J. Chromatogr. A* **2007,** *1144*, 14-29.

21. Cabooter, D.; Lynen, F.; Sandra, P.; Desmet, G., *J. Chromatogr. A* **2007,** *1157*, 131-141.

22. Hlushkou, D.; Bruns, S.; Tallarek, U., *J. Chromatogr. A* **2010,** *1217*, 3674-3682.

23. Fang, Y.; Tolley, H. D.; Lee, M. L., *J. Chromatogr. A* **2010,** *1217*, 6405-6412.

24. V. Gupta; Jena, A., *Adv. Flitr. Sep. Technol.* **1999,** *13b*, 833-844.

25. Jena, A.; Gupta, K., *Chem. Eng. Technol.* **2010,** *33*, 1241-1250.

26. Gu, B.; Li, Y.; Lee, M. L., *Anal. Chem.* **2007,** *79*, 5848-5855.

27. Trojer, L.; Bisjak, C. P.; Wieder, W.; Bonn, G. K., *J. Chromatogr. A* **2009,** *1216*, 6303-6309.

28. Viklund, C.; Svec, F.; Fréchet, J. M. J.; Irgum, K., *Chem. Mater.* **1996,** *8*, 744-750.

29. Li, Y.; Tolley, H. D.; Lee, M. L., *Anal. Chem.* **2009,** *81*, 4406-4413.

# CHAPTER 3 CORRELATION OF CHROMATOGRAPHIC PERFORMANCE WITH MORPHOLOGICAL FEATURES OF ORGANIC POLYMER MONOLITHS*

## 3.1 Introduction

Organic monolithic stationary phases offer broad chromatographic selectivity, high porosity, and independent optimization of through-pore and skeleton sizes in LC [1-6]. However, the chromatographic performance of these organic monoliths has generally not reached the level of particle packed columns, particularly for small molecules, which can be attributed to large average through-pore size, random (heterogeneous) spatial through-pore distribution, variable through-pore geometry (tortuosity), and inconsistent skeletal lattice and pore dimensions along the column length (axial heterogeneity) and across the column diameter (radial heterogeneity) [1,2,5,7,8]. These structural features, inherent in monoliths because of the nature of their fabrication processes cause significant band broadening along a column, which can be explained in terms of the classical van Deemter coefficients. The variable through-pore geometry (i.e., tortuosity) can be related to the B-term, while the other structural features contribute to eddy dispersion (A-term of the van Deemter equation) because of the mobile phase flow velocity inequalities within the column [7]. Giddings divided the contributions of these flow velocity inequalities into categories of trans-skeleton, trans-channel, inter-channel and trans-column, depending on their magnitudes in time and length [9]. The trans-skeleton and trans-channel velocity biases were directly related to average skeleton thickness and macropore size, respectively. The inter-channel velocity bias was reported to be governed by the heterogeneity of the pore space, while the trans-column bias was related to the radial heterogeneity of the monolith. All of these relationships were initially reported for particle packed columns [10], which were then extended to silica monoliths [7,9,11,12]. However, information about

*This chapter was largely reproduced from: Aggarwal, P.; Asthana V.; Lawson, J. S.; Tolley, H. D.; Wheeler, H. D.; Mazzeo, B. A.; Lee, M.L. *J. Chromatogr. A* **2014,** *1334*, 20-29.

morphology-transport relationships, which is essential for improving the material properties of any porous medium [13], is very limited for organic monoliths [1]. The ability to correlate measurements of chromatographic efficiency to qualitative and quantitative descriptors of monolith bed morphology would greatly aid in structure-directed optimization of synthetic methods.

A number of characterization methods, stated in Section 2.1, have provided limited descriptors of monolith morphology (i.e., pore size and pore size distribution) with no information about the skeletal dimensions and bed uniformity across the column radius. Moreover, the relevance of these bulk measurements to chromatographic column performance has proven to be highly speculative because of poor correlation between measurements of bulk samples and monoliths confined in capillaries [14,15]. The work with capillary flow porometry (CFP) [16,17] in Chapter 2 verifies the need for in-column measurements. Three-dimensional reconstructions of monoliths would provide useful insights into their formation, and aid in establishing morphology-performance relationships for organic monoliths in terms of van Deemter coefficients.

Therefore, researchers have developed a small number of in situ characterization techniques, such as SEM [18], TEM [19], ISEC [20], TPB [21], Donnan-exclusion method [22] capacitively-coupled contactless conductivity detection ($C^4D$) [23] and CLSM [24,25] for analyzing stationary phase bed structures in the column format, several of which are capable of providing three-dimensional (3D) information. However, the use of organic solvents as mobile phase or pore blocking agents in ISEC and TPB, respectively, may alter the morphology of certain organic monoliths, compromising their 3D characterization [19,20]. $C^4D$ allows rapid scanning of heterogeneities along the column length; however, it fails to detect radial

heterogeneity, and the information available is insufficient for 3D reconstruction [11]. CLSM has proven to provide 3D structural information about silica monoliths; however, the refractive index mismatch between the capillary wall and polymeric monoliths has limited its application in characterization of organic polymer monoliths. Two-dimensional (2D) SEM has long been used for obtaining structural information about monolith morphology [18], membrane filters [26] and biological samples [27], however, in only one geometric plane. The same information can be obtained in all three (x, y and z) dimensions by serial sectioning and imaging of many cross-sections using dual-beam SEM with subsequent image processing [28-32]. There have been several attempts at extending the application of these 2D characterization techniques (TEM and SEM) to polymeric monolith morphology [19], the most recent being the work of Tallarek et al. [33]. These authors used serial block-face scanning electron microscopy to analyze the solvated structures of hyper-crosslinked poly(styrene-divinylbenzene) monoliths within capillary columns. However, the procedure involves adsorption of the staining agent on the monolith being characterized. The extent of this adsorption differs for different monoliths, thus requiring optimization of the staining agent concentration to achieve the desired contrast in the images.

In this chapter, a slice-and-view procedure using a dual-beam focused ion beam-SEM (DB FIB/SEM) was developed for 3D characterization of PEGDA monolith morphology. The images collected were used to reconstruct the sample volume; also, chord length distributions (CLD) representing pore sizes, radial homogeneities, and porosities [15,19,25] were derived. These 3D data sets were further utilized to compute pore space tortuosity in all three spatial directions. The results of these computational predictions were verified using experimental techniques based on measurement of ionic transport properties of electrolyte filled in the pore space. The information derived from these techniques was used to compare morphological

differences between chromatographic columns as well as areas located spatially at different locations within the same capillary column. These quantitative measurements of morphological differences aided in identifying the factors affecting the chromatographic performance of these columns.

## 3.2 Experimental

### 3.2.1 Chemicals and reagents

2,2-Dimethoxy-2-phenyl-acetophenone (DMPA), 3-(trimethoxysilyl)propyl methacrylate (TPM), and poly(ethylene glycol) diacrylate (PEGDA, $M_n \sim 700$) were purchased from Sigma-Aldrich (St. Louis, MO, USA). Analytical reagent grade 2-propanol (Mallinckrodt Baker, Phillipsburg, NJ, USA) and hexanes (Fischer Scientific, Fair Lawn, NJ, USA) were used as porogens. Tergitol 15-S-20, a surfactant also used as a porogen, came from Dow Chemical, Midland, MI, USA. UV transparent fused-silica capillary tubing was purchased from Polymicro Technologies (Phoenix, AZ, USA). LR white resin (medium grade) came from Ted Pella, Redding, CA, USA, and the staining agent, lead II methacrylate, came from Gelest, Morrisville, PA, USA.

### 3.2.2 Monolith fabrication

Monoliths were fabricated inside pretreated UV transparent Teflon coated capillaries. The inner surface of the capillary was functionalized with TPM following the procedure described in Section 2.2.2. The pre-polymer solution containing monomer (PEGDA, $M_n \sim 700$), porogens (hexane, isopropanol and tergitol 15-S-20) of variable composition, and a fixed amount of DMPA (1% w/w of monomer) was introduced into the surface treated capillary using helium gas pressure. The capillary was then placed under a PRX 1000-20 UV lamp (TAMARACK Scientific, Corona, CA) for 3 min (390 ± 15 nm). After polymerization, the capillary column was

flushed with methanol and then HPLC grade water using an HPLC pump. The two columns selected (i.e., C1 and C2) for characterization (see Section 3.3.1) differed in chromatographic performance. They both had the same capillary dimensions (i.e., ~15 cm long and 150 μm diameter) and contained the same pre-polymer constituents. Table 3.1 lists the reagent compositions, column dimensions and column efficiencies for these different monolithic columns. A van Deemter curve was plotted for each column using thiourea (0.2 mg/mL) as analyte and HPLC grade water as mobile phase (Figure 3.1). The capillary LC system used for efficiency measurements was an Ultimate 3000 high-pressure gradient LC system (Dionex, Sunnyville, CA) equipped with an FLM-3300 nanoflow manager (1:1000 split ratio).

**3.2.3 Sample preparation for SEM**

A 4 % (w/w) solution of lead methacrylate (staining agent) was made in LR white (medium grade) resin by sonicating the mixture for 20 min, making sure there were no visible air bubbles in the solution. The fabricated PEGDA columns were flushed with ethanol-water mixtures having successively higher ethanol concentrations (i.e., 30 %, 50 %, 70 % and 95 %, w/w), followed by flushing with an equi-portion mixture of stained resin and 95 % (w/w) ethanol/water. Finally, the columns were filled with the stained resin using a syringe pump, followed by thermal polymerization of the resin inside the column at 55 °C in an oven. The columns were observed to be completely filled and polymerized (Figures 3.2C and 3.2D). The column was cut into short lengths (i.e., 0.5-1 cm) and mounted on an SEM stub; the capillary ends were then gold coated (10 nm) to overcome sample charging during SEM.

**Table 3.1.** Column performance, specifications and reagent compositions for different monolithic columns.

| Specifications | Column 1 (C1) | Column 2 (C2) |
|---|---|---|
| Percentage of monomer | 20 | 30 |
| Porogen ratio[a] | 2.81 | 0.96 |
| Percentage of tergitol | 35 | 25 |
| Column length (cm) | 14.7 | 14.5 |
| Column diameter (µm) | 150 | 150 |
| Back pressure (MPa)/(psi) | 2.41/350 | 9.99/1,450 |
| $H_{min}$(µm) [b] | 19.5 | 15.3 |
| A (µm) [b] | 6.95 | 6.12 |
| B (x $10^3$ $\mu m^2/s$ ) [b] | 1.43 | 0.96 |
| C (x $10^{-2}$ s) [b] | 2.79 | 2.21 |
| Column porosity ($\varepsilon_{ext}$) [c] | 0.65 | 0.49 |

[a] Porogen ratio = w/w ratio of isopropanol/hexane
[b] Measured using non-retained compound thiourea
[c] Measured using thyroglobulin as large biomolecule

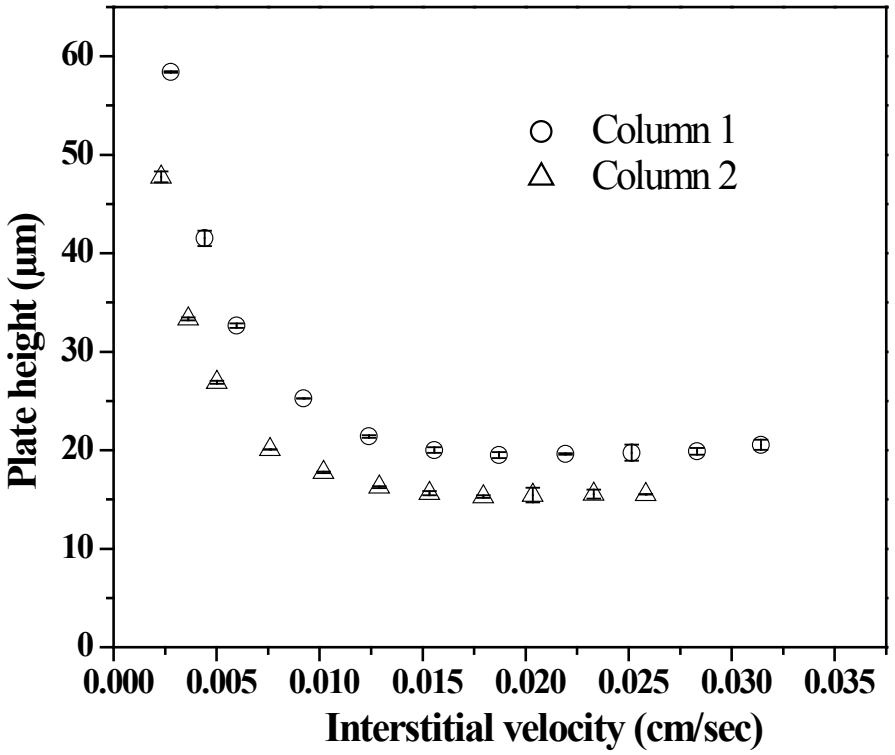


**Figure 3.1.** Plots of plate height (H) vs linear velocity using thiourea as an non-retained compound for two monolithic columns prepared using the same reagents and procedure. Error bars include the total range in values from three repetitive measurements.

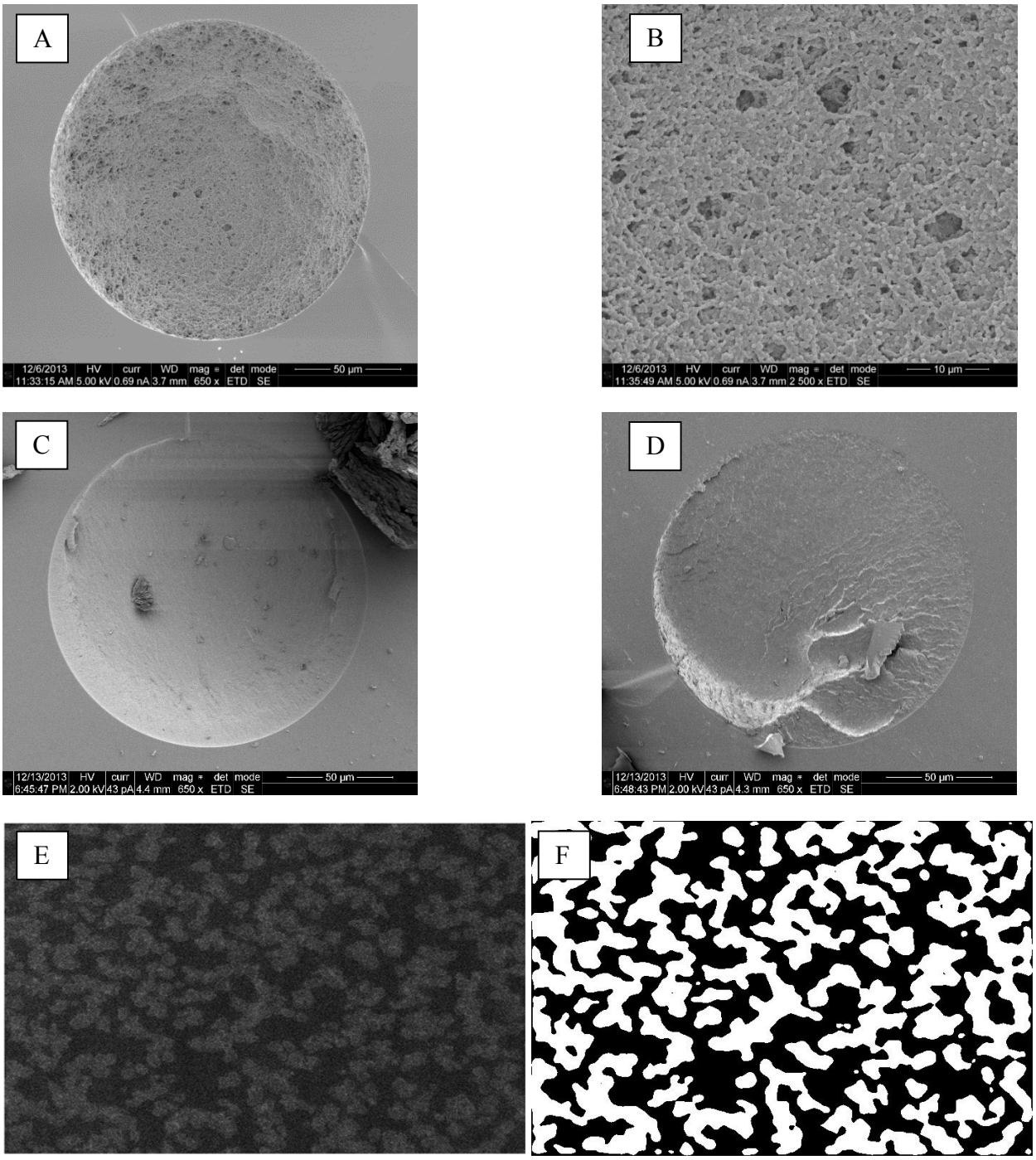


**Figure 3.2.** SEM images of (A) column 1; (B) column 1 at higher magnification, which shows a fused morphology; (C) monolith-free capillary filled with stained LR white solution; (D) column 1 embeded with LR white; (E) raw SEM image taken in the back-scattered electron mode; and (F) binary image after noise removal and Otsu's thresholding.

### 3.2.4 Image acquisition and processing

Image acquisition was performed using a Helios dual-beam SEM. A trough (~50×50×25 μm) was created and subsequently sectioned (100 nm slice thickness) along the z-axis using a gallium ion beam. A backscattered electron image of 1024 x 884 pixels with a pixel size of 35.3 x 44.8 $nm^2$ was acquired. The collected images were cropped to eliminate the poorly illuminated dark area at the bottom of the trough and to select the desired area, thereby yielding a sample size of 24.7 x 21.7 x 10.00 $\mu m^3$. The images were acquired in backscatter electron mode with a beam energy of 2 kV and probe current of 0.69 nA, at a working distance of 4.1 mm and tilt angle of 52°. The acquired SEM images are compressed along the Y axis because of imaging at a tilted angle. The actual length of the cross section was obtained by dividing the compressed pixel length along the Y axis with the sine of the tilt angle [34]. The images collected were then processed using an in-house written MATLAB program. I applied four consecutive processing steps to convert the gray-scale images to binary images (solid skeleton and void spaces): (1) median filter and wiener filter (with kernel size 6 x 3) to remove the grainy noise while preserving the edges of the pore structure, (2) open filter (with disc radius of 30 pixels) to remove the non-homogenous illumination from the images [35], (3) Gaussian filter and histogram equalization to remove noise in the images and enhance the contrast, respectively, and (4) Otsu's thresholding to make the images binary for segmentation, giving the best visual match between binary and raw images (Figures 3.2E and 3.2F). These binary images (100 in number) were stacked to represent a 3D structure for each sample (Figure 3.3). Images were collected for four sample sets (C1C, C1E, C2C and C2E), with two sample sets from each column (C1 and C2). The letters E and C represent the edge and center of the columns, respectively.

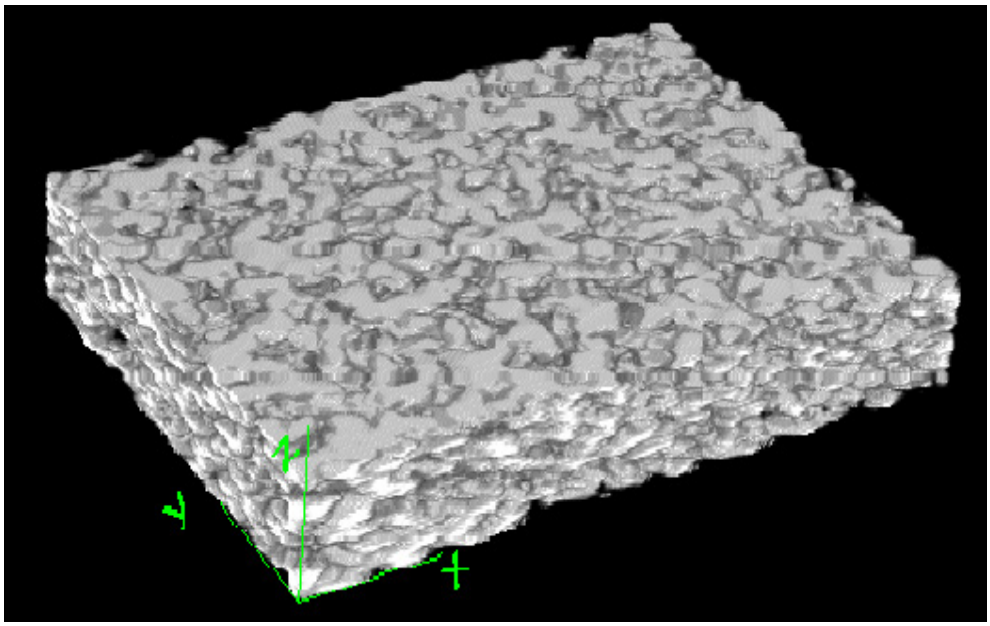

**Figure 3.3.** Volume rendered 3D representation of the reconstructed PEGDA monolith. The white areas represent pores, while the black areas represent the monolithic skeleton.

### 3.2.5 Data acquisition and analysis

To extract quantitative morphological information from the segmented image stack, chords were generated by randomly (but uniformly) choosing points in the void space. Uniformity in selecting points was achieved by dividing the image into grids and then randomly selecting a point within each grid. Vectors were then projected from these points at an equi-spaced angle until they hit the monolith skeleton or the boundaries of the image. The distance spanned by a vector pair at 180º was designated as a chord length. Any chord touching the image boundary at either end was censored, since its actual length would be longer than the measured value. The total number of chords drawn were 5 x 55 x 100 (27,500 chords) for each data set. The number of points selected and the number of chords drawn were determined such that a stable representation of the statistical distribution was obtained (i.e., small standard error). The mean of these measured chord lengths was used to represent the average pore size ($\mu$), while the distribution range represented the bed heterogeneity (described as the non-parametric homogeneity factor, $\kappa$) along the column radius. The non-parametric estimates of the mean and homogeneity factor were determined for the combined censored and un-censored data. Also, the column porosity was calculated for each image as the ratio of number of white pixels to total number of pixels [36], and the average of 100 images was used to represent the porosity of the entire column. The standard deviation of the porosities was calculated by first fitting an autoregressive moving average model to determine the existence of any correlation between successive image slices [37]. Resulting estimates were compared with estimates of the standard deviation made assuming no correlation.

### 3.2.6 Tortuosity determination

Both experimental and computational modeling methods were used to determine the tortuosities of monolithic columns [38,39]. A current-controlled AC impedance experiment was performed by applying an alternating current axially across the monolithic column filled with electrolyte solution (20 % w/w NaCl) and measuring the electrical impedance (i.e., resistance and capacitance) of the column. The frequency of the AC signal was varied from 100 Hz to 10 MHz using a precision impedance analyzer (4294A) from Agilent Technologies. From this measured impedance, the column resistance was calculated based on a parasitic capacitance model in an intermediate frequency range (i.e., 0.1 to 10 kHz) using an in-house written MATLAB program. The resistance values were measured for three different capillary lengths (3, 5 and 7 cm) to ensure that the measured value was not a function of capillary length. Since the concentration in an AC impedance measurement is effectively constant at intermediate frequencies in the kHz range, the effective conductivity of the electrolyte can be directly related to the measured resistance per unit length ($\Delta R/\Delta L$) by

$$k_{eff} = \left(\frac{\Delta L}{\Delta R}\right)\left(\frac{1}{A}\right) \tag{3.1}$$

where $k_{eff}$ is the effective conductivity of the electrolyte-filled monolithic column and A is the column cross-section. Subsequently, the tortuosity of the monolithic column was calculated using the measured $k_{eff}$ value [40]

$$\tau = \left(\frac{k_{electrolyte}}{k_{eff}}\right)\varepsilon = \frac{\varepsilon}{K} \tag{3.2}$$

where K is the relative conductivity, $\tau$ is the tortuosity, $\varepsilon$ is the porosity of the monolith, and $k_{electrolyte}$ is the conductivity of the NaCl solution, which was measured by repeating the above

experiment with a monolith-free capillary filled with NaCl solution. The $k_{electrolyte}$ was found to be 187.2 mS/cm, which was within 1.5 % of the bulk conductivity measurement.

The experimental measurements were verified using computational predictions of tortuosity conducted on the binary images computed for both monolithic columns. An in-house written Fortran code was used to compute K in each direction for the collected 3D structures. These in turn were used to derive the tortuosity values for the pore space in three different axial directions [41]. The K value of an ion through the monolith (in three axial directions) at the applied potential ($\Phi$) was computed based on the differential version of Ohm's law and the principle of conservation of current using

$$0 = \nabla \cdot (K \nabla \varphi) \tag{3.3}$$

The computed relative conductivity was used to determine $\tau_i$ (i.e., the tortuosity in three axial directions) using equation 3.2. The data sets were coarse-grained (with a final voxel size of 141.2 x 179.2 x 100 $nm^3$) so as to give a balance between the computational cost of analysis and the accuracy of the results. Coarse-graining was done with a resampling factor of 0.25, keeping in mind the effect of coarse-graining on measured structural parameters. The same code was also used to compute the porosity values for the monolith, so as to check the effect of coarse-graining on computed parameters.

Some additional computational modeling was conducted to verify whether or not the sample size collected was representative of the entire column. The relative conductivities ($K_x$, $K_y$, and $K_z$) of samples were collected from two different spatial locations in the same column, i.e., edge and center) in order to determine means and standard deviations of $K_x$, $K_y$, and $K_z$. A large virtual column (150 µm diameter, 200 µm length) was constructed with voxels having the same volume as the two experimental samples. Each voxel was given a random conductivity in

each direction from a Gaussian distribution having the same mean and standard deviation as the two experimental samples. An effective column axial conductivity was then calculated using the finite element program COMSOL Multiphysics 3.0. In this way, I extrapolated from the two samples a finite size column to determine the effect of spatial variability on overall conductivity.

### 3.3 Results and discussion

#### 3.3.1 Column selection

The two PEGDA columns in this study were chosen from a larger group of columns that had been fabricated earlier. Initially, 64 different columns were fabricated. These columns were created with various compositions of one monomer and three porogens. The monomer for each column was selected from a list of four potential monomers, and the porogens for each column were selected from a list of twelve potential porogens. The 64 different compositions were chosen as a D-optimal subset of an extreme-vertices mixture design [42], where lower and upper constraints were placed on the amount of each potential monomer and porogen in the mixture. Homogenous monoliths resulted from 44 of the 64 compositions. Logistic regression was used to relate the physico-chemical properties of each composition to the probability of achieving a homogeneous monolith, and a region was identified in the physico-chemical property space that had a high probability of resulting in a homogeneous monolith. Next, chromatographic performances were measured for a subset of the columns that resulted in homogeneous monoliths, plus a few other columns fabricated based on predictions of the Logistic regression model.

Regression analysis was used to model the column performance as a function of the physico-chemical properties of the columns. Monomer viscosity was found to be the most important factor governing column performance. I believe that monomer viscosity governs the

reaction kinetics by affecting the diffusion rate of the propagating radicals in the solution and the time of phase separation. The viscosity of the polymerizing solution has previously been shown to affect the monolith morphology [43]. Moreover, different monomers with different chain lengths further alter the reaction kinetics of polymerization. Although no other physical/chemical properties were found to have as strong a correlation with column performance, there was still considerable variability in column performance among columns prepared from the same monomer. The reason for this variability has yet to be explained. In this study, I investigated two columns prepared from the same monomer and viscosity but different proportions of the monomer and three porogens (2-propanol, hexane and tergitol 15-S-20). This was done to investigate their morphological differences and, hopefully, obtain some insight to help improve the prediction of column performance as a function of physical/chemical properties.

**3.3.2. Column preparation**

Monolithic samples were filled with low viscosity resin (LR white), which was cured before taking SEM images to stabilize the structure and provide depth discrimination during the imaging process. The low viscosity of the resin was an advantage during filling of the monolithic columns using a simple syringe pump; other high viscosity resins, such as Spurrs, were difficult to push inside the column, even with high pressure. The step-wise infiltration of the column (explained in Section 3.2.3) at low flow rate followed by polymerization at low temperature aided in overcoming the cure shrinkage associated with LR white polymerization. This was evident from the SEM micrographs of an empty capillary filled with polymerized LR white resin and a monolithic column embedded with LR white (Figures 3.2C and 3.2D). Slow gradient infiltration of LR white provided effective and continuous filling of pores with low stress on the

monolith structure. Subsequent slow polymerization of the resin because of low polymerization temperature was observed to relieve the effect of LR white shrinkage on the polymeric structure.

In addition to filling the pores, either the monoliths or the pores must be stained to provide contrast between the pores and the monolithic skeleton. Staining using electron-dense agents such as lead, tungsten, osmium or uranium has been reported for this purpose [19,44,45]. Staining has a limitation in that the staining agent must react with the surface of the material in a specific way [19,45], which may influence the morphology of the stained material. Furthermore, since my samples did not contain any ionic groups, I added staining agent to the filling resin (negative staining), giving micrographs with bright pores and dark skeletal structures. experimented with different staining agents, such as tetraphenyl lead and lead methacrylate, as well as several different concentrations of these staining agents, to determine an optimum staining reagent. A 4 % (w/w) solution of lead methacrylate in LR white resin provided a contrast sufficient for assessment of the macropore morphology.

Some sections in the binary images of these samples show the pore space to have a convex structure, contrary to the concave morphology expected for globular monolith morphology. However, SEM micrographs of non-embedded monolithic columns showed a fused morphology in contrast to conventional globular morphology (Figures 3.2A and 3.2B). Such fused morphology has been observed and reported for several diacrylate organic monolithic columns [46,47] in which microglobular structural features have become less distinct or totally eliminated. Therefore, the pore space in a binary image could have either convex or concave features.

### 3.3.3. Column porosity

Monolith porosity was computed for each image slice and plotted as a function of the slice number (representing the distance along the column radius) as shown in Figure 3.4. These individual porosity values were used to calculate the overall porosity of the monolith. The porosity of column 1 was computed to be 0.59 (mean porosity of C1C and C1E) with a standard deviation of 0.005 in comparison to 0.49 for column 2 (mean porosity of C2C and C2E) with a standard deviation of 0.01 (Table 3.2). The higher porosity of column 1 correlates with its lower back pressure of 2.41 MPa in comparison to 9.99 MPa for column 2. Moreover, the measured chromatographic porosity values of 0.65 and 0.49 for column 1 (sample C1C and C1E) and column 2 (sample C2C and C2E), respectively, were found to be in reasonable agreement with the computed values (Table 3.2). The ratios of the measured back pressures for the columns were compared with the pressure drop ratios calculated using the Kozeny-Carman equation

$$\Delta P = \frac{\eta L u_f}{l^2} \frac{(1-\varepsilon_e)^2}{\varepsilon_e^3} \tag{3.4}$$

where $l$ is a scale parameter related to the average size of the through-pores, their distribution and tortuosity [1] as represented by the mean chord length in this work. The external porosity ($\varepsilon_e$) used for calculating the pressure drop was computed from SEM images. The ratio of the measured back pressure was found to be in close agreement (differing by a factor of 1.23) with the ratio of the pressure drops calculated from porosities determined from microscopy images. These results further validate the procedure of image binarization and the fact that the white areas in the images correctly represent the through-pores in the monolithic structure.

I also compared porosities from data sets collected from different spatial locations in the same column. The center sections of both columns (i.e., samples C1C and C2C) were found

A

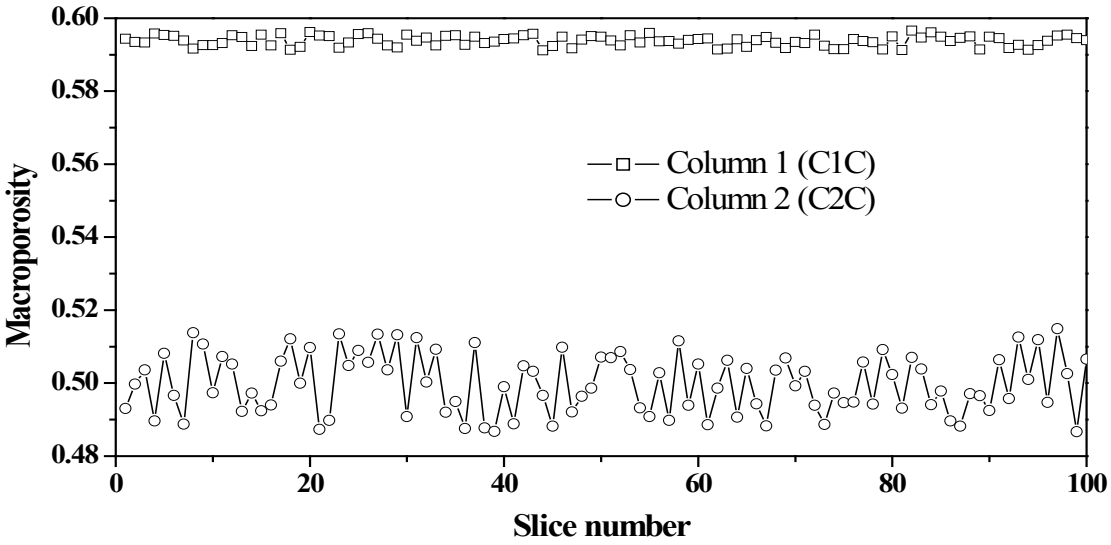


B

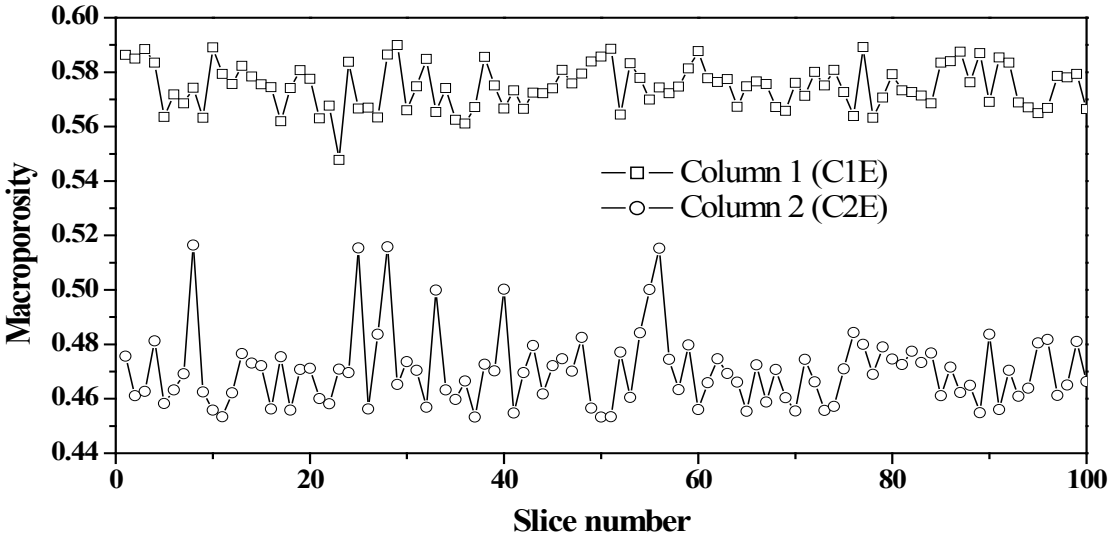


**Figure 3.4.** Macroporosity profiles of reconstructed sample volumes from (A) the centers of two columns, i.e., samples C1C and C2C, and (B) the edges of two columns, i.e., samples C1E and C2E.

**Table 3.2.** Porosities, mean chord lengths and homogeneity factors from 3D SEM analyses of two chromatographic columns.

| Sample[a] | Plate height (μm) | Computed porosity[b] | μ (μm)[c] | σ [d] | Homogeneity factor ( κ ) |
|---|---|---|---|---|---|
| C1C | 19.5 | 0.59 (0.001) | 5.90 (0.08) | 2.54 | 5.39 |
| C1E | 19.5 | 0.58 (0.008) | 5.46 (0.02) | 2.48 | 4.89 |
| C2C | 15.3 | 0.50 (0.008) | 5.23 (0.02) | 2.46 | 4.53 |
| C2E | 15.3 | 0.47(0.01) | 5.16 (0.02) | 2.48 | 4.33 |

[a]Samples C1C and C1E represent the center and edge cross-sections of column 1, respectively, while sample C2C and C2E represent the center and edge cross-sections of column 2.
[b]standard deviations in parenthesis.
[c]μ represents the mean chord length with standard deviation for three repetitive measurement in parenthesis.
[d] standard deviation in mean chord lengths for each repetation.

to have slightly higher porosities in comparison to the edge sections of the columns (Figure 3.4). The standard deviations were higher for the data sets along the capillary wall (i.e., samples C1E and C2E) in comparison to those for data sets from the center (i.e., samples C1C and C2C) of the monoliths (Table 3.2). The slight increase in porosity in moving away from the column wall can be ascribed to faster polymerization at the wall because of higher UV light intensity than at the center. Apart from these different reaction kinetics, pre-functionalization of the inner surface has been reported to produce a dense polymer layer along the capillary wall [48]. Similar trends in macroporosity variation were reported by Tallerek et al. [33] for PS-DVB monoliths.

### 3.3.4. Overall through-pore size and bed heterogeneity

The pore space and degree of heterogeneity of a monolith were characterized in terms of chord length measurements and their distribution, respectively. The mean chord length was based on a significant number of randomly generated linear paths between the pore walls with no assumptions about the pore geometry, and was used to represent the mean through-pore size. I used the non-parametric mean ($\mu$) and standard deviation ($\sigma$) to compute the non-parametric homogeneity factor, kappa ($\kappa$), defined as

$$\kappa = \frac{\mu^2}{\sigma^2} = \left(\frac{1}{CV}\right)^2 \tag{3.5}$$

which is the square of the reciprocal of the coefficient of variation (CV). This formulation of a homogeneity factor is comprable with the k-factor when the chord length distribution follows a gamma distribution. The non-parametric estimates of $\mu$ and $\sigma^2$ were calculated using statistical methods for censored data [49]. Also, Efron's correction was employed when the largest observed chord length was a censored one [50].

I used these non-parametric estimates because the computed chord length distribution (Figure 3.5A) did not follow a gamma distribution. Figure 3.5B gives a Q-Q plot of the data

A

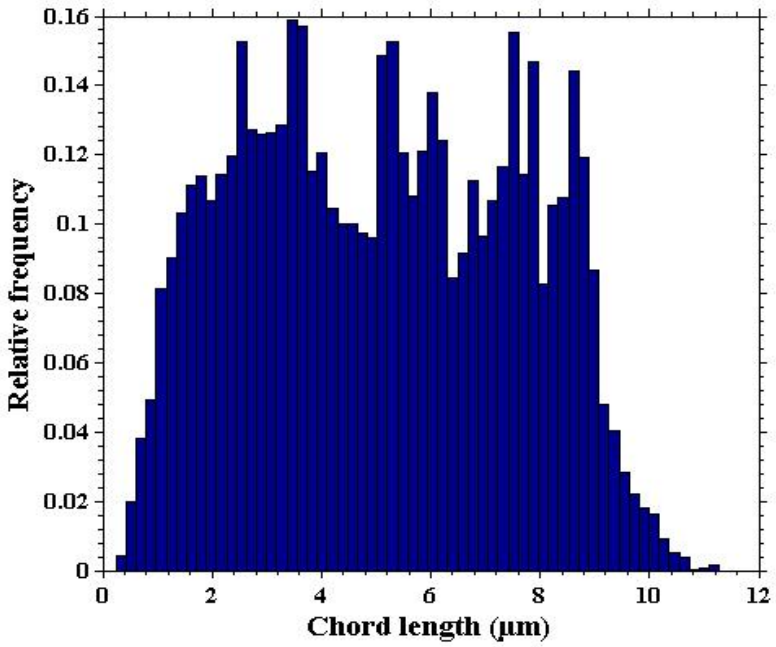


B

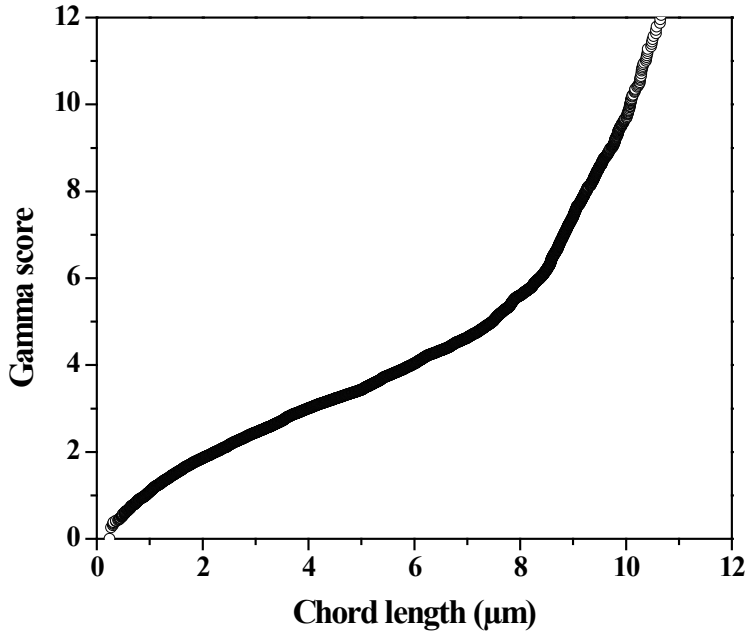


**Figure 3.5.** Plots showing (A) chord length distribution of column C2C, and (B) Q-Q graph of CLD data relative to the quantiles of a gamma distribution.

relative to the quantiles of a gamma distribution. If the data were distributed as a gamma distribution, the plot should have been a straight line. The observed deviation from a straight line is an indication that the data are not distributed as a gamma distribution, but have short tails with too much of the distribution in the "middle." This non-gamma chord distribution may be attributed to the non-conventional fused morphology of these organic monoliths. The sample volume was not found to be a factor responsible for truncating the long chords (making it a non-gamma distribution), since the CLD distribution was found to be similar for two different sample volumes differing by a factor of 7. The sample volume could have been a problem if the censoring would have occurred selectively for the longer chord lengths. However, I observed that the censoring took place randomly for all of the measured lengths and did not selectively truncate the longer chords. Auto-correlation between the measured parameters for different slices could have been another reason for making these distributions appear more homogenous than expected. Therefore, I calculated the correlated standard deviation in porosity for different data sets and compared it with the standard deviation under the assumption of independence. Less than 6 % of the variation in the data can be attributed to correlations in chord length from image to image, thereby making auto-correlation an insignificant contributor towards higher homogeneity factor values.

Column 2 (sample C2C and C2E), which showed better chromatographic performance and higher backpressure, was found to have lower porosity and smaller average pore diameter (mean chord length) in comparison to column 1, represented by sample C1C and C1E (Table 3.2). The SEM results correlate well with the chromatographic performances of the columns and agree well with reports in the literature [51,52]. However, the heterogeneity was found to increase (as the non-parametric homogeneity factor decreased from 5.39 to 4.53) with a decrease

in pore dimensions for both samples of column 2 (i.e., C2C and C2E). Increased heterogeneity of the column associated with a reduction in pore size may hinder further improvements in column performance as explained later in this manuscript [52,53]. Therefore, reducing the dimensions of the monolithic structures should be done while preserving the same structural homogeneity. There have been some reports of fabricating submicron silica monoliths with conserved macropore space homogeneity [54], and the same needs to be done for organic polymer monoliths. The measured mean chord length values for all four samples were found to be accurate with a maximum deviation of only 0.08 μm for three repetitive measurements. The t-test value for samples collected from the same spatial location in the different columns, i.e, center and edge, were found to be 23.59 and 10.47, respectively. These much greater t-test values (>1.96, reference value) indicate that the difference between the calculated mean chord length values and the homogeneity factors for the two columns was statistically significant.

**3.3.5. Radial heterogeneity**

The two columns were also evaluated quantitatively for radial heterogeneity by reconstructing their 3D structures from different spatial locations (i.e., edge and center) of the same column. In both columns, the edge portions (samples C1E and C2E) had smaller pore size and were less homogenous than the center portions of the respective columns (Table 3.2). The difference in homogeneity factor and mean chord length value was again found to be statistically significant with calculated t-test values of 16.03 and 2.72 (in comparison to a reference t value of 1.96) for columns 1 and 2, respectively. High UV light intensity and the presence of a methacrylate layer (due to capillary pretreatment) along the capillary wall caused more rapid polymerization near the wall than at the center of the column, leading to smaller pore size [48]. Moreover, the presence of two types of vinyl bonds, methacrylate bonded to the wall and

monomers bonded to each other in the bulk, led to increased short-range heterogeneity in the monolithic structure near the column wall.

The difference in homogeneity factors for the center and edge portions of column 1 was found to be 0.5 in comparison to 0.2 for column 2. This indicates that column 1 is radially more heterogenous in comparison to column 2. This higher radial heterogeneity can be a significant contributor to the lower chromatographic performance of column 1, and can be correlated with the trans-column velocity bias present along the column radius because of variation in pore size and porosity. This trans-column velocity bias has long been considered to be a contributor to eddy dispersion in the van Deemter equation [55], which was recently reported to behave as a pseudo-C term for capillary columns with low aspect ratio [56].

**3.3.6. Column tortuosity**

The tortuosities for columns 1 and 2 were measured to be 2.34 and 1.50, respectively, using AC impedance experiments (Table 3.3). The tortuosity values were found to be independent of column length since the resistances measured for different column lengths gave a linear relationship (Figure 3.6). This shows that, for these columns, the tortuosity measured in one section of the column is a good representation of the entire column.

The tortuosity values for both columns were also predicted from relative conductivity values computed using computational modeling, along three different axial directions in the SEM images. The samples were coarse-grained to reduce computational cost, while maintaining relevant structural features. The effect of coarse-graining becomes significant if the resampled voxel size exceeds the relevant length scale of the microstructure, which in this case is pore diameter. Since the resampled voxel size was around 100 times smaller than the computed mean pore diameter in my samples, the effect of coarse-graining can be considered insignificant. This

**Table 3.3.** Monolith tortuosity values from experimental measurements.

| Column number | ΔR/ΔL | $k_{eff}$ | Relative conductivity (K) | Experimental tortuosity ($\tau_y$) |
|---|---|---|---|---|
| 1 | 118.9 | 47.62 | 0.254 | 2.34 |
| 2 | 89.52 | 63.25 | 0.337 | 1.50 |

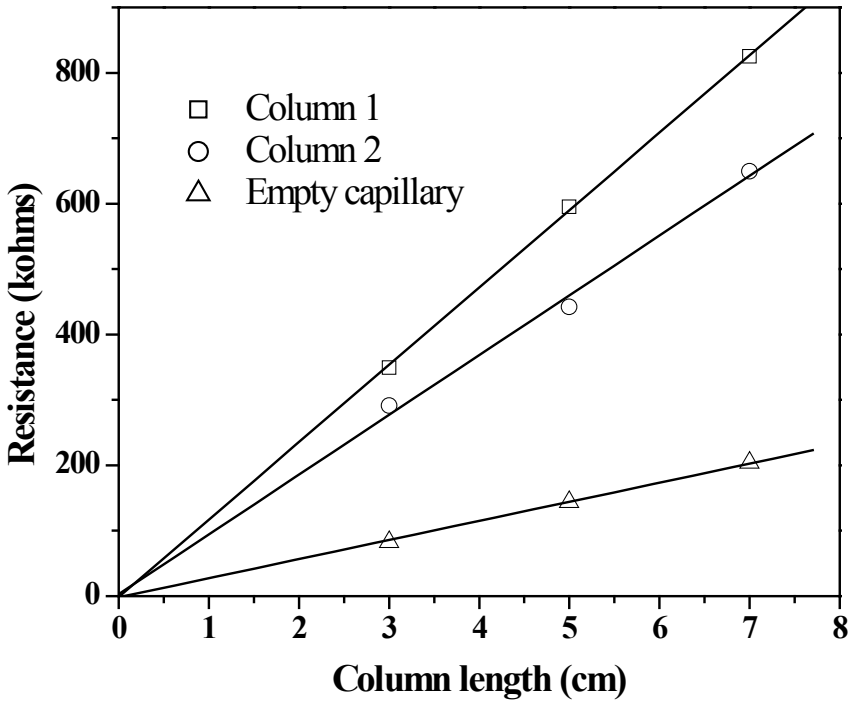


**Figure 3.6.** Plots showing linear relationships between measured resistances and column lengths for two monolithic columns and a monolith-free capillary.

was confirmed when the value of porosity was found to be unaffected by different levels of coarse-graining, similar to reports in the literature [57].

Since, the experimentally determined tortuosity values mainly represent the axial tortuosity ($\tau_y$) of the pore network with minor contributions from the tortuosities along the radial ($\tau_z$) and azimuthal ($\tau_x$) directions; therefore, the experimentally measured values were compared with the computed tortuosity in the axial direction (Table 3.4). The computed axial tortuosity ($\tau_y$) value of 2.32 for column 1 (arithmetic mean tortuosity for samples C1C and C1E) was in excellent agreement with the experimental value of 2.34; however, the computed axial tortuosity value for column 2 was found to be higher than the experimental value (2.13 vs 1.50) by a factor of 1.4. However, the computed values correctly represent the correct trend of lower column tortuosity for column 2 compared to column 1.

As mentioned in Section 3.2.6, additional computation was conducted to determine if the sample size was the limiting factor that caused the mismatch between the measured and computed tortuosity values. The effective axial tortuosity values (i.e., $\tau_y$) computed for reconstructed columns 1 and 2 were found to be 2.27 and 2.09, respectively. These differ from the simple arithmatic mean tortuosity values ($\tau_y$) of 2.34 and 2.13 for the original sample (35.3 x 44.8 x 10 $\mu m^3$) by only 2.1 and 1.8 %, respectively. This verifies that the sample size collected was an adequate 3D representation of the column. The observed difference in the computed and measured tortuosity values for column 2 might alternatively be attributed to issues in the binarization process. I tried to alter the binarization process by modifying the size of noise filters and image thresholding index. The lowest column tortuosity value for column 1 was computed to be 2.01, which is still higher than the measured value. I believe that further investigation is needed to determine the reason for this discrepancy.

**Table 3.4.** Monolith tortuosity values from computational predictions.

| Column number | Sample | Relative conductivity[a] | | | Axial tortuosity ($\tau_y$) | Axial tortuosity ($\tau_y$)[b] |
|---|---|---|---|---|---|---|
| | | $K_x$ | $K_y$ | $K_z$ | | |
| 1 | C1C | 0.274 | 0.248 | 0.279 | 2.37 | 2.32 |
| | C1E | 0.247 | 0.27 | 0.213 | 2.27 | |
| 2 | C2C | 0.221 | 0.217 | 0.177 | 2.22 | 2.13 |
| | C2E | 0.223 | 0.231 | 0.161 | 2.03 | |

[a] $K_x$, $K_y$, and $K_z$ are relative conductivities along azimuthal, axial and radial directions.
[b] arithmetic mean of axial tortuosity of different samples from the same column

### 3.3.7. Correlation of monolith structure with performance

The structural parameters of chord length, homogeneity factor and column tortuosity can be used to diagnose the chromatographic performance of columns in terms of van Deemter coefficients (Table 3.1). A lower monolith porosity and smaller mean chord length indicate the presence of smaller pores in column 2 (samples C2C and C2E), corresponding to lower resistance to mass transfer in the mobile phase. This was verified by a lower C coefficient value of $2.21 \times 10^{-2}$ for column 2 in comparison to $2.79 \times 10^{-2}$ for column 1. Another reason for lower performance of column 1 can be high column tortuosity, which correlates to a higher B-term ($1.43 \times 10^{3}$ in comparison to $0.96 \times 10^{3}$ $\mu m^2/s$) observed for column 1.

Columns with good homogeneity throughout show a squared dependence of efficiency on through-pore size; however, in this particular study, the improvement in performance was not significant. This can be attributed to the short-range heterogeneity or radial heterogeneity in the monolithic structures as observed from the 3D characterization and estimation of non-parametric homogeneity factors. Similar structural heterogeneities have also been reported in silica [58-60] and hybrid monoliths [61], and have been correlated with inter-channel and trans-column eddy dispersions. The relationship of short-range heterogeneity to inter-channel eddy dispersion was determined by calculating the non-parametric homogeneity factors for the two columns. The difference in the non-parametric homogeneity factors of edge and center portions of the same monolithic columns was used to determine the radial heterogeneity of the columns.

Column 2 was expected to have a much higher value for the A coefficient in the van Deemter equation because of the much lower value of non-parametric homogeneity factor. However, the A-term was found to have a value of 6.12 μm for column 2 in comparison to 6.95 μm for column 1. A closer inspection of various factors contributing to the A coefficient, i.e.,

trans-channel, short-range interchannel and transcolumn dispersion, provides an explanation for this. Column 2 should have a much larger short-range interchannel eddy dispersion because of higher short-range heterogeneity. However, the lower trans-channel and trans-column eddy dispersion negates the effect of the former on the overall value of A. This can be a consequence of the fact that smaller pore size corresponds to smaller contribution to eddy dispersion arising from the lateral distribution of velocities within each through-pore (i.e., trans-channel eddy dispersion) and smaller radial heterogeneity.

The combined effects of reduced pore size (i.e., reduced resistance to mass transfer and trans-channel eddy dispersion) and better column tortuosity explain the improved column performance of column 2. However, the increased short-range heterogeneity accompanying a reduction in skeletal dimensions may lead to less improvement in column performance than expected with reduction in skeletal dimensions. The performance of monoliths fabricated from the same pre-polymer constituents and under similar experimental conditions is inherently limited by the nature of the fabrication process or the initiation method. There have been reports of different initiation methods, such as living radical polymerization, that yield more homogenous polymer networks. Living polymerization provides fine control of polymerization dynamics and mechanism which can be used for producing well-defined bicontinuous structures [62,63].

**3.4 Conclusions**

Sample volumes of PEGDA monoliths were characterized quantitatively using dual beam 3D SEM. Morphological parameters, including chord length, homogeneity factor and tortuosity, were correlated to monolith chromatographic performance using quantitative descriptors and van Deemter coefficients. The average through-pore size of column 2, which demonstrated higher

efficiency, was found to be 5.23 μm with a homogeneity factor of 4.53. Chromatographic performance improved with a reduction in through-pore size, column tortuosity and bed porosity. However, reductions in structural dimensions were found to be associated with increased bed heterogeneity, compromising the positive effects of reduced structural dimensions on column performance. The 3D SEM technique described in this chapter aided in identifying and quantifying the existing radial heterogeneity in the monolithic columns.

These results provide useful insights into the process of monolith fabrication, and indicate the importance of reducing the through-pore dimensions with simultaneous improvement in bed homogeneity if improved chromatographic performance is to be achieved. The initiation method was identified as the major source of heterogeneity, since both columns were fabricated using the same pre-polymer constituents. Columns synthesized using different polymerization methods may be able to provide better control over homogeneity of the macropore space [62,63]. This work clearly indicates a need for different, improved methods for polymer synthesis; living polymerization may be a good candidate.

**3.5 References**


[1] Guiochon, G. *J. Chromatogr. A* **2007**, *1168*, 101-168.

[2] Aggarwal, P.; Tolley, H.D.; Lee, M.L. *J. Chromatogr. A* **2012**, *1219*, 1-14.

[3] Unger, K.K.; Skudas, R.; Schulte, M.M. *J. Chromatogr. A* **2008**, *1184*, 393-415.

[4] Svec, F.; Huber, C.G. *Anal. Chem.***2006**, *78*, 2100-2107.

[5] Nordborg, A.; Hilder, E.F.; Haddad, P.R. *Annu. Rev. anal. Chem.* **2011**, *4*, 197-226.

[6] Leinweber, F.C.; Tallarek, U. *J. Chromatogr. A* **2003**, *1006*, 207-228.

[7] Gritti, F.; Guiochon, G. *J. Chromatogr. A* **2009**, *1216*, 4752-4767.

[8] Cabrera, K. *J. Sep. Sci.* **2004**, *27*, 843-852.

[9] J.C. Giddings, Dynamics of Chromatogrpahy, Part 1: Principles and Theory Marcel Deker (**1965**) New York.

[10] Khirevich, S.; Höltzel, A.; S-Morgenstern, A.; Tallarek, U. *Anal. Chem.* **2009,** *81*, 7057-7066.

[11] Hormann, K. ; Müllner, T.; Bruns, S.; Höltzel, A.; Tallarek, U. *J. Chromatogr. A* **2012**, *1222*, 46-58.

[12] Hlushkou, D.; Bruns, S.; Höltzel, A.; Tallarek, U. *Anal. Chem.* **2010,** *82*, 7150-7159.

[13] Gostovic, D.; Vito, N.J.; O'Hara, K.A.; Jones, K.S.; Wachsman, E.D. *J. Am. Ceram. Soc.* **2011**, *94*, 620-627.

[14] Gigova, A. *J. Power Sources* **2006**, *158*, 1054-1061.

[15] Bruns, S.; Müllner, T.; Kollmann, M.; Schachtner, J.; Höltzel, A.; Tallarek, U. *Anal. Chem.* **2010**, *82*, 6569-6675.

[16] Aggarwal, P.; Tolley, H.D.; Lee, M.L. *Anal. Chem.* **2011,** *84*, 247-254.

[17] Fang, Y.; Tolley, H.D.; Lee, M.L. *J. Chromatogr. A* **2010**, *1217*, 6405-6412.

[18] Liang, C.; Dai, S.; Guiochon, G. *Anal. Chem.* **2003**, *75*, 4904-4912.

[19] Courtois, J., Szumski, M.; Georgsson, F.; Irgum, K. *Anal. Chem.* **2007,** *79*, 335-344.

[20] Lubda, D.; Lindner, W.; Quaglia, M.; Hohenesche, C.d.F.v.; Unger, K.K. *J. Chromatogr. A* **2005**, *1083*, 14-22.

[21] Cabooter, D.; Lynen, F.; Sandra, P.; Desmet, G. *J. Chromatogr. A* **2007,** *1157*, 131-141.

[22] Jung, S.; Ehler, S.; Pattky, M.; Tallarek, U. *J. Chromatogr. A* **2010,** *1217*, 696-704.

[23] Connolly, D.; Floris, P.; Paull, B.; Nesterenko, P.N. *TrAC-Trend. Anal. Chem.* **2010**, *29*, 870-884.

[24] Hlushkou, D.; Bruns, S.; Tallarek, U. *J. Chromatogr. A* **2010,** *1217*, 3674-3682.

[25] Bruns, S.; Tallarek, U. *J. Chromatogr. A* **2011,** *1218*, 1849-1860.

[26] Masselin, I.; Durand-Bourlier, L.; Laine, J.-M.; Sizaret, P.-Y.; Chasseray, X.; Lemordant, D. *J. Membr. Sci.* **2001**, *186*, 85-96.

[27] Leser, V.; Drobne, D.; Pipan, Z.; Milani, M.; Tatti, F. *J. Microsc.* **2009**, *233*, 309-319.

[28] Plummer, C.J.G.; Hilborn, J.G. *Polymer* **1995**, *36*, 2485-2489.

[29] Denk, W.; Horstmann, H. *PLoS Biology* **2004**, *2*, 1900-1909.

[30] Young, R.J.; Dingle, T.; Robinson, K.; Pugh, P.J.A. *J. Microsc.* **1993**, *172*, 81-88.

[31] Reingruber, H.; Zankel, A.; Mayrhofer, C.; Poelt, P. *J. Membr. Sci.* **2011**, *372*, 66-74.

[32] Holzer, L.; Indutnyi, F.; Gasser, P.; Munch, B.; Wegmann, M. in, *Wiley-Blackwell*, **2004**, p. 84.

[33] Müllner, T.; Zankel, A.; Mayrhofer, C.; Reingruber, H.; Höltzel, A.; Lv, Y.; Svec, F.; Tallarek, U. *Langmuir* **2012**, *28*, 16733-16737.

[34] Kato, M.; Ito, T.; Aoyama, Y.; Sawa, K.; Kaneko, T.; Kawase, N.; Jinnai, H. *J. Polym. Sci. Part B Polym. Phys.* **2007**, *45*, 677-683.

[35] Russ, J.C. *The Image Processing Handbook*, CRC Press, North Carolina, **1995**.

[36] Courtois, J.; Szumski, M.; Georgsson, F.; Irgum, K. *Anal. Chem.* **2006**, *79*, 335-344.

[37] Box, G.E.P.; Jenkins, G.M.; Reinsel, G.C. *Time Series Analysis Forecasting & Control*, Prentice Hall, New Jersey, **1994**.

[38] Thorat, I.V.; Stephenson, D.E.; Zacharias, N.A.; Zaghib, K.; Harb, J.N.; Wheeler, D.R. *J. Power Sources* **2009**, *188*, 592-600.

[39] Stephenson, D.E.; Walker, B.C.; Skelton, C.B.; Gorzkowski, E.P.; Rowenhorst, D.J.; Wheeler, D.R. *J. Electrochem. Soc.* **2011,** *158*, A781-A789.

[40] Doyle, M.; Newman, J.; Gozdz, A.S.; Schmutz, C.N.; Tarascon, J.M. *J. Electrochem. Soc.* **1996**, *143*, 1890-1903.

[41] Hutzenlaub, T.; Asthana, A.; Becker, J.; Wheeler, D.R.; Zengerle, R.; Thiele, S. *Electrochem. Commun.* **2013**, *27*, 77-80.

[42] Lawson, J. *Design and Analysis of Experiments with SAS*, CRC Press, Boca Raton FL, **2010**.

[43] Aoki, H.; Kubo, T.; Ikegami, T.; Tanaka, N.; Hosoya, K.; Tokuda, D.; Ishizuka, N. *J. Chromatogr. A* **2006**, *1119*, 66-79.

[44] Spurr, A.R. *J. Ultrastruct. Res.* **1969,** *26*, 31-43.

[45] Martin, C.; Coyne, J.; Carta, G. *J. Chromatogr. A* **2005**, *1069*, 43-52.

[46] Li, Y.; Tolley, H. D.; Lee, M. L. *J. Chromatogr. A* **2012**, *1217*, 4934-4945.

[47] Li, Y.; Tolley, H. D.; Lee, M. L. *J. Chromatogr. A* **2012**, *1218*, 1399-1408.

[48] Nischang, I.; Svec, F.; Frechet, J.M.J. *Anal. Chem.* **2009,** *81*, 7390-7396.

[49] Klein, J. P.; Moeschberger, M.L. *Survival Analysis : Techniques for Censored and Truncated Data* **1997** Ney York.

[50] Efron, B. *Proceedings of the Fifth Berkeley Symposium on Mathematical Statistics and Probability* **1997,** *4*, 831.

[51] Minakuchi, H.; Nakanishi, K.; Soga, N.; Ishizuka, N.; Tanaka, N. *J. Chromatogr. A* **1997**, *762*, 135-146.

[52] Altmaier, S.; Cabrera, K. *J. Sep. Sci.* **2008**, *31*, 2551-2559.

[53] Gzil, P.; De Smet, J.; Desmet, G. *J. Sep. Sci.* **2006,** *29*, 1675-1685.

[54] Hormann, K.; Tallarek, U. *J. Chromatogr. A* **2013**, *1312*, 26-36.

[55] Vervoort, N.; Gzil, P.; Baron, G.V.; Desmet, G. *J. Chromatogr. A* **2004**, *1030*, 177-186.

[56] Burns, S.; Grinias, J. P.; Blue, L. E.; Jorgenson, J. W.; Tallarek, U. *Anal. Chem.* **2012,** *84*, 4496-4503.

[57] Hutzenlaub, T.; Becker, J.; Zengerle, R.; Thiele, S. *ECS Electrochem. Lett.* **2012,** *2*, F14-F17.

[58] Minakuchi, H.; Nakanishi, K.; Soga, N.; Ishizuka, N.; Tanaka, N. *J. Chromatogr. A* **1998,** *797*, 121-131.

[59] Kobayashi, H.; Tokuda, D.; Ichimaru, J.; Ikegami, T.; Miyabe, K.; Tanaka, N. *J. Chromatogr. A* **2006**, *1109*, 2-9.

[60] Vervoort, N.; Gzil, P.; Baron, G.V.; Desmet, G. *J. Chromatogr. A* **2004,***1030*, 177-186.

[61] Bruns, S.; Hara, T.; Smarsly, B. M.; Tallarek, U. *J. Chromatogr. A* **2011**, *1218*, 5187-5194.

[62] Kanamori, K.; Hasegawa, J.; Nakanishi, K.; Hanada, T.; Yamango, S. *Macromolecules* **2008**, *41*, 7186-7193.

[63] Hasegawa, J.; Kanamori, K.; Nakanishi, K.; Hanada, T.; Yamango, S. *Macromol. Rapid Commun.* **2009**, *30*, 986-990.

# CHAPTER 4 FLOW RATE DEPENDENT EXTRA-COLUMN VARIANCE FROM INJECTION IN CAPILLARY LIQUID CHROMATOGRAPHY*

## 4.1 Introduction

Over the last 40 years, LC performance has improved significantly by optimizing both column selectivity and efficiency [1-3]. As stated in previous chapters, improvements have been associated with evolution of stationary phase packing materials in areas such as particle synthesis and characterization [4-6], different bonding chemistries [7] and reduction in particle size [8-11]. Reduction in particle size has been accompanied by concomitant decrease in column diameter to alleviate consequences of heat generated in these columns by percolation of mobile phase at high flow rates [12-14]. Reductions in column and particle dimensions result in greatly reduced column volumes and low column permeability. Reduced column volume causes extra-column volumes associated with LC instrumentation to become significant contributors to analyte band dispersion [3,14]. Inherent extra-column band broadening of chromatographic peaks severely limits the separation potential of improved column packing materials.

This issue of extra-column band broadening is well known, and considerable attention has been paid to reduce contributions arising from valves, connecting tubes, sampling devices (injectors), and detector cells [15-18]. The first notable study of extra-column volumes was conducted by Sternberg over 40 years ago, related to gas chromatography [19]. This study provided simple methods for calculating specifications that an instrument should meet, applicable to both GC and LC. Extra-column contributions were grouped into three different categories: (1) axial dispersion of the injection plug in the injection device [20], (2) axial dispersion of the injected band of analyte in any connecting tubing and detector cell [21], and (3) difference between the actual injection profile and the signal provided by the detector.

* This chapter was largely reproduced from: Aggarwal, P.; Liu; K.; Sharma, S.; Lawson, J. S.; Tolley, H. D.; Lee, M.L., submitted.

Guiochon et al. [22-24] carried out numerous studies to theoretically and experimentally characterize extra-column variances arising from different components of an instrument, and compared these contributions for two different commercially available systems. These studies included investigations of injection volume, injection time, sampling technique, diameter of connecting tubes, detector flow cell volume and detector response time. They provided a thorough investigation of all components with mathematical explanations for the observed phenomena. Most studies were conducted using 4.6 to 2.1 mm columns. Suggested methods to reduce this extra-column variance included reducing the sample volume, reducing the internal diameters of the sample loop and connecting capillary tubes, reducing the detector flow cell volume and optimizing the detector response rate [20]. These methods have proven to be useful in reducing extra-column variance; however, with the use of capillary LC columns, these contributions still prove to be significant.

In an effort to minimize extra-column variance, on-column detection with no connecting tubing was used for all experiments, thereby eliminating any extra-column variance associated with factors 2 and 3 stated above. Extra-column variance due to the injection valve was minimized somewhat by optimizing a variety of factors as described in the literature; however, it could not be eliminated [18,25,26]. In the past, extra-column variance due to the injector was described as a constant function of injection volume, with some contributions from valve geometry and mixing inside the valve [22]. However, this has never been fully characterized. Therefore, in this chapter, the injection valve contribution to band-broadening for a commercially available capillary LC system (used in my work) was characterized experimentally, and a new mathematical model was constructed to explain the observed

behavior. The effects of differences in extra-column variance on chromatographic performance for both retained and non-retained compounds were considered.

## 4.2 Experimental

### 4.2.1 Chemicals and reagents

Poly(ethylene glycol) diacrylate (PEGDA, $M_n \sim 700$) was purchased from Sigma-Aldrich (St. Louis, MO, USA). Analytical reagent grade *n*-dodecanol (Acros Organics, NJ, USA), *n*-decanol (Acros) and *n*-decane (Spectrum Chemical, New Burnswick, NJ, USA) were used as porogens. Tergitol 15-S-20, also used as a porogen, was obtained from Dow Chemical, Midland, MI, USA. UV transparent fused-silica capillary tubing was purchased from Polymicro Technologies (Phoenix, AZ, USA). All aqueous solutions and mixed mobile phases were prepared with HPLC-grade water and acetonitrile received from Fischer Scientific (Fair Lawn, NJ, USA). Test analytes included uracil, phenol, resorcinol, catechol and pyrogallol (Sigma-Aldrich). All samples were prepared in appropriate volumes of mobile phase to prevent the appearance of minor peak disturbances.

### 4.2.2 Instrumentation

The LC experiments were performed using an Ultimate 3000 high-pressure gradient LC system [Dionex (now Thermo Scientific), Sunnyville, CA] equipped with an FLM-3300 nanoflow manager (1:1000 split ratio). The injection system was a ten-port injection valve fitted with a zero dead-volume nanoViper (Thermo) sample loop having a volume of 1 μL. The injection valve had a 104 nL groove in the rotor and two connecting bore holes of 116 nL each, making a total swept volume of 336 nL. The swept volume is defined as the total volume in the injector, including the sample loop/groove and connecting bore holes, and is different from the actual volume selected by the sampling valve for introduction into the column. The sample

volume injected in all experiments was 30 nL unless stated otherwise. Time-gated injections were carried out in all experiments with the injection valve being switched at different time intervals as a function of flow rate. On-column detection was accomplished immediately after the monolithic stationary phase at a detection wavelength of 214 nm using a Crystal 100 variable wavelength UV-Vis absorbance detector (Thermo). The detector rise time was set at 1 s (corresponding to a sampling rate of 10 Hz), with a detector sensitivity set at 0.0005 AUFS. Data acquisition was performed with Chrom Perfect software (Mountain View, CA, USA), and all peak analysis was done using Microsoft Excel. Every reported value represents the average of three repetitive measurements under the same conditions. All of the experiments were conducted at room temperature.

A second LC system was used to compare the differences in extra-column variance. This recently reported system consisted of a nano-flow pumping system with integrated injection valve [27]. The integrated 8-port injection valve had an internal 130-nL V-shaped sample loop. Detection was carried using the same Crystal 100 variable wavelength UV detector in the previous paragraph (Figure 4.1).

**4.2.3 Chromatographic column and conditions**

The column used was a PEGDA monolithic capillary column fabricated using UV polymerization as stated in Section 2.2.2. Table 4.1 lists the column dimensions and reagent composition (i.e., amount of monomer, ratio of porogens, etc.) for the monolith. The mobile phase composition used was 98% water in acetonitrile (w/w) for determining the extra-column variance of the injection valve using a non-retained analyte (uracil, 0.2 mg/mL). The mobile

A

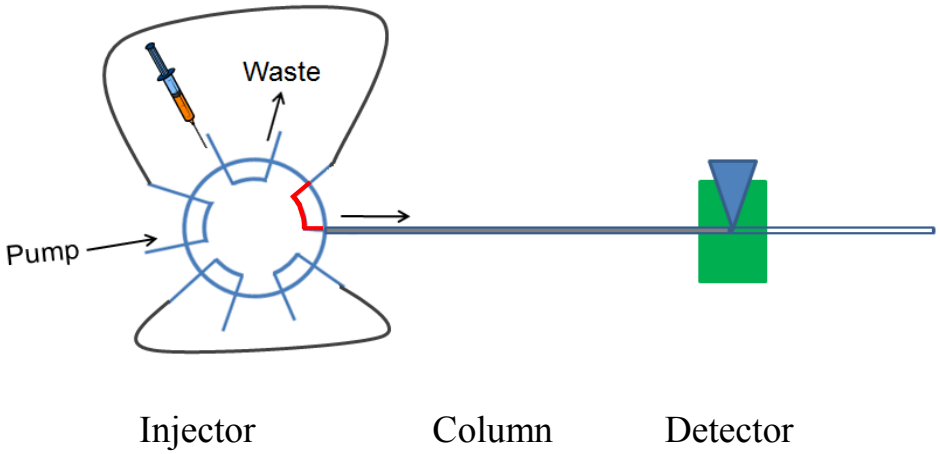


B

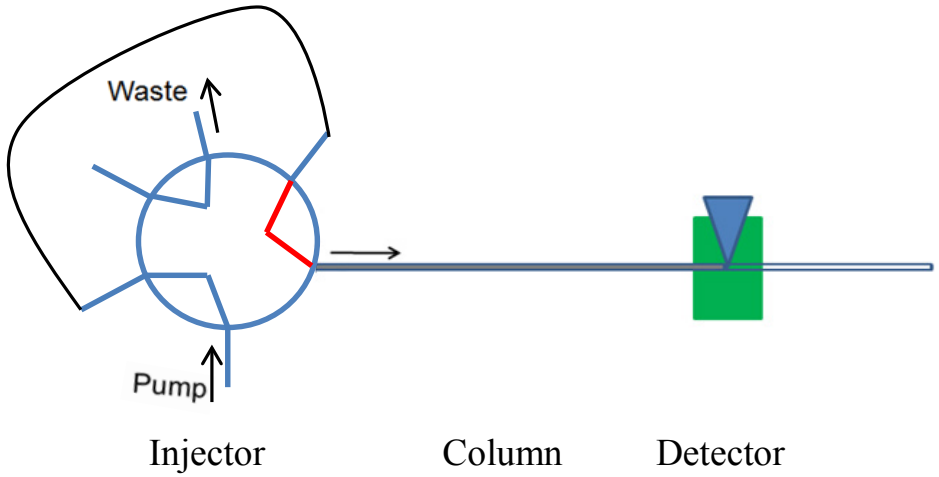


**Figure 4.1.** Schematics of the LC systems used. (A) Commercial capillary LC system with injector valve having 336 nL swept volume, (B) nano-flow LC system with injector valve having 130 nL swept volume. The actual sample injection volumes for all measurements were 30 or 60 nL.

**Table 4.1.** Specifications and reagent compositions for the PEGDA monolithic column.

| Specification | Value |
|---|---|
| Back pressure[a] (MPa)/(psi) | 17.9/2600 |
| Column length (cm) | 15.1 |
| Column diameter (μm) | 150 |
| Percentage of monomer (% w/w) | 20 |
| Amount of tergitol 15-S-20 (g) | 0.30 |
| Porogen ratio[b] | 1.03/1.35/1 |
| Column porosity, $\varepsilon_t$ | 0.42 |

[a] Measured at 0.4 μL/min

[b] Porogen ratio = w/w/w ratio of dodecanol/decanol/decane

phase flow rates used in this study covered the range of 0.05-0.4 µL/min, corresponding to a linear velocity range of 0.28-2.26 cm/min.

### 4.2.4 Extra-column variance

In capillary LC, the effect of extra-column variance on separation efficiency has been well documented and proven to be significant. Assuming that all contributions to peak variance are independent, the total variance of a peak is the sum of these contributions:

$$\sigma^2_{\text{tot}} = \sigma^2_{\text{col}} + \sigma^2_{\text{inj}} + \sigma^2_{\text{cap}} + \sigma^2_{\text{det}} \quad (4.1)$$

Since, in this study we used on-column detection with no connecting tubing, the peak variance due to the detection cell ($\sigma^2_{det}$) and connecting tubes ($\sigma^2_{cap}$) were negligible. Moreover, the sampling rate at the detector was 10 Hz, providing 460 points in the narrowest peak measured at 0.4 µL/min. The high sampling rate and low detection time constant (corresponding to 0.0005 AUFS) minimized any residual contribution of detection cell to extra-column variance. Therefore, the total variance was essentially restricted due to the column ($\sigma^2_{\text{col}}$) and injection valve ($\sigma^2_{\text{inj}}$). All peak variances measured in this study have been expressed in time units, i.e., $\text{min}^2$.

Several methods have been used in the past to calculate extra-column band broadening, including a linear extrapolation method (LEM) using a homologous series of compounds, LEM using empty column lengths [28], and whole column detection [29-31]. The method employed in this study to measure the extra-column variance was LEM using a monolith-free capillary (same internal diameter as the monolithic column) and measuring the peak variance as a function of capillary length. By plotting the total variance versus the length of capillary tube and extrapolating this line to zero length, the extra-column variance due to the injector was obtained. Variances were measured for four different capillary lengths (15 cm to 30 cm) and eight different

flow rates. The smallest capillary length used was 15 cm, as it was the minimum length required between the injector and the detector. Also, to ensure the delivery of accurate flow rates from the LC pump, a monolithic column was attached to the empty capillary after the detection point. This provided a back pressure for the LC system.

### 4.2.5 Chromatographic analysis

Peak broadening is normally expressed in terms of number of theoretical plates (N). In calculating N, the peaks were assumed to have Gaussian shapes, which are rarely observed in LC. As a result, large errors can be introduced in the computed efficiency values [32,33]. Therefore, to minimize this error, the exponentially modified Gaussian function-based Foley-Dorsey equations were used for calculating variance ($\sigma^2$) and plate count (N) [34,35]:

$$\sigma_{tot}^2 = \frac{W_{0.1}^2}{1.764(B/A)^2 - 11.15(B/A) + 28} \tag{4.2}$$

$$N = \frac{41.7(t_R/W_{0.1})^2}{1.25 + (B/A)} \tag{4.3}$$

where $t_R$ is the retention time of the analyte, $W_{0.1}$ is the width at 10% peak maximum, B is the width from the center of the peak to the tail of the peak, and A is the width from the front of the peak to the center of the peak, both at 10% peak height. Calculating peak width at 10% peak height provides more accurate measurement of plate count than when using half peak width [32,36].

## 4.3 Results and Discussion

With the advent of highly efficient capillary columns in LC, extra-column variance plays a significant role in determining the performance of these columns. Extra-column contributions due to the injector were examined extensively in this work, both experimentally and theoretically. A new mathematical expression that describes this behavior was derived.

### 4.3.1 Extra-column variance from the injector

The contribution of the sampling device (i.e., injection valve) to peak variance has been shown to depend on the injection profile and size of the sample plug [15,37]. The volumetric contribution has been described in the literature and is based on the assumption that the sample is uniformly distributed throughout the injection volume:

$$\sigma_{inj}^2 = \frac{V_i^2}{12} \tag{4.4}$$

where $V_i$ represents the injection volume and 12 is a constant from assuming that the sample plug has a rectangular shape. $V_i$ was calculated in units of time based on the flow rate and the path length of the sample plug. This mathematical expression represents the smallest possible contribution from the injection process. There have been other reports of additional contributions to band broadening from the injection valve due to dispersion inside the device [7,16,20,22]; however, these were not fully characterized either experimentally or theoretically. Therefore, we used LEM to fully explore these phenomena.

Figure 4.2 shows the measurement of total variance as a function of column length, where the intercept on the y axis corresponds to dispersion caused by the injection valve. The intercept at each flow rate was found to be different, varying from 33.9 nL to 21.5 nL with change in flow rate from 0.05 µL/min to 0.40 µL/min. This variation in extra-column volume indicates the presence of an additional flow-related contribution of the injection valve to total peak variance. This additional contribution to peak variance can be attributed to dispersion of the analyte inside the bore holes connecting the sample loop, mixing of the analyte with the mobile phase, and valve switching events [37].This flow rate dependent contribution was modeled to establish a mathematical relationship between the flow rate and observed peak variance, and was found to be an inverse square of the flow rate times an exponential function of the flow rate:

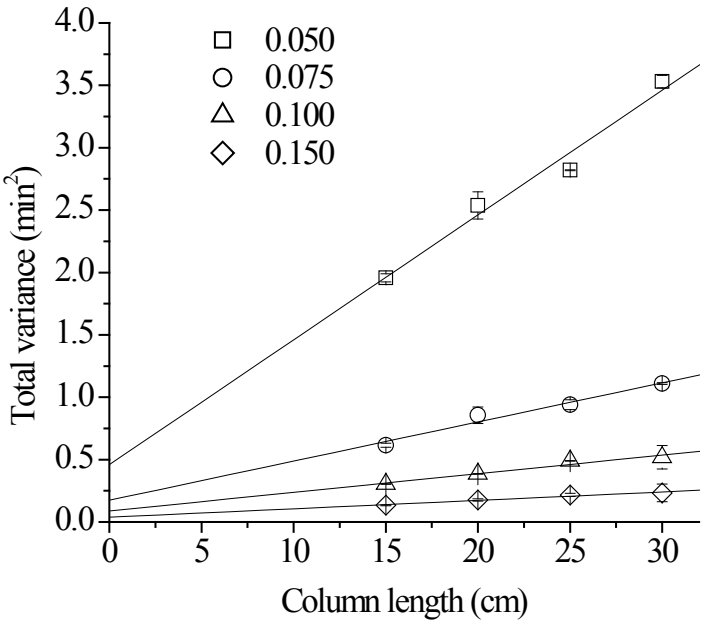


**Figure 4.2.** Total variance versus column length for a non-retained analyte, uracil, at four different flow rates (0.050 µL/min, 0.075 µL/min, 0.100 µL/min, and 0.150 µL/min); similar plots were constructed for four additional flow rates from 0.200 to 0.400 µL/min at increments of 0.050 µL/min (not shown in this figure for clarity). Each data point represents an average value of three replicate measurements. Conditions: 150 µm i.d. empty capillary column; 98:2 w/w water/acetonitrile mobile phase; on-column UV detection at 214 nm; 30 nL injection volume.

$$\sigma^2_{inj} = \frac{1}{u^2} e^{(\alpha + \frac{\beta}{u})} \quad (4.5)$$

where α and β are fixed coefficients having values of -7.38 and 0.03, respectively, for our system. This equation predicts well the additional contribution to the extra-column variation due to the injector ($R^2$ = 0.999), Figure 3. The coefficients listed in equation 5 have constant numerical values for a particular valve, analyte, and mobile phase system, which are due to the geometrical parameters of the valve such as shape and diameter, and the physical/chemical properties of the mobile phase and the analyte. The exponential tail is evident only at very low flow rates; at high flow rates, the $\beta/u$ term becomes insignificant, leading to a constant extra-volume contribution of the injector. This is clearly evident in Figure 4.3 as the variance becomes constant above a flow of 0.2 µL/min. The removal of the exponential term (or β = 0) from the equation reduces the $R^2$ value to 0.992, and examination of the residuals of the fit show a pattern that indicates an incomplete model. Moreover, the p-value for the coefficient β was found to be 2.04 x $10^{-7}$, indicating the statistical significance of the coefficient. This observed exponential dependence on flow rate can be explained on the basis of axial and radial diffusion of analyte, which in turn governs solute dispersion and mixing [23]. The groove in the rotor and connecting bore holes in the stator were considered as open capillaries with very short lengths. The analyte band spreads largely longitudinally with small radial dispersion at very low flow rates because of the inverse dependence of axial dispersion on flow rate and direct correlation between radial dispersion and flow rate. This results in a long exponential tail in addition to the rectangular plug shape at lower flow rates used in capillary LC.

An exponential extra-column variance due to the injection valve was suggested by Fountain et al. [10] for an injection volume of 1 µL on a 2.1 mm column using an ultra-high pressure LC. However, the exponential contribution to extra-column variance would become

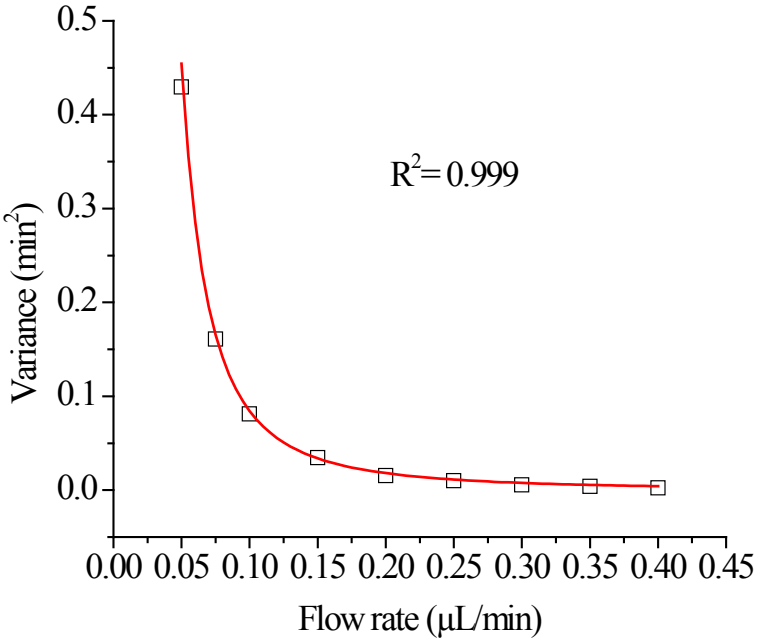


**Figure 4.3.** Extra-column variance due to the commercial capillary LC injector (swept volume of 336 nL) as a function of flow rate. Conditions are the same as in Figure 4.2.

much more evident for lower injection volumes (i.e., 100 nL), which are commonly used in capillary LC. When the sample plug is small, dispersion acting at the rear of the sample zone is influenced by dispersion occurring at the front boundary, which is diluted by the mobile phase. This prevents the sample plug from reaching a plateau or rectangular distribution as is normally seen with large sample volumes. As explained in the previous paragraph, exponential tailing becomes more evident at low flow rates, as it leads to more axial dispersion. Therefore, the addition of higher dispersion due to low flow rates and small injection volumes explains the existence of exponential tailing in extra-column band broadening due to injection profiles in capillary LC. This effect of sample volume and dispersion was also observed by Prub et al. [20] in their characterization of extra-column dispersion in capillary LC.

**4.3.2 Effect of extra-column volume on plate height (H) for a non-retained compound**

Using the previously described model, the extra-column dispersion caused by the injector can be calculated and used to determine the actual chromatographic efficiency of the column. For the commercial LC system used in this study, the extra-column variance was found to be at least 60% of the total column variance at every measured flow rate for the non-retained analyte uracil. This indicates an approximate 130% loss in column performance. Therefore, the monolithic column analyzed in this study should give a maximum theoretical plate count of 186,000 plates/m as shown in Figure 4.4. The van Deemter plots shown in Figure 4.4 were obtained after minimizing the contributions of extra-column variances from already known factors. This included sample volume, diameter of external sample loop, data acquisition rate and sampling method. The sample volume injected (30 nL) was optimized by striking a balance between column volume to prevent sample overloading and detector sensitivity. The diameter of the external sample loop was found to be inconsequential since time-gated injection [38,39] was

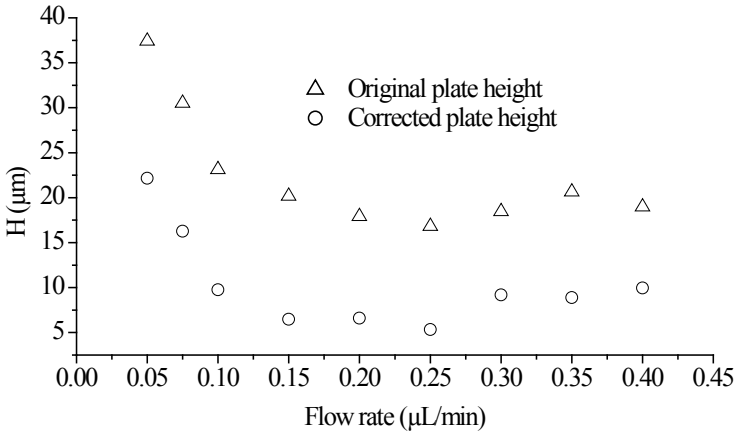


**Figure 4.4.** Plate height versus flow rate of a non-retained analyte (uracil) with (o) and without (Δ) dead-volume corrections at different flow rates. Conditions: 15 cm×150 μm i.d. PEGDA monolithic column; 98:2% w/w water/acetonitrile mobile phase; on-column UV detection at 214 nm; 30 nL injection volume.

used [25]. These observations were in agreement with previously reported observations in the literature [20]. A data acquisition rate of 10 Hz was found to be sufficient for all flow rates tested with a minimum peak width of 10.8 s at the highest flow rate.

To further verify our observations of the effects of extra-column variance on chromatographic performance, a second injection system that was specially fabricated with the sampling system integrated in a nano-flow pump to minimize extra-column variance was evaluated using the same column and detection system as was used for the commercial instrument. The chromatographic efficiency almost doubled with the more carefully designed system and a 130 nL sample volume. Dispersion was reduced in the internal sample loop of the injector because of the smaller diameter connecting bore holes and V-shape sample groove geometry, which provided better mixing.

Less dispersion was clearly evident in the peak shapes for the non-retained analyte at a flow rate of 0.42 µL/min as shown in Figure 4.5A, and from the van Deemter plots for the different injectors in Figure 4.5B. The small difference in retention times (i.e., 0.17 s) of uracil at 0.42 µL/min can be attributed to the small change in column length (0.1 cm) due to connections and injector configurations. In summary, the overall band dispersion of the non-retained analyte depends mostly on axial dispersion and mixing dispersion that takes place inside the extra-column variance, which was found to have an exponential dependence on the flow rate.

**4.2.3 Effect of extra-column volume on plate height (H) for retained compounds**

The same monolithic column was used for separating a mixture of phenols under isocratic reversed-phase conditions (80:20 w/w water/acetonitrile) as shown in Figure 4.6. The smallest uncorrected plate height was 10 µm for phenol, corresponding to a retention factor (k) of 3.06, which is much lower than the uncorrected plate height of the non-retained uracil, i.e.,

A

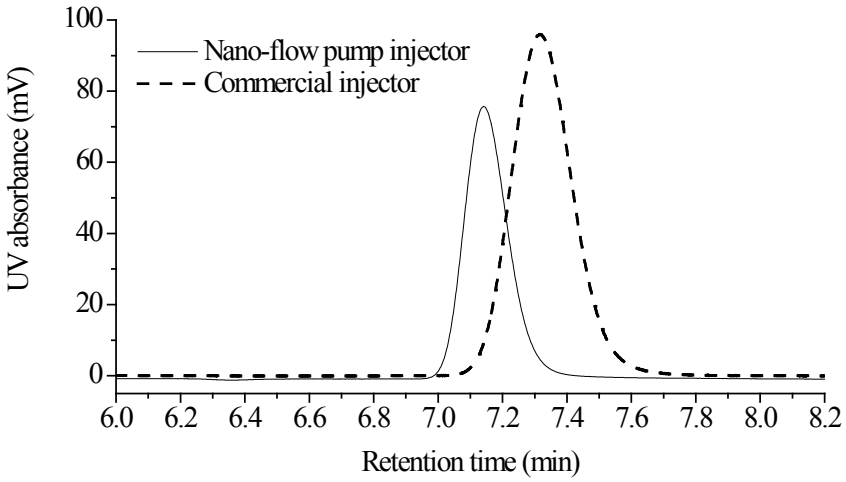


B

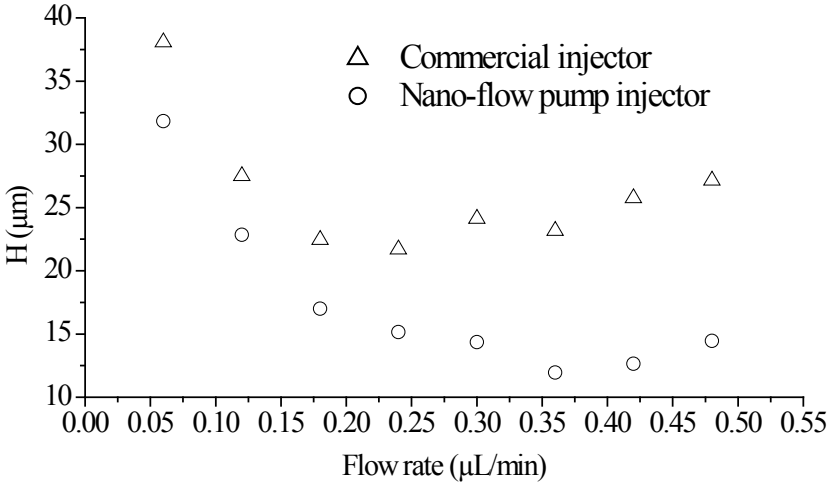


**Figure 4.5.** Comparison between dead volume contributions of a non-retained analyte (uracil) for injectors having swept volumes of 336 nL and 130 nL, respectively. (A) peak profiles at 0.42 µL/min, (B) plate height versus flow rate. Conditions: 15 cm×150 µm i.d. PEGDA monolithic column; 98:2 w/w water/acetonitrile mobile phase; on-column UV detection at 214 nm; 60 nL injection volume.

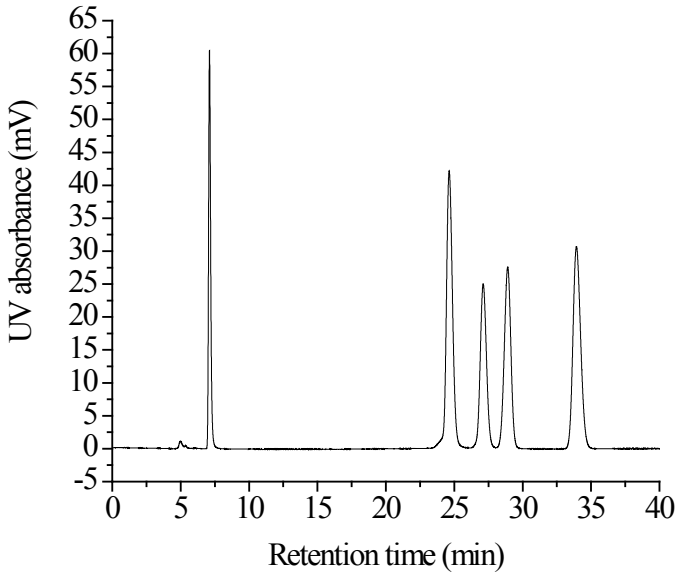


**Figure 4.6.** LC separation of phenols using a commercial capillary LC system. Conditions: 15 cm × 150 µm i.d. PEGDA monolithic column; 80:20 w/w water/acetonitrile; 400 nL/min flow rate; on-column UV detection at 214 nm. Peak identifications: uracil, pyrogallol, catechol, phenol, and resorcinol in order of elution.

18.2 µm. This is expected since the effect of extra-column variance decreases with increasing peak width, i.e., increasing retention. Retention of an analyte on the chromatographic column aids in reducing the effects of axial and mixing dispersion that occurs in the extra-column volume. The effect of extra-column volume on peak variance for a retained compound can be calculated using [7]:

$$\sigma^2_{\text{retained}} = \frac{\sigma^2}{\epsilon_t^2(1 + k)^2} \tag{4.6}$$

where σ is the peak variance of a non-retained compound, $\epsilon_t$ is the total column porosity (0.42 for this particular column) and k is the retention factor.

Table 4.2 lists the corrected and measured efficiencies for both retained and non-retained compounds. The measured plate count was found to increase with an increase in retention factor, while the trend was opposite after correction for the extra-column variance. This is because errors made in estimating the column efficiency decrease with increasing retention. For a retained compound, the effect of extra column variance decreases with an increase in analyte retention factor (Figure 4.7). The column efficiency is underestimated by 6% for a retention factor of 2.5, which drops to 1.6 % when the retention factor exceeds 3.5. These conclusions are for an extra-column volume that was minimized for a particular LC system with on-column detection and no connecting tubes. One may expect a greater effect of extra-column volume on retained compounds when using larger sample volumes and connecting tubes for off-column detection.

**4.4 Conclusions**

Our results demonstrate two volume independent contributions to extra-column variance due to the injection valve. One of these arises from axial and mixing dispersion that occurs inside the injection valve groove, and is an exponential function of flow rate. We report for the first

**Table 4.2**. Efficiencies of a PEGDA monolithic column for non-retained and retained compounds with and without correction for extra-column variance.

| Analyte | Retention time (min)[a] | Retention factor (k) | Measured plate number [a] | Corrected plate number |
|---|---|---|---|---|
| Uracil | 7.11 (0.1) | | 8,300 (1.1) | 15,800 |
| Pyrogallol | 24.6 (0.2) | 2.46 | 14,600 (2.0) | 15,500 |
| Catechol | 27.0 (0.1) | 2.81 | 15,000 (1.2) | 15,650 |
| Phenol | 28.9 (0.1) | 3.06 | 15,200 (2.1) | 15,700 |
| Resorcinol | 33.9 (0.1) | 3.77 | 15,100 (1.0) | 15,500 |

[a] % RSD in parenthesis for three repetitive measurements

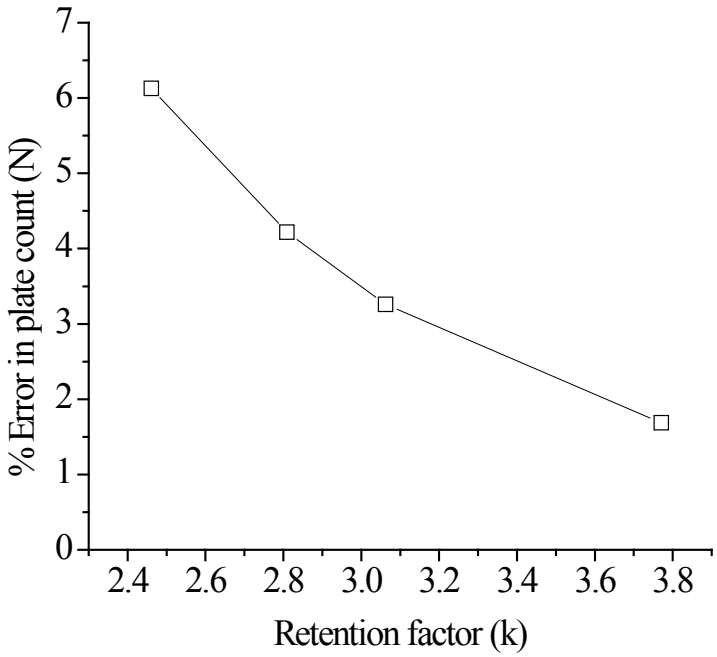


**Figure 4.7.** Percent error of the estimated column efficiency of retained compounds (pyrogallol, catechol, phenol and resorcinol) as a function of retention factor.

time a mathematical model that describes this relationship. The overall extra-column volume was calculated to be 35 nL after optimization of the instrument and reducing/eliminating all possible sources of extra-column dispersion. The theoretical corrections for column performance were verified using a new nano-flow pump with integrated injection system having a smaller sample loop and different geometry. The chromatographic efficiency doubled with the use of the new injection valve. The extra-column variance results in a measured efficiency that is approximately half of the actual column efficiency for a non-retained analyte, 6% less for a compound with a retention factor of approximately 2, and approximately 1% less for a compound with a retention factor > 3.5. Therefore, the extra-column band broadening should be characterized in order to determine the actual performance of capillary LC columns.

**4.5 References**


1. Shi, Y.; Xiang, R.; Horváth, C.; Wilkins, J. A. *J. Chromatogr. A* **2004**, *1053*, 27-36.
2. Neue, U. D.; O'Gara, J. E.; Méndez, A. *J. Chromatogr. A* **2006**, *1127*, 161-174.
3. Gritti, F.; Guiochon, G. *J. Chromatogr. A* **2012**, *1228*, 2-19.
4. Neue, U. D., In *Encyclopedia of Analytical Chemistry*, Meyers, R. A., Ed. Wiley and Sons, Ltd.: Chichester, **2000**; pp 11450-11472.
5. Wyndham, K. D.; O'Gara, J. E.; Walter, T. H.; Glose, K. H.; Lawrence, N. L.; Alden, B. A.; Izzo, G. S.; Hudalla, C. J.; Iraneta, P. C. *Anal. Chem.* **2003**, *75*, 6781-6788.
6. Liu, Y.; Grinberg, N.; Thompson, K.; Wenslow, R.; Neue, U.; Morrison, D.; Walter, T.; O'Gara, J.; Wyndham, K. *Anal. Chim. Acta* **2005**, *554*, 144-151.
7. O'Gara, J. E.; Alden, B. A.; Walter, T. H.; Petersen, J. S.; Niederlaender, C. L.; Neue, U. D. *Anal. Chem.* **1995**, *67*, 3809-3813.
8. Gritti, F.; Guiochon, G. *J Chromatogr. A* **2010**, *1217*, 1604-15.

9. Gritti, F.; Guiochon, G. *J Chromatogr. A* **2010**, *1217*, 1485-95.

10. Fountain, K. J.; Neue, U. D.; Grumbach, E. S.; Diehl, D. M. *J. Chromatogr. A* **2009**, *1216*, 5979-5988.

11. Mazzeo, J. R.; D. Neue, U.; Kele, M.; Plumb, R. S. *Anal. Chem.* **2005**, *77*, 460 A-467 A.

12. Colon, L. A.; Cintron, J. M.; Anspach, J. A.; Fermier, A. M.; Swinney, K. A. *Analyst* **2004**, *129*, 503-504.

13. MacNair, J. E.; Lewis, K. C.; Jorgenson, J. W. *Anal. Chem.* **1997**, *69*, 983-989.

14. Wu, N.; Bradley, A. C.; Welch, C. J.; Zhang, L. *J. Sep. Sci.* **2012**, *35*, 2018-2025.

15. Kirkland, J. J.; Yau, W. W.; Stoklosa, H. J.; Dilks, C. H. *J. Chromatogr. Sci.* **1977**, *15*, 303-316.

16. Colin, H.; Martin, M.; Guiochon, G. *J. Chromatogr. A* **1979**, *185*, 79-95.

17. Classens, H. A.; Cramers, C. A.; Kuyken, M. A. J. *Chromatographia* **1987**, *23*, 189-194.

18. Tsuda, T.; Novotny, M. *Anal. Chem.* **1978**, *50*, 632-634.

19. Sternberg, J. C., In *Advances in Chromatography*. Giddings, J.C.; Keller, R.A., Eds.; Marcel Deckker: New York, 1966; pp 205-270.

20. Prüß, A.; Kempter, C.; Gysler, J.; Jira, T. *J. Chromatogr. A* **2003**, *1016*, 129-141.

21. Aris, R. *P. Roy. Soc. Lond. A Mat.* **1959**, *252*, 538-550.

22. Gritti, F.; Felinger, A.; Guiochon, G. *J. Chromatogr. A* **2006**, *1136*, 57-72.

23. Gritti, F.; Guiochon, G. *J. Chromatogr. A* **2010**, *1217*, 7677-7689.

24. Gritti, F.; Sanchez, C. A.; Farkas, T.; Guiochon, G. *J. Chromatogr. A* **2010**, *1217*, 3000-3012.

25. Vissers, J. P. C.; de Ru, A. H.; Ursem, M.; Chervet, J.-P. *J. Chromatogr. A* **1996**, *746*, 1-7.

26. Colin, H.; Martin, M.; Guiochon, G. *J. Chromatogr. A* **1979**, *185*, 79-95.

27. Sharma, S.; Plistil, A.; Simpson, R. S.; Liu, K.; Farnsworth, P. B.; Stearns, S. D.; Lee, M. L. *J. Chromatogr. A* **2014**, *1327*, 80-89.

28. Kirkland, J.; Yau, W.; Stoklosa, H.; Dilks, C. *J. Chromatogr. Sci.* **1977**, *15*, 303-316.

29. Lauer, H.; Rozing, G. *Chromatographia* **1981**, *14*, 641-647.

30. Freebairn, K.; Knox, J. *Chromatographia* **1984**, *19*, 37-47.

31. Claessens, H.; Cramers, C.; Kuyken, M. *Chromatographia* **1987**, *23*, 189-194.

32. Bidlingmeyer, B. A.; Warren Jr, F. V. *Anal. Chem.* **1984**, *56*, 1583A-1596A.

33. Schudel, J. V.; Guiochon, G. *J. Chromatogr. A* **1988**, *457*, 1-12.

34. Foley, J. P.; Dorsey, J. G. *J. Chromatogr. Sci.* **1984**, *22*, 40-46.

35. Foley, J. P.; Dorsey, J. G. *Anal. Chem.* **1983**, *55*, 730-737.

36. Berthod, A. *J. Liq. Chromatogr.* **1989**, *12*, 1169-1185.

37. Bakalyar, S. R.; Phipps, C.; Spruce, B.; Olsen, K. *J. Chromatogr. A* **1997**, *762*, 167-185.

38. Harvey, M. C.; Stearns, S. D. *J. Chromatogr. Sci.* **1983**, *21*, 473-477.

39. Harvey, M. C.; Robinson, R. E.; Harvey, M. C.; Stearns, S. D. *J. Chromatogr. Sci.* **1994**, *32*, 190-194.

# CHAPTER 5 HIGH EFFICIENCY POLY(ETHYLENE GLYCOL) DIACRYLATE MONOLITHS FOR REVERSED-PHASE CAPILLARY LIQUID CHROMATOGRAPHY OF SMALL MOLECULES*

## 5.1 Introduction

Monolithic columns were introduced in the early 1990's as a low pressure alternative to particle packed columns [1,2]. An additional advantage of monolithic stationary phases compared to particle packed columns is that through-pore size and skeletal dimensions (analogous to particle diameter in packed columns) can be varied nonlinearly [3]. This offers the potential to engineer monolithic stationary phases with high porosities and thin skeletal sizes to reduce the resistance to mass transfer (i.e., improve chromatographic efficiency) without decreasing column permeability. Other attractive advantages of monolithic columns, such as easy preparation, wide selectivity, and applicability to most LC separation modes, have been illustrated in a number of recent excellent review articles [3-9].

Organic polymer monoliths typically exhibit agglomerated, inter-adhered globular morphologies intertwined with through-pores. Since they have relatively low surface areas and can be synthesized from biocompatible monomers, they have proven advantageous for separation of large bio-molecules such as proteins and peptides [10-13]. The research group I worked in at Brigham young University previously showed that polyethylene glycol diacrylate (PEGDA) monoliths are well-suited for separation of proteins and peptides under hydrophobic interaction chromatography (HIC) conditions [12,14]. This is due in large part to the low total mesopore volume in the polymer backbone, which severely limits diffusion of biomacromolecules into the stagnant mobile phase in the swollen monolith gel structure [15,16]. The surface areas for organic polymer monoliths generally range from single $m^2/g$ to tens of $m^2/g$ [17,18]. Therefore, radial mass transfer for large molecules is dominated by mobile phase convection, with little

* This chapter was largely reproduced from: Aggarwal, P.; Lawson, J. S.; Tolley, H. D.; Lee, M.L., submitted.

contribution from diffusion into and in the stationary phase [19]. On the other hand, organic polymer monoliths have proven to be relatively ineffective for separation of small molecules because of high gel porosity and low mesopore volume [20-22].

Several new approaches have been reported for fabricating organic monoliths with larger surface areas to improve their separation performance for small molecules. These include copolymerization of stearyl methacrylate with several dimethacrylate crosslinkers differing in chain length and branching fragments [17], use of higher polymerization temperature [23], post-polymerization hyper-cross linking [18,24,25], early termination of the polymerization reaction [26] and addition of nanostructures such as carbon nanotubes and fullerenes [27]. All of these methods lead to higher crosslinking density (i.e., higher surface area), a major factor leading to improved column performance. Another straightforward approach to obtain highly crosslinked monolithic structures is to use a high concentration of crosslinking monomer in a multi-monomer system or use a single monomer crosslinker [28,29]. Our previous work has demonstrated the advantages associated with single monomer synthesis, including better mechanical stability, improved reproducibility, simpler optimization of polymerization conditions and, particularly important in this study, higher surface area [12,30-32]. Several moderately efficient RPLC monolithic columns have been synthesized using single diacrylate or dimethacrylate crosslinkers (e.g., pentaerythritol diacrylate monostearate [30] and neopentyl glycol dimethacrylate [32]), and demonstrated for separation of small alkyl benzene and alkyl paraben molecules.

This chapter presents the fabrication and application of monoliths prepared from PEGDA monomers for RPLC of small molecules. The PEGDA monoliths were demonstrated for separation of phenols, hydroxy benzoic acids, alkyl parabens, pharmaceutical compounds (i.e., non-steroidal anti-inflammatory drugs) and acidic herbicides (i.e., phenylurea derivatives). The

fabrication conditions were optimized using statistical principles with column efficiency as the guiding parameter. To my knowledge, this is the first study that demonstrates a quantitative correlation between physical/chemical properties of the pre-polymer constituents and column efficiency, leading to the rational selection of porogens.

## 5.2 Experimental

### 5.2.1 Chemicals and reagents

The reagents, 2,2-dimethoxy-2-phenyl-acetophenone (DMPA, 99%), 3-(trimethoxysilyl)propyl methacrylate (TPM, 98%) and poly(ethyleneglycol) diacrylate (PEGDA, Mn 258, 302, 575, and 700), were purchased from Sigma–Aldrich (St Louis, MO, USA). All porogenic solvents and chemicals were HPLC or analytical reagent grade, respectively, and were used as received. Tergitol surfactant (T15-S-12, T15-S-15, T15-S-20), also used as a co-porogen, was obtained from Dow Chemical, Midland, MI, USA. The standard compounds, phenol, catechol, resorcinol, pyrogallol, benzoic acid, 2-hydroxy benzoic acid, 3-hydroxy benzoic acid, 3,4-dihydroxy benzoic acid, 2,4-dihydroxy benzoic acid and 3,4,5-trihydroxybenzoic acid were obtained from Sigma-Aldrich. Methyl paraben, ethyl paraben, propyl paraben and butyl paraben were purchased from Fluka (Buchs, Switzerland). Mixtures of phenylurea herbicides (i.e., isoproturon, monuron, monolinuron, diuron and linuron) and pharmaceutical compounds (i.e., paracetamol, ibuprofen, aspirin and indomethacin) were purchased from Sigma-Aldrich.

### 5.2.2 Polymer monolith preparation

Monoliths were synthesized inside pre-treated UV transparent Teflon-coated capillaries (150 µm i.d.) functionalized using the procedure listed in Section 2.2.2. Pre-polymer solutions were prepared in 1-dram (4 mL) glass vials by admixing initiator, monomer, and porogen

**Table 5.1.** Compositions of fabricated monolithic columns.

| Column Number | Composition[a] (wt.%)[b] | | | | | | | | | | | | Efficiency (plates/m) |
|---|---|---|---|---|---|---|---|---|---|---|---|---|---|
| | Monomer | T15S20 | T15S12 | T15S15 | Dodecanol | Decanol | Hexane | Decane | Iso butanol | Iso propanol | Ethylether | Methanol | |
| PEGDA-258 | | | | | | | | | | | | | |
| C1 | 0.35 | 0.30 | 0 | 0 | 0 | 0 | 0 | 0 | 0.25 | 0 | 0 | 0.10 | 14,000 |
| C2 | 0.20 | 0 | 0.30 | 0 | 0 | 0 | 0 | 0 | 0 | 0 | 0.25 | 0.25 | 9,800 |
| C3 | 0.35 | 0 | 0.15 | 0 | 0 | 0.25 | 0 | 0 | 0 | 0.25 | 0 | 0 | 11,500 |
| C4 | 0.20 | 0 | 0.30 | 0 | 0 | 0.25 | 0.25 | 0 | 0 | 0 | 0 | 0 | 13,800 |
| C5 | 0.35 | 0 | 0.15 | 0 | 0 | 0 | 0.25 | 0 | 0 | 0 | 0.25 | 0 | 16,100 |
| C6 | 0.35 | 0.15 | 0 | 0 | 0.25 | 0 | 0 | 0 | 0 | 0 | 0.25 | 0 | 12,700 |
| C7 | 0.35 | 0 | 0 | 0.30 | 0 | 0.25 | 0 | 0 | 0 | 0.25 | 0 | 0 | 11,400 |
| C8 | 0.20 | 0 | 0 | 0.30 | 0.25 | 0 | 0 | 0 | 0 | 0.25 | 0 | 0 | 10,200 |
| C9 | 0.35 | 0 | 0.15 | 0 | 0 | 0 | 0 | 0 | 0.25 | 0 | 0.25 | 0 | 11,600 |
| C10 | 0.20 | 0.30 | 0 | 0 | 0.25 | 0 | 0 | 0 | 0 | 0 | 0 | 0.25 | 12,400 |
| C11 | 0.35 | 0.15 | 0 | 0 | 0 | 0 | 0 | 0 | 0 | 0 | 0.35 | 0.15 | 12,500 |
| C12 | 0.35 | 0 | 0 | 0.20 | 0.15 | 0.30 | 0 | 0 | 0 | 0 | 0 | 0 | 12,200 |
| C13 | 0.35 | 0 | 0.30 | 0 | 0 | 0 | 0 | 0 | 0 | 0.15 | 0.20 | 0 | 14,200 |
| C14 | 0.35 | 0 | 0 | 0.20 | 0.20 | 0 | 0.25 | 0 | 0 | 0 | 0 | 0 | 7,100 |
| C15 | 0.35 | 0 | 0 | 0.25 | 0 | 0 | 0.20 | 0 | 0.20 | 0 | 0 | 0 | 9,800 |
| PEGDA-302 | | | | | | | | | | | | | |
| C16 | 0.35 | 0 | 0.15 | 0 | 0 | 0 | 0 | 0 | 0 | 0.25 | 0 | 0.25 | 15,500 |
| C17 | 0.20 | 0 | 0 | 0.30 | 0 | 0.25 | 0 | 0 | 0 | 0.25 | 0 | 0 | 13,800 |
| C18 | 0.35 | 0.30 | 0 | 0 | 0 | 0 | 0 | 0 | 0 | 0.10 | 0.25 | 0 | 18,400 |
| C19 | 0.35 | 0 | 0 | 0.30 | 0 | 0.10 | 0 | 0 | 0 | 0 | 0 | 0.25 | 13,700 |
| C20 | 0.35 | 0 | 0.15 | 0 | 0.25 | 0 | 0 | 0 | 0.25 | 0 | 0 | 0 | 13,200 |
| C21 | 0.20 | 0 | 0.30 | 0 | 0 | 0 | 0 | 0 | 0.25 | 0.25 | 0 | 0 | 12,700 |
| C22 | 0.35 | 0 | 0 | 0.30 | 0 | 0.25 | 0.10 | 0 | 0 | 0 | 0 | 0 | 12,800 |
| C23 | 0.20 | 0 | 0 | 0.30 | 0 | 0.25 | 0 | 0 | 0 | 0.25 | 0 | 0 | 11,900 |
| C24 | 0.20 | 0 | 0 | 0.30 | 0 | 0.25 | 0 | 0 | 0 | 0.25 | 0 | 0 | 11,900 |
| C25 | 0.20 | 0.30 | 0 | 0 | 0 | 0.25 | 0 | 0 | 0 | 0 | 0.25 | 0 | 13,300 |
| PEGDA-575 | | | | | | | | | | | | | |
| C26 | 0.20 | 0.30 | 0 | 0 | 0 | 0 | 0 | 0 | 0.25 | 0.24 | 0 | 0 | 38,600 |
| C27 | 0.20 | 0.30 | 0 | 0 | 0 | 0 | 0 | 0 | 0.25 | 0.25 | 0 | 0 | 76,400 |
| C28 | 0.25 | 0 | 0 | 0.17 | 0 | 0 | 0 | 0 | 0 | 0.29 | 0.29 | 0 | 45,700 |
| C29 | 0.25 | 0 | 0.17 | 0 | 0 | 0 | 0 | 0 | 0.29 | 0 | 0.29 | 0 | 30,700 |
| C30 | 0.20 | 0.30 | 0 | 0 | 0 | 0 | 0 | 0 | 0.25 | 0.25 | 0 | 0 | 48,400 |
| C31 | 0.20 | 0 | 0 | 0.30 | 0.25 | 0 | 0 | 0 | 0 | 0 | 0.25 | 0 | 33,000 |

| | | | | | | | | | | | | | |
|---|---|---|---|---|---|---|---|---|---|---|---|---|---|
| C32 | 0.20 | 0.30 | 0 | 0 | 0 | 0 | 0 | 0 | 0.25 | 0.25 | 0 | 0 | 33,200 |
| C33 | 0.20 | 0.30 | 0 | 0 | 0 | 0 | 0 | 0 | 0.25 | 0.25 | 0 | 0 | 27,300 |
| C34 | 0.35 | 0 | 0.15 | 0 | 0.25 | 0 | 0 | 0 | 0 | 0 | 0.25 | 0 | 41,800 |
| C35 | 0.20 | 0.30 | 0 | 0 | 0 | 0 | 0 | 0 | 0.25 | 0.25 | 0 | 0 | 46,800 |
| C36 | 0.20 | 0.30 | 0 | 0 | 0 | 0 | 0 | 0 | 0.25 | 0.25 | 0 | 0 | 41,600 |
| C37 | 0.35 | 0 | 0.15 | 0 | 0.25 | 0 | 0 | 0 | 0 | 0 | 0.25 | 0 | 43,000 |
| C38 | 0.35 | 0 | 0 | 0.05 | 0 | 0.25 | 0.10 | 0 | 0 | 0.25 | 0 | 0 | 41,300 |
| C39 | 0.35 | 0 | 0 | 0.15 | 0 | 0.25 | 0 | 0 | 0.25 | 0 | 0 | 0 | 33,800 |
| C40 | 0.20 | 0 | 0.30 | 0 | 0.25 | 0.25 | 0 | 0 | 0 | 0 | 0 | 0 | 40,100 |
| C41 | 0.35 | 0 | 0.15 | 0 | 0 | 0.25 | 0 | 0 | 0 | 0 | 0.25 | 0 | 28,000 |
| C42 | 0.35 | 0.30 | 0 | 0 | 0 | 0.10 | 0 | 0 | 0 | 0.25 | 0 | 0 | 29,800 |
| C43 | 0.35 | 0 | 0.15 | 0 | 0.25 | 0.25 | 0 | 0 | 0 | 0 | 0 | 0 | 31,300 |
| | | | | | | PEGDA-700 | | | | | | | |
| C44 | 0.20 | 0.35 | 0 | 0 | 0 | 0 | 0.12 | 0 | 0 | 0.34 | 0 | 0 | 49,600 |
| C45 | 0.30 | 0.24 | 0 | 0 | 0 | 0 | 0.23 | 0 | 0 | 0.22 | 0 | 0 | 64,600 |
| C46 | 0.20 | 0.17 | 0 | 0 | 0 | 0 | 0.30 | 0 | 0 | 0.33 | 0 | 0 | 66,100 |
| C47 | 0.25 | 0.17 | 0 | 0 | 0 | 0 | 0.25 | 0 | 0 | 0.33 | 0 | 0 | 62,900 |
| C48 | 0.20 | 0.22 | 0 | 0 | 0 | 0 | 0.22 | 0 | 0 | 0.33 | 0 | 0 | 58,700 |
| C49 | 0.20 | 0 | 0.30 | 0 | 0.15 | 0.15 | 0 | 0.20 | 0 | 0 | 0 | 0 | 75,000 |
| C50 | 0.20 | 0 | 0.30 | 0 | 0.13 | 0.13 | 0 | 0 | 0 | 0 | 0.25 | 0 | 55,400 |
| C51 | 0.25 | 0.17 | 0 | 0 | 0 | 0.29 | 0 | 0 | 0 | 0 | 0.23 | 0 | 56,600 |
| C52 | 0.20 | 0.30 | 0 | 0 | 0 | 0 | 0 | 0 | 0.25 | 0.25 | 0 | 0 | 31,600 |
| C53 | 0.20 | 0 | 0 | 0.30 | 0.25 | 0 | 0 | 0 | 0 | 0 | 0.25 | 0 | 54,900 |
| C54 | 0.20 | 0.30 | 0 | 0 | 0 | 0 | 0 | 0 | 0.25 | 0.25 | 0 | 0 | 2,900 |
| C55 | 0.35 | 0 | 0.15 | 0 | 0.25 | 0 | 0 | 0 | 0 | 0 | 0.25 | 0 | 35,200 |
| C56 | 0.20 | 0.30 | 0 | 0 | 0 | 0 | 0 | 0 | 0.25 | 0.25 | 0 | 0 | 39,200 |
| C57 | 0.20 | 0 | 0.30 | 0 | 0.25 | 0 | 0 | 0 | 0 | 0 | 0.25 | 0 | 53,200 |
| C58 | 0.35 | 0 | 0.05 | 0 | 0.25 | 0 | 0.10 | 0 | 0.25 | 0 | 0 | 0 | 52,700 |
| C59 | 0.20 | 0 | 0.30 | 0 | 0 | 0.25 | 0 | 0 | 0 | 0 | 0.25 | 0 | 32,800 |
| C60 | 0.275 | 0 | 0.18 | 0 | 0.25 | 0 | 0 | 0 | 0.125 | 0 | 0.175 | 0 | 30,400 |
| C61 | 0.35 | 0.15 | 0 | 0 | 0.25 | 0 | 0 | 0 | 0 | 0.25 | 0 | 0 | 44,300 |
| C62 | 0.20 | 0 | 0.30 | 0 | 0.125 | 0.125 | 0 | 0 | 0 | 0 | 0.25 | 0 | 62,900 |
| C63 | 0.35 | 0 | 0 | 0.15 | 0 | 0.25 | 0 | 0 | 0.25 | 0 | 0.25 | 0 | 8,300 |

[a] All monoliths contained 1 wt% DMPA to monomer.
[b] wt % related to total polymerization mixture.
[c] Efficiencies were measured for a non-retained compound, uracil.

solvents (Table 5.1). The solution was vortexed and then degassed by sonicating for 2 min if nonvolatile solvents were used as porogens. For volatile porogens, the solution was only vortexed to prevent vaporization of the porogen. A section of the surface treated capillary was cut and filled with pre-polymer solution using helium gas pressure. One end of the capillary was left empty for on-column UV detection. After introducing the reagent solution, the capillary was sealed with rubber septa at both ends and placed directly under a PRX 1000-20 Exposure Unit UV lamp (390±15 nm, 1000 W, TAMARACK Scientific, Corona, CA). Columns were exposed to a light intensity of 1 mW/cm$^2$ for a time period of 5 min. The light intensity was measured using an ACCU-CAL$^{tm}$-30 UV intensity meter (DYMAX, Torrington, CT, USA). Monoliths obtained after exposing with UV light were flushed with methanol and then water until stable pressure readings were obtained. An FEI Helios Nanolab 600 dual-beam scanning electron microscope (SEM) (Hillsboro, OR) was used to provide visual images of the monolith surface structures. SEM images were collected from 0.5 cm long monolithic columns coated with a conducting gold layer to overcome charging of the samples.

**5.2.3 Capillary liquid chromatography**

The capillary liquid chromatography system was an Ultimate 3000 high-pressure gradient LC system (Dionex, Sunnyvale, CA) equipped with an FLM-3300 nanoflow manager (1:1000 spilt ratio). The system was operated with Chromeleon software. A zero dead-volume nanoViper (Thermofisher Scientific, Sunnyvale, CA) loop having a volume of 1 µL was used as sample loop. The sample injection volume was kept constant at 30 nL for all experiments using time-gated injection by switching the injection valve at a specific time interval for each mobile phase flow rate. The dead volume of the system was determined to be 18 to 35 nL, depending on the flow rate [33]. On-column detection was performed using a Crystal 100 variable wavelength

UV–Vis absorbance detector at a wavelength of 214 nm. The detector rise time was set at 1 s, with a detector sensitivity set at 0.0005 AUFS. Data acquisition was performed using ChromPerfect software (Mountain View, CA, USA). Chromatograms were transferred to an Excel file and redrawn using Microcal Origin (Northampton, MA).

The mobile phases used were mixtures of acetonitrile and water with specific compositions and gradient programs as listed in the figure captions. For investigating the retention mechanism, ammonium formate buffered mobile phases were used. A 1 M ammonium formate buffer stock solution was prepared, and the pH was adjusted to any desired value using formic acid. Buffered mobile phases were prepared by mixing the desired amounts of 1 M ammonium formate solution, acetonitrile and water, and then filtering them through a 0.22-µm membrane filter. Each sample was prepared in a solution with the initial mobile phase composition for each respective separation. The reported mobile phase pH values refer to the aqueous portions only.

**5.2.4 Column permeability and stability**

Darcy's law was used to calculate column permeabilities from pressure drop and flow rate measurements. Plots of back pressure versus flow rate were constructed for selected monolithic columns (listed in Table 5.2) by flowing water through a 10 cm length of column at flow rates from 100 to 600 nL/min. The slope of each plot was used to determine the respective column permeability. Permeability values were also computed using acetonitrile as mobile phase to evaluate poly(PEGDA) monolith stabilities in different polarity solvents.

**5.2.5 Design of experiments**

The variables included in this study were (1) type of monomer (i.e., 4 different molecular weight PEGDA monomers), (2) surfactant porogen (i.e., different molecular weight tergitol

**Table 5.2.** Permeabilities and efficiencies of selected monolithic columns.[a]

| Column number | Monomer | Permeability ($K \times 10^{-5}$ $m^2$)[b] | Efficiency (plates/m) |
|---|---|---|---|
| 1 | PEGDA-258 | 5.41 | 9,800 |
| 2 | PEGDA-302 | 1.64 | 18,400 |
| 3 | PEGDA-575 | 0.30 | 33,000 |
| 4 | PEGDA-700 | 0.26 | 75,000 |

[a] Monolith composition is given in Table 5.1.

[b] $K = \eta Lu/\Delta P$, where $\eta$ is the viscosity, L is the column length (10 cm in this case), u is the mobile phase linear velocity, and $\Delta P$ is the column back pressure. The values for $u/\Delta P$ are based on plots of back pressure versus flow rate using water as mobile phase.

surfactant) and (3) porogenic solvent (i.e., 10 different liquids). The list of experimental mixtures to test was chosen as a D-optimal subset of an extreme-vertices mixture design, where lower and upper constraints were placed on the weight proportion of each variable (i.e., pre-polymer constituent in the mixture). The percentage of initiator (DMPA) was kept constant in all experiments (i.e., 1.0% w/w of monomer). The sum of the weight fractions of all components in the polymerization mixture equaled 100% (Table 5.1). From the weight proportion of the components (i.e., monomer, surfactant and porogen) in each experimental mixture, six physical/chemical properties were calculated. The properties used were viscosity and Hansen solubility parameter values of the pre-polymer constituents (Table 5.3). The viscosities were investigated both individually as well as in a ratio (X1 and X6). The Hansen solubility parameters included numerical solubility values due to the various possible chemical interactions between the porogens and monomer (i.e., dispersion, polarity and hydrogen-bonding). The numerical values for the solubility parameters were defined as the ratio of solubility value of the porogen mixture to that of the monomer for each chemical interaction, i.e., X2 for dispersion, X3 for polarity, X4 for hydrogen bonding and X5 for overall solubility ratio. The overall solubility is defined as the square root of the summed solubility value due to individual chemical interactions:

$$\delta_t^2 = \delta_d^2 + \delta_p^2 + \delta_h^2 \qquad (5.1)$$

Next, each experimental mixture was polymerized. Some mixtures resulted in homogeneous monoliths, while others were gels or clear liquids. Logistic regression was used to fit a model relating the probability of obtaining a homogeneous monolith to the relative proportion of the pre-polymer constituents in the mixture. However, this model was not an

**Table 5.3.** Physical/chemical properties of porogens, surfactants, and monomers.

| Component | Viscosity (cP)[a] | Hansen parameter for solubility[b] | | | |
|---|---|---|---|---|---|
| | | Dispersion | Polarity | Hydrogen bonding | Total |
| **Porogen** | | | | | |
| Dodecanol | 16.13 | 17.6 | 2.70 | 10.0 | 20.0 |
| Decanol | 11.79 | 15.5 | 6.50 | 10.8 | 20.4 |
| Hexane | 0.31 | 14.9 | 0 | 0 | 14.9 |
| Decane | 0.92 | 15.8 | 0 | 0 | 15.8 |
| Isobutanol | 3.33 | 15.1 | 5.70 | 16.0 | 22.7 |
| Isopropanol | 2.40 | 15.8 | 6.10 | 16.4 | 23.5 |
| Ethylether | 0.24 | 14.5 | 2.90 | 5.10 | 15.8 |
| Methanol | 0.59 | 14.7 | 12.3 | 22.3 | 29.6 |
| Water | 1.00 | 15.6 | 16.0 | 42.3 | 47.8 |
| 1,4-Butanediol | 71.5 | 16.6 | 10.0 | 21.5 | 28.9 |
| **Surfactant** | | | | | |
| T-15-S-12 | 85 | 19.4 | 1.12 | 7.59 | 20.9 |
| T-15-S-15 | 87 | 19.6 | 1.07 | 7.65 | 21.1 |
| T-15-S-20 | 98 | 19.9 | 0.97 | 7.72 | 21.4 |
| **Monomer** | | | | | |
| PEGDA-258 | 3.0 | 22.1 | 2.22 | 6.99 | 23.2 |
| PEGDA-302 | 4.0 | 21.9 | 2.06 | 7.15 | 23.1 |
| PEGDA-575 | 10 | 21.8 | 1.51 | 7.86 | 23.2 |
| PEGDA-700 | 13 | 21.4 | 1.38 | 7.64 | 22.8 |

[a] Viscosity data were from online CRC Handbook of Chemistry and Physics, 89th ed., CRC, Boca Raton, 2008–2009.

[b] Solubility parameter values were from Solvents and Solvent Effects in Organic Chemistry, 3rd ed., Wiley-VCH, KGaA, Weinheim, 2003.

accurate predictor of the probability of obtaining a monolith. As an alternative, a model relating the probability of obtaining a monolith was fit to the physical/chemical properties of each mixture, again by logistic regression. This model fit better and was useful in identifying regions in the property space that had a high probability of resulting in monolithic structures.

Finally, chromatographic efficiencies were measured for all of the macroscopically observable continuous monoliths. Regression analysis was used to fit a model that related the log(efficiency) for each of the monoliths to the physical/chemical values that were calculated from their respective pre-polymer components. The model was used to predict other combinations of physical/chemical properties that should produce monoliths with high chromatographic efficiency. Various mixtures with these combinations of properties were made, and the efficiencies of the resulting monoliths were measured. The results were added to the data base to refine the regression model.

## 5.3 Results and Discussion

### 5.3.1 Preparation of PEGDA monoliths

An important practice when fabricating monolithic columns for capillary LC is optimizing the monolith morphology (i.e., skeletal dimensions, porosity and pore-size distribution) to yield the best chromatographic efficiency with an acceptable column permeability (i.e., for this study, an arbitrarily selected permeability value of $1 \times 10^{-14}$ $m^2$). Therefore, all of the factors governing monolithic bed structure must be considered and optimized to obtain the desired morphology. These can be grouped into two main categories, i.e., polymerization conditions and pre-polymer components. Polymerization conditions, such as polymerization type (thermal or photo initiation), polymerization temperature, polymerization time, irradiation wavelength and intensity (if using photo-initiation) and column dimensions have

been reported to be major parameters that must be optimized [20,34,35]. Other important factors related to the pre-polymer components are their physical/chemical properties and weight proportions. There are reports in the literature of the use of solubility and polarity index values as guides for selection of porogens [36,37]; however, weight proportion optimization has been based more on practical experience and guess-work than on scientific rules. Such an approach is extremely time-consuming and labor-intensive and, therefore, is not feasible to evaluate all possible combinations.

Therefore, to make the process of porogen selection more scientific and efficient, I used numerical values of the physical/chemical properties of the monomers and porogens to guide the selection of pre-polymer solution combinations. In the results obtained from logistic regression, the parameters X3, X4, X5 and X6 were found to be the determining factors for predicting the probability of obtaining a monolithic column (Figure 5.1A). The dotted lines in the figure represent 50% probability of obtaining a monolithic column. The probability was found to increase with increase in solubility ratio due to interaction of polar groups, total solubility ratio and viscosity ratio. However, the solubility ratio due to hydrogen bonding interactions was found to have a negative effect. In previous work in this research group [14] and in the work by Courtois et al. [36], it was observed that a solvent with a solubility value similar to that of the monomer could be considered to be a good solvent, resulting in a monolith with low permeability and small pore size. I observed a similar trend in my analysis; the probability of obtaining a monolith was found to be maximum with a Hansen solubility parameter ratio around 1 (i.e., X4 and X5). Monoliths fabricated from this pre-polymer composition were found to have lower permeability than other monoliths. The negative response curve for solubility ratio due to

A

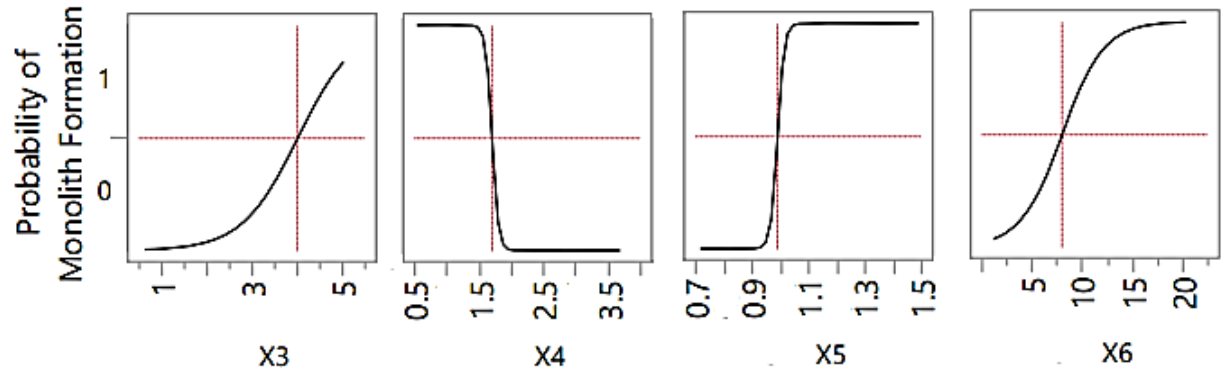


B

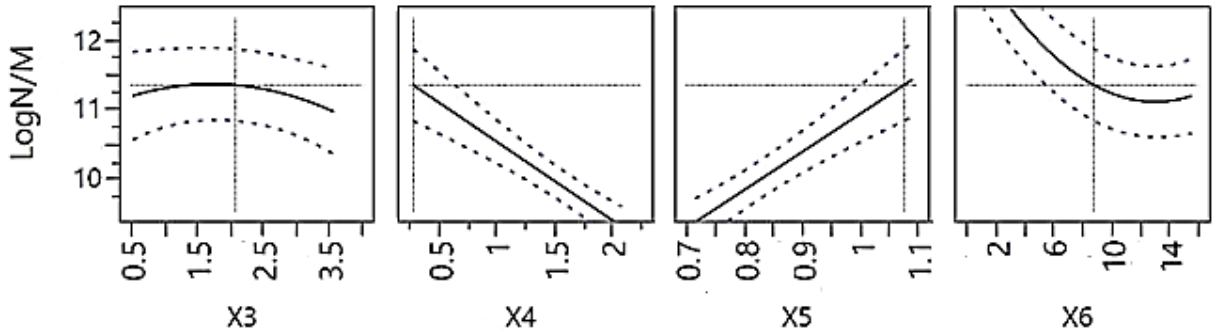


**Figure 5.1.** Prediction profile plots showing the effects of physical/chemical properties on (A) probability of obtaining a monolith and (B) chromatographic efficiency of the monolith. The variables are: (X3) ratio of Hansen solubility parameters of porogen mixture to monomer due to polarity, (X4) hydrogen bonding, (X5) square root sum of all three solubility parameters and (X6) ratio of viscosity of porogen mixture to monomer.

hydrogen bonding could be explained by a tendency for phase separation. Small pore size or low column permeability is always a consequence of delayed phase separation in the polymerizing reaction mixture, which is beneficial for fabricating efficient monoliths. However, prolonged delay in phase separation results in macroscopically visible non-continuous monoliths. Therefore, pre-polymer compositions with water and 1,4-buatendiol as porogens resulted in non-continuous monoliths because of extensive hydrogen bonding. As a result, these two porogens were not included in subsequent pre-polymer composition optimization for highly efficient columns.

Other than solubility, the other physical/chemical parameter that was found to be an important predictor of monolith formation was the viscosity ratio (X6). A higher viscosity ratio resulted in an increased probability of obtaining a monolithic column. Monomers with low viscosities showed high probability of forming monoliths from high viscosity porogens, while monomers with high viscosities showed increased probability of forming monoliths when mixed with intermediate to low viscosity porogens. Up to a limit, viscous pre-polymer compositions were found to have higher probability of forming monoliths. The polymerizing mixture viscosity governs the reaction kinetics by affecting the diffusion rate of the propagating radicals in the solution, as well as the time of phase separation. Therefore, the probability of monolith formation increases with an increase in viscosity of the pre-polymer mixture. However, above a certain viscosity, excessive delay in phase separation occurs (similar to the trend with solubility ratio), thereby resulting in formation of a gel or non-continuous monolith. This statistical design aided in selecting suitable porogens and their weight proportions (i.e., 74% accuracy) and reduced the time involved in column development and optimization.

The other factors optimized for monolith fabrication were polymerization time and UV light intensity. A polymerization time of 5 min and a light intensity of 10 mW/cm$^2$ were found to be optimum for obtaining continuous monolithic columns for all pre-polymer compositions listed in Table 5.1. The polymerization time was optimized to provide complete polymerization within a relatively short time. The light intensity was varied to observe the effects of slow and rapid polymerization on monolith morphology and resultant chromatographic performance. A light intensity below 1 mW/cm$^2$ necessitated longer polymerization time (~10-15 min) without any significant gain in column performance or change in monolith morphology. On the other hand, a light intensity in excess of 10 mW/cm$^2$ caused a rise in reaction chamber temperature without any significant improvement in column performance.

**5.3.2 Chromatographic efficiencies of PEGDA monoliths**

The measured column efficiencies were modeled with respect to the physical/chemical properties of the pre-polymer constituents. The same four factors (i.e., solubility ratio due to hydrogen bonding, polarity and total chemical interactions (X3, X4, and X5), and viscosity ratio (X6) were found to have significant effects (Figure 5.1B). The column efficiencies were found to improve with increasing value of X5, reaching a maximum around 1. The effect of solubility ratio due to individual chemical interactions was found to have the same effect as it did on probability of obtaining a monolith. The optimum value for X3 was found to be 1.5, while the efficiency decreases with an increase in value of X4 from 0.3 to 2.0. The effect of solution viscosity on column efficiency was found to be opposite to that observed for probability of forming a monolith. Column efficiency was found to improve with a decrease in viscosity ratio (X6), indicating that monomers with high viscosities (i.e., longer ethylene oxide chains) produced more efficient columns (Table 5.2). These results also indicate that the most efficient

columns are obtained just at the boundary beyond which the probability of obtaining a monolith reduces dramatically. Obviously, the statistically designed experiments and regression modeling described in this work were helpful in identifying conditions which most likely would not have been found following typical optimization practices.

The improvement in efficiency can be attributed to reduced pore size as indicated by decreasing column permeability (Table 5.2) and accompanying change in monolith morphology. SEM images in Figure 5.2 show that the monolith morphology changes from a totally globular morphology for PEGDA-258 to a completely fused morphology for PEGDA-700. Globular monoliths have higher structural heterogeneity compared to fused structures. This change in monolith morphology affects the diffusion dynamics of an analyte as a function of its molecular weight [16]. Molecules with small hydrodynamic radii show greater dispersion in monolithic columns with globular morphologies [38], indicating greater mass-transfer resistance during transport though the material [20]. In contrast, monolithic columns with fused morphologies possess lower structural heterogeneity, thereby providing better column performance for small molecule separations. Large molecules with hydrodynamic radii in the nanometer range [39] would not be influenced as significantly by this structural heterogeneity, greatly minimizing any reduction in separation efficiency [15]. In past studies, it was observed that conventional globular monoliths showed good separation performance for large molecule separations, while fused morphologies performed better for small molecules [30]. The highest chromatographic efficiency measured in this study was 75,000 plate/m for a non-retained compound (i.e., uracil) at a mobile phase flow rate of 250 nL/min on a PEGDA-700 column.

The commercial LC instrument used for these experiments was found to have a flow rate dependent extra-column dead volume of 27 nL at 250 nL/min [33]. Therefore, the column

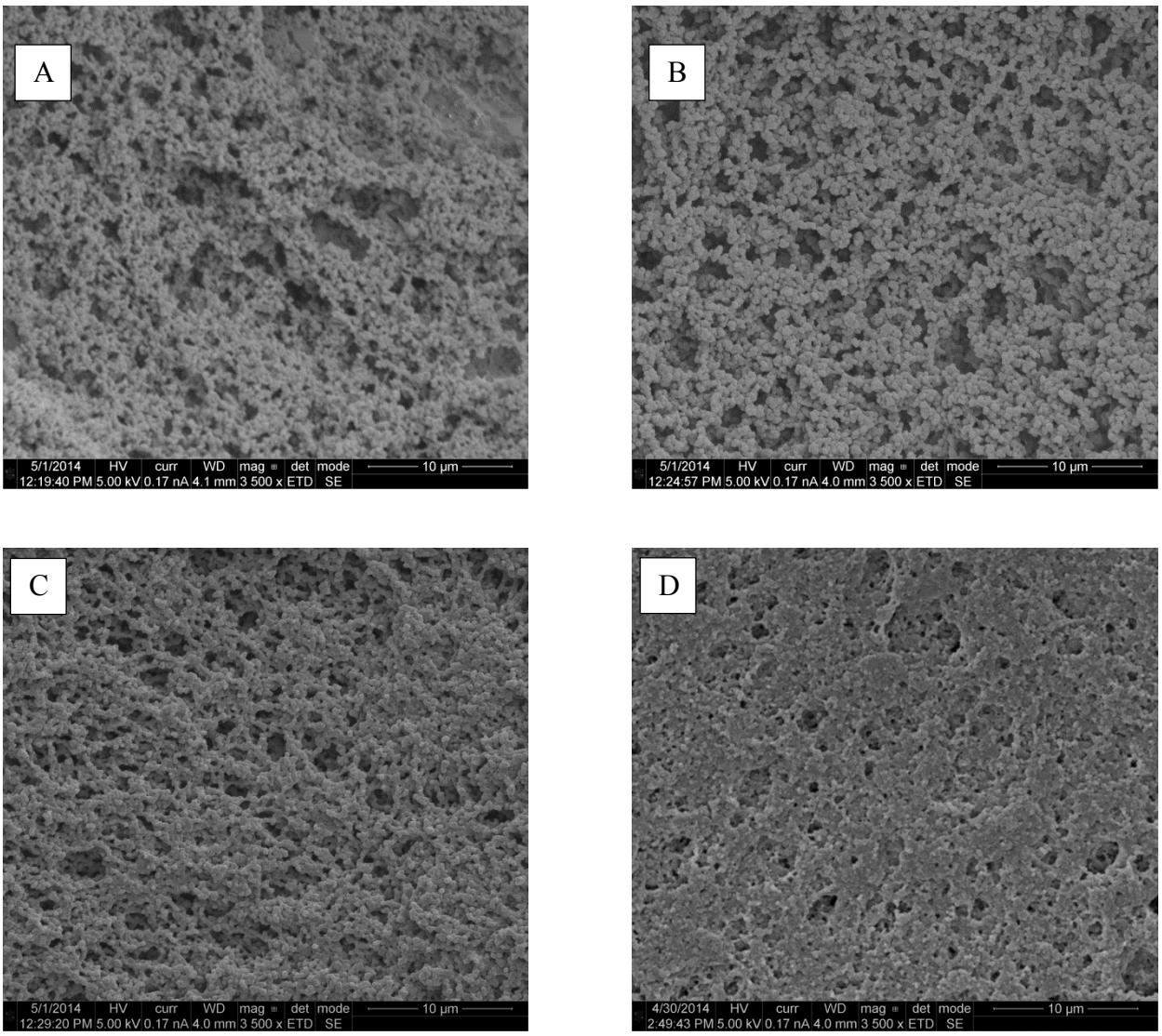


**Figure 5.2.** SEM images of selected monoliths. Monolith compositions for images A to D are the same as for columns 1 to 4 in Table 5.2.

performance should be corrected to an actual plate number of 186,000 plates/m. All measured efficiencies reported in this chapter are approximately 30-60% of the actual column performance and should be corrected by a factor of ~2.5-3.0. All of the efficiencies reported in this manuscript were measured at 10% peak height in order to provide accurate values.

### 5.3.3 Separation of small molecules

The highly efficient PEGDA-700 monolithic column with fused monolith morphology provided excellent separations of acidic compounds (benzoic acids), basic compounds (phenols and alkyl parabens) and some commonly used pharmaceutical drugs and herbicides. The results observed from separations of these classes of small molecules are described in the following sections.

*Hydroxy benzoic acids.* The retention mechanism using the PEGDA monolithic stationary phase was investigated using hydroxy benzoic acids as test analytes. Figure 5.3 shows an isocratic separation of 6 benzoic acid derivatives in less than 25 min with an elution order of benzoic acid (BA), 2-hydroxy benzoic acid (2-HB), 3-hydroxy benzoic acid (3-HB), 3,4-dihydroxy benzoic acid (3,4-DHB), 3,4,5-trihydroxy benzoic acid (3,4,5-THB) and 2,4-dihydroxy benzoic acid (2,4-DHB). The flow rate was 400 nL/min with an isocratic mobile phase composition of 40:60 (w/w) acetonitrile/water at pH 2.5. The six compounds were baseline resolved with a measured column efficiency of more than 100,000 plates/m and tailing factor less than 1.30. The retention mechanism was initially thought to be based on hydrophilic interactions, with compounds having more hydroxyl groups eluting later. However, the higher retention of 2,4-DHB (k = 2.5) in comparison to 3,4,5-THB (k = 2.0) indicated the presence of another interaction mechanism. Therefore, the retention mechanism was investigated in more

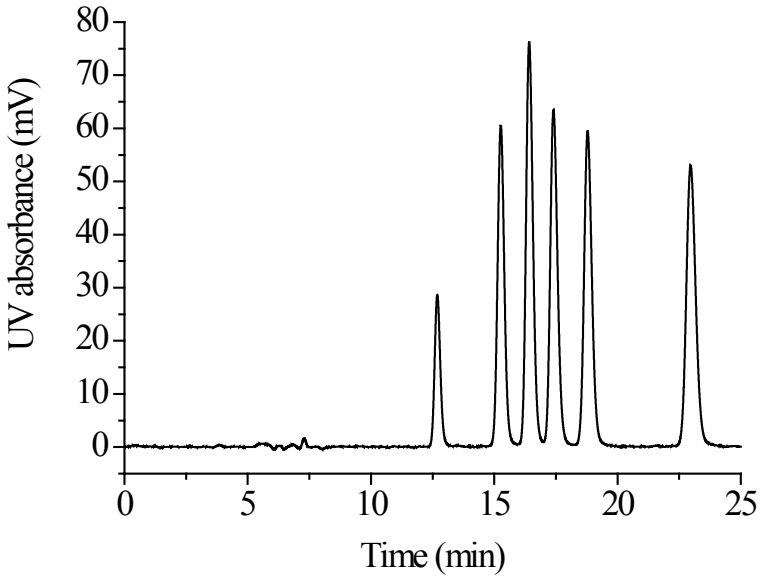


**Figure 5.3.** RPLC separation of hydroxy benzoic acids on a PEGDA-700 monolithic column. The monolith composition is given in the footnote of Table 5.3. Conditions: 15 cm × 150 μm i.d. monolithic column; mobile phase component A was acetonitrile with 1% formic acid (pH = 2.5), and B was water with 1% formic acid (pH = 2.5); isocratic elution with 40% A/60% B; 400 nL/min flow rate; on-column UV detection at 214 nm. Peak identifications in order of elution: benzoic acid (BA), 2-hydroxy benzoic acid (2-HB), 3-hydroxy benzoic acid (3-HB), 3,4-dihydroxy benzoic acid (3,4-DHB), 3,4,5-trihydroxy benzoic acid (3,4,5-THB) and 2,4-dihydroxy benzoic acid (2,4-DHB).

detail. The interactions occurring between analytes and stationary phase were investigated by varying the mobile phase acetonitrile concentration, pH and salt concentration.

The effect of acetonitrile concentration on the retention factors of the hydroxy benzoic acids is shown in Figure 5.4A. Resolution and selectivity were found to decrease with an increase in the amount of acetonitrile in the mobile phase, indicating typical RP behavior. The retention times decreased dramatically with an increase in acetonitrile content from 20 to 50% followed by a gradual decrease from 50 to 80%. Baseline resolution was obtained for all six benzoic acid derivatives in the range of 30 to 50% acetonitrile. The higher partition coefficient (i.e., 1.64) of 2,4-DHB compared to 3,4,5-THB (0.91) led to a higher retention of 2,4-DHB, and indicates hydrophobic interactions between the stationary phase and the analyte. The elution order of hydroxy benzoic acids did not strictly follow molecular polarity. This behavior can be explained by considering additional hydrogen bonding interactions between the hydroxyl groups of the analytes and the polar ethylene chains in the PEGDA monolith. The extent of hydrogen bonding should increase with an increase in number of hydroxyl groups, giving a retention order of THB>DHB>HBA>BA. For the structural isomers, 2-HB and 3-HB, intra-molecular hydrogen bonding in 2-HB reduces its interaction with the stationary phase, thereby reducing its retention compared to 3-HB.

To further investigate the possibility of ionic interactions between the analyte and stationary phase, the pH and salt concentration of the mobile phase was varied. The effect of mobile phase pH on the retention times of the hydroxyl benzoic acids was investigated by changing the pH of the aqueous portion before mixing with acetonitrile. The pH of the aqueous portion was varied from pH 2.0 to 3.0 using formic acid (Figure 5.4C). The maximum resolution of the six benzoic acid derivatives was observed at pH 2.5, which decreased with further rise in

A

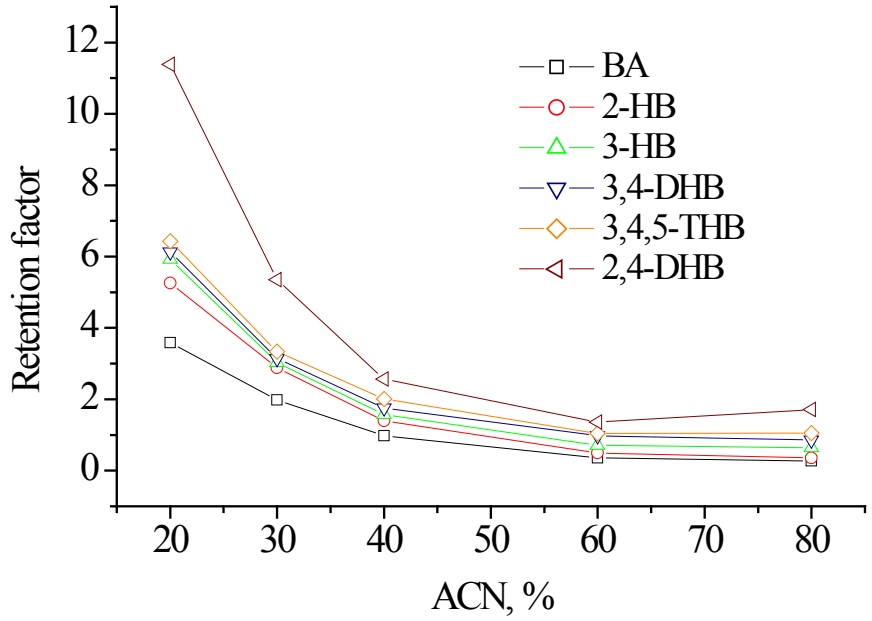


B

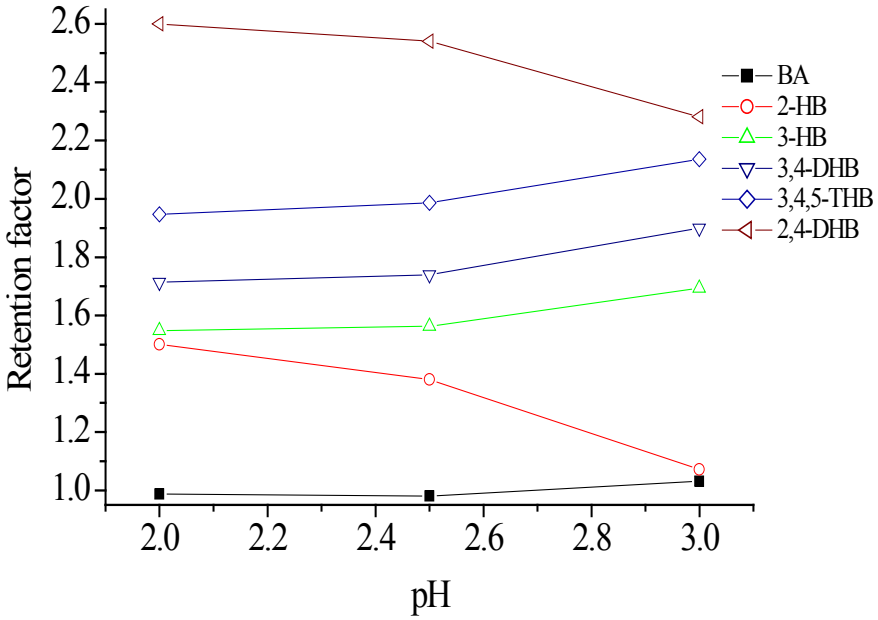

C

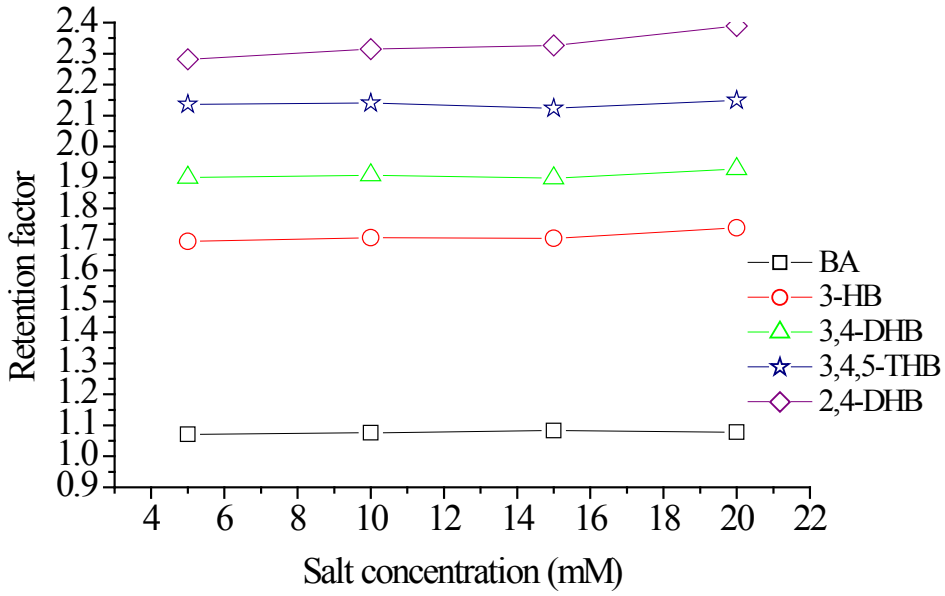


**Figure 5.4.** Effect of mobile phase properties on the separation of benzoic acid derivatives. Conditions: (A) mobile phase containing 20% to 80% ACN at pH 2.5, (B) water mobile phase containing 40% (v/v) ACN with pH ranging from 2.0 to 3.0, (C) water mobile phase containing 40% (v/v) ACN at pH 3.0 with ammonium formate salt concentration ranging from 5 to 20 mM. Other conditions are the same as in Figure 5.1. Compound identifications: benzoic acid (BA), 2-hydroxy benzoic acid (2-HB), 3-hydroxy benzoic acid (3-HB), 3,4-dihydroxy benzoic acid (3,4-DHB), 3,4,5-trihydroxy benzoic acid (3,4,5-THB) and 2,4-dihydroxy benzoic acid (2,4-DHB).

pH. Above pH 3, the first two compounds co-eluted while the other compounds showed significant tailing. At neutral pH, the whole mixture co-eluted with no individual peaks. The reduced retention and selectivity above pH 3.0 indicates reduced hydrophobic interaction between stationary phase and analyte because of negative charges on the analytes. This phenomenon of reduced retention of charged analytes was observed in past studies in RPLC.

The reduced retention of negatively charged analytes could be due, as well, to the presence of negatively charged groups on the monolith surface. Therefore, to determine if this was a factor in this study, different salt concentrations from 0 to 20 mM ammonium formate were added to the mobile phase at pH 3.0. It was previously reported that 20 mM salt concentration is needed to form a layer of electrically neutral counter ions on a surface. If there had been any negative charges on the monolith surface, the retention factors of the benzoic acids would have increased with an increase in salt concentration. However, the retention factors of all hydroxy benzoic acid derivatives were found to remain constant with increase in salt concentration (Figure 5.4C). Therefore, the retention mechanism was confirmed to primarily involve hydrophobic interactions with additional hydrogen bonding between the polar groups of the analytes and the ethylene groups in the monolith backbone.

*Separation of phenols.* Figure 5.5 shows an isocratic separation of uracil, pyrogallol, catechol, phenol and resorcinol using the PEGDA-700 column listed in Table 5.2. The flow rate was 400 nL/min with mobile phase mixture of 20:80 (v/v) acetonitrile/water. The 4 phenols were baseline resolved with column efficiency >100,000 plates/m with tailing factors < 1.28. The retention mechanism was determined to be the same as for the benzoic acid derivatives, involving hydrophobic interactions and hydrogen bonding between polar groups. The elution order of the structural isomers, i.e., catechol followed by resorcinol, can be explained on the

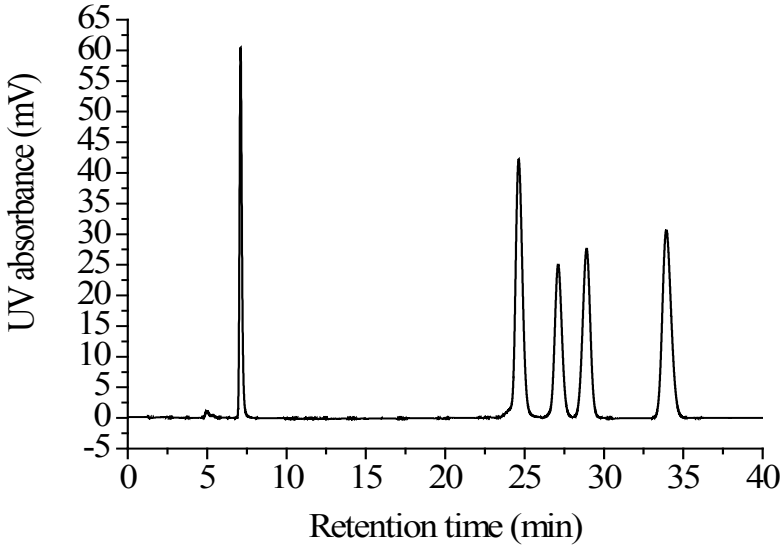


**Figure 5.5.** RPLC separation of phenols on a PEGDA-700 monolithic column. The monolith composition is given in the footnote of Table 5.3. Conditions: 15 cm × 150 μm i.d. monolithic column; mobile phase component A was acetonitrile, and B was water; isocratic elution with 20% A/80% B; 400 nL/min flow rate; on-column UV detection at 214 nm. Peak identifications in order of elution: uracil, pyrogallol, catechol, phenol and resorcinol.

basis of hydrogen bonding. The intra-molecular hydrogen bonding in catechol reduces its interaction with the stationary phase, thereby reducing its retention time. The retention times of the phenol derivatives decreased with an increase in amount of acetonitrile in the mobile phase (data not shown), indicating the typical RPLC retention mechanism.

*Separation of alkylparabens.* Figure 5.6 shows an isocratic separation of four alkyl parabens (i.e., methyl, ethyl, propyl and butyl parabens) using the PEGDA-700 column listed in Table 5.2 (separation conditions listed in the figure caption). The four analytes were baseline resolved in < 22 min with a column efficiency of >100,000 plates/m and tailing factors < 1.20. Retention time was found to increase with alkyl chain length in the analyte molecule. Methyl paraben, which is the least hydrophobic due to only a methyl group, eluted first, followed by the three other compounds. These results confirmed RPLC behavior.

*Separation of pharmaceutical compounds and herbicides.* To further demonstrate the excellent performance of this PEGDA-700 monolithic column, mixtures of commercially available pharmaceutical compounds (non-steroidal anti-inflammatory drugs, NSAID's) and phenyl-urea herbicides were separated. The herbicides are most commonly used in the agricultural industry and are major water pollutants that are analyzed for water purity. A mixture of four NSAID's were baseline resolved in < 15 min (Figure 5.7) using a linear gradient of increasing acetonitrile content from 10% to 100 % in 5 min, followed by isocratic elution with 100% acetonitrile for 15 min at 400 nL/min. The peaks were sharp and focused, with peak widths at 10% peak height < 10 s for all of the peaks.

The 5 herbicides were baseline resolved in < 18 min (Figure 5.8) using a 10-100% acetonitrile linear gradient in 15 min, followed by isocratic elution with 100% acetonitrile at a flow rate of 400 nL/min. The herbicides had very similar polarities since they differed in only

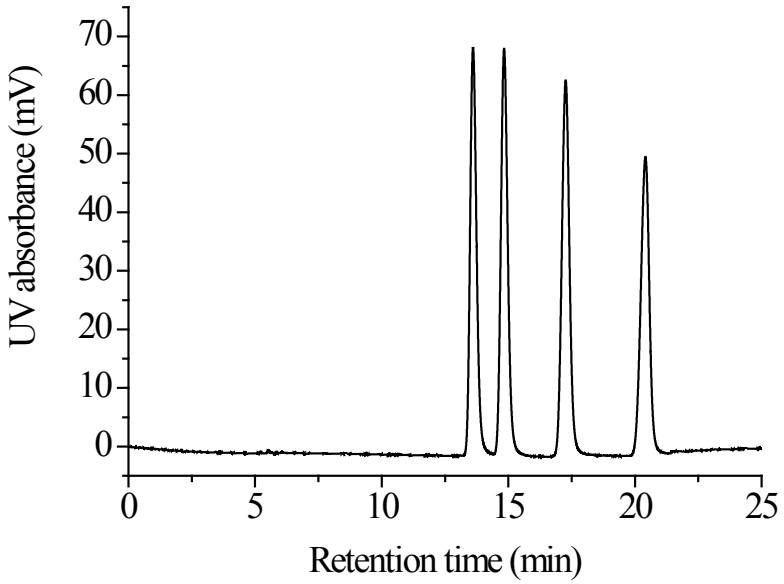


**Figure 5.6.** RPLC separation of alkylparabens on a PEGDA-700 monolithic column. The monolith composition is given in the footnote of Table 5.3. Conditions: 15 cm × 150 µm i.d. monolithic column; mobile phase component A was acetonitrile with 1% formic acid (pH = 2.5), and B was water with 1% formic acid (pH = 2.5); isocratic elution with 35% A/65% B; 400 nL/min flow rate; on-column UV detection at 214 nm. Peak identifications in order of elution: methyl paraben, ethyl paraben, propyl paraben and butyl paraben.

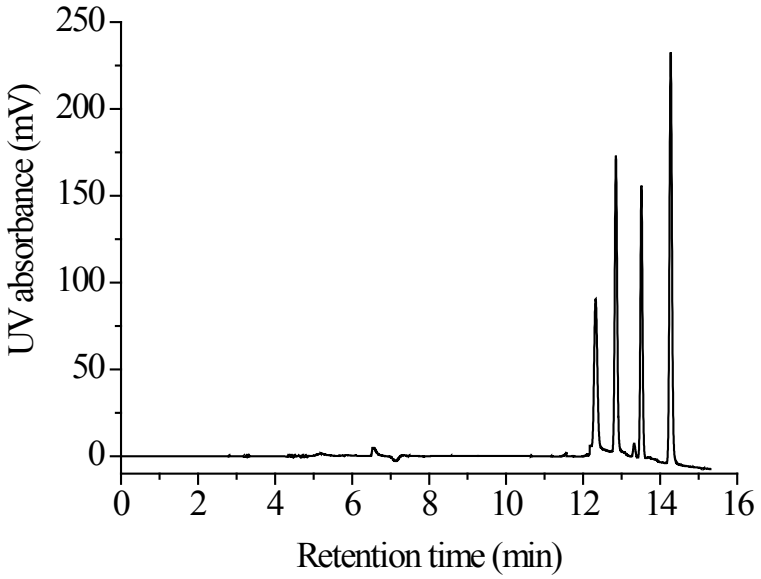


**Figure 5.7.** RPLC separation of nonsteroidal anti-inflammatory drugs (NSAIDs) on a PEGDA-700 monolithic column. The monolith composition is given in the footnote of Table 5.3. Conditions: 15 cm × 150 μm i.d. monolithic column; mobile phase component A was acetonitrile with 1% formic acid (pH = 2.5), and B was water with 1% formic acid (pH = 2.5); linear gradient from 10% A to 100% A in 5 min, and then isocratic elution with 100% B; 400 nL/min flow rate; on-column UV detection at 214 nm. Peak identifications in order of elution: paracetamol, aspirin, ibuprofen and indomethacin.

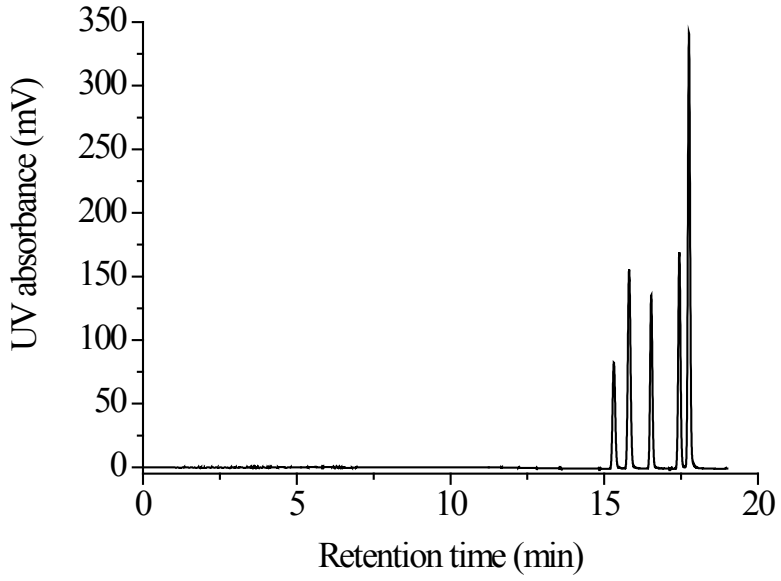


**Figure 5.8.** RPLC separation of urea herbicides on a PEGDA-700 monolithic column. The monolith composition is given in the footnote of Table 5.3. Conditions: 15 cm × 150 µm i.d. monolithic column; mobile phase component A was acetonitrile, and B was water; linear gradient from 10% A to 100% A in 15 min, and then isocratic elution with 100% B; 400 nL/min flow rate; on-column UV detection at 214 nm. Peak identifications in order of elution: isoproturon, monuron, monolinuron, diuron and linuron.

one functional group. The peaks were again sharp and focused with a maximum peak width of 11 s at 10% peak height.

### 5.3.4 Reproducibility, permeability and stability

Column reproducibility and stability are important performance characteristics of monolithic columns that must be verified for their use in routine analysis. The run-to-run and column-to-column RSD values based on retention times of phenols and uracil (n = 3) were < 0.2% and < 2.1%, respectively (Table 5.4). More than 150 injections were made to test the stability of the PEGDA-700 columns; no noticeable change was observed in column performance. Column stability was also evaluated in terms of column permeability, calculated based on Darcy's Law as explained in Section 5.2.4 using water as mobile phase. Linear relationships between back pressure and flow rate ($R^2 > 0.999$) for all four monoliths (Table 5.2) clearly indicated good mechanical stability. Column permeabilities for a PEGDA-700 column measured using two additional mobile phases (acetonitrile and methanol) showed the same linear relationship, indicating little to no shrinkage or swelling of monoliths in mobile phases of different polarity (Figure 5.9). As demonstrated here and by previous work in this group, monoliths synthesized from single crosslinking monomers generally exhibit excellent column stability.

## 5.4 Conclusions

Monolithic RPLC stationary phases showing chromatographic efficiencies >100,000 plates/m, tailing factors < 1.28 and low flow resistance were fabricated using UV initiated polymerization of diacrylate-based single cross-linking monomers (PEGDA) of different molecular weights. The monolithic columns were successfully used to separate low molecular weight polar compounds such as hydroxy benzoic acids, phenols, NSAID's and phenylurea

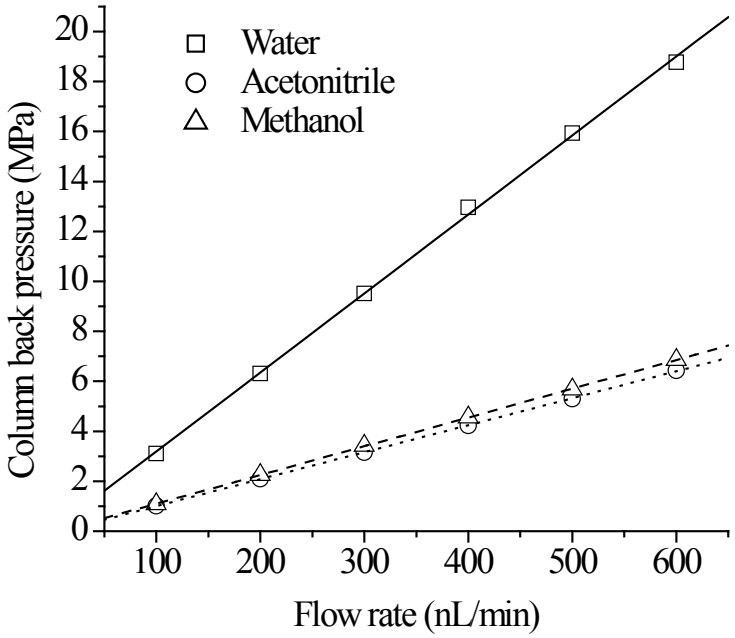


**Figure 5.9.** Effect of mobile phase flow rate on column back pressure. Conditions: 10 cm x 150 µm i.d. PEGDA-700 monolithic column. The monolith composition is given in the footnote of Table 5.4.

**Table 5.4.** Retention times of uracil and phenols showing column-to-column reproducibility of three independently prepared PEGDA-700 columns.[a,b]

| | Retention time (min) | | | | |
|---|---|---|---|---|---|
| | Uracil | Pyrogallol | Catechol | Phenol | Resorcinol |
| Column 1 | 7.0 | 24.4 | 26.9 | 28.7 | 33.7 |
| Column 2 | 6.9 | 23.8 | 26.3 | 28.0 | 32.3 |
| Column 3 | 6.9 | 24.0 | 26.7 | 29.0 | 33.0 |
| RSD[c] | 1.0 | 1.41 | 1.40 | 2.01 | 2.13 |

[a] Conditions as listed in Figure caption 5.5.
[b] Pre-polymer composition was PEGDA-700 (0.20 g), Tergitol-15-S-12 (0.30 g), dodecanol (0.15 g), decanol (0.15 g) and decane (0.20 g). The initiator used was DMPA (1 wt% of monomer).
[c] RSD is relative standard deviation in percentage.

herbicides. The retention mechanism was found to follow typical reversed-phase behavior with additional hydrogen bonding interactions, making the column suitable for separation of polar compounds, which are otherwise poorly retained on C18 columns. The fabricated columns demonstrated excellent reproducibility with RSD values for run-to run and column-to-column < 0.25% and 2.1%, respectively. Excellent column stability was evident from little shrinkage or swelling in solvents of different polarity.

The fabrication method and process of porogen selection were rationalized using physical-chemical properties such as solubility and viscosity. The solubility values used were classified based on the nature of the possible interactions of the reagents (i.e., dispersion, polarity, and hydrogen bonding). A statistical model was developed for optimizing the reagents and conditions based on scientific principles, which could be applied to simplify the fabrication development process. The model predicted the probability of obtaining a monolith with 74% accuracy, and column performance was successfully correlated to pre-polymer solubility and viscosity values. The statistical approach not only made the fabrication process more scientific, but also aided in identifying possible compositions that would result in highly efficient columns, which might be missed in normal experimental procedures.

**5.5 References**


[1] Svec, F.; Fréchet, J.M. *Anal. Chem.* **1992**, *64*, 820-822.

[2] Hjertén, S.; Liao, J.-L.; Zhang, R. *J. Chromatogr. A* **1989**, *473*, 273-275.

[3] Guiochon, G. *J. Chromatogr. A* **2007**, *1168*, 101-168.

[4] Grushka, E.; Grinberg, N. *Advances in chromatography*, CRC Press, **2012**.

[5] Liu, K.; Aggarwal, P.; Lawson, J.S.; Tolley, H.D.; Lee, M.L. *J. Sep. Sci.* **2013**, *36*, 2767-2781.

[6] Urban, J.; Jandera, P. *Anal. Bioanal. Chem.* **2013**, *405*, 2123-2131.

[7] Svec, F. *J. Sep. Sci.* **2004**, *27*, 747-766.

[8] Cabrera, K. *J. Sep. Sci.* **2004**, *27*, 843-852.

[9] Vlakh, E.; Tennikova, T. *J. Chromatogr. A* **2009**, *1216*, 2637-2650.

[10] Premstaller, A.; Oberacher, H.; Huber, C.G. *Anal. Chem.* **2000**, *72*, 4386-4393.

[11] Gu, B.; Chen, Z.; Thulin, C.D.; Lee, M.L. *Anal. Chem.* **2006**, *78*, 3509-3518.

[12] Li, Y.; Tolley, H.D.; Lee, M.L. *J. Chromatogr. A* **2010**, *1217*, 4934-4945.

[13] Ivanov, A.R.; Zang, L.; Karger, B.L. *Anal. Chem.* **2003,** *75*, 5306-5316.

[14] Li, Y.; Tolley, H.D.; Lee, M.L. *Anal. Chem.* **2009,** *81*, 9416-9424.

[15] Hahn, R.; Panzer, M.; Hansen, E.; Mollerup, J.; Jungbauer, A. *Separ. Sci. Technol.* **2002**, *37*, 1545-1565.

[16] Nischang, I.; Brueggemann, O.; Svec, F. *Anal. Bioanal. Chem.* **2010**, *397*, 953-960.

[17] Xu, Z.; Yang, L.; Wang, Q. *J. Chromatogr. A* **2009**, *1216*, 3098-3106.

[18] Urban, J.; Svec, F.; Fréchet, J.M. *Anal. Chem.* **2010**, *82*, 1621-1623.

[19] Jungbauer, A.; Hahn, R. *J. Sep. Sci.* **2004**, *27*, 767-778.

[20] Nischang, I.; Brüggemann, O. *J. Chromatogr. A* **2010**, *1217*, 5389-5397.

[21] Greiderer, A.; Trojer, L.; Huck, C.W.; Bonn, G.K. *J. Chromatogr. A* **2009**, *1216*, 7747-7754.

[22] Svec, F. *J. Chromatogr. A* **2010**, *1217*, 902-924.

[23] Peters, E.C.; Svec, F.; Fréchet, J. *Adv. Mater.* **1999**, *11*, 1169-1181.

[24] Lv, Y.; Lin, Z.; Svec, F. *Anal. Chem.* **2012**, *84*, 8457-8460.

[25] Urban, J.; Svec, F.; Fréchet, J.M. *J. Chromatogr. A* **2010**, *1217*, 8212-8221.

[26] Nischang, I.; Teasdale, I.; Brüggemann, O. *Anal. Bioanal. Chem.* **2011**, *400*, 2289-2304.

[27] Chambers, S.D.; Holcombe, T.W.; Svec, F.; Fréchet, J.M. *Anal. Chem.* **2011,** *83*, 9478-9484.

[28] Santora, B.P.; Gagné, M.R.; Moloy, K.G.; Radu, N.S. *Macromolecules* **2001,** *34*, 658-661.

[29] Viklund, C.; Svec, F.; Fréchet, J.M.; Irgum, K. *Chem. Mater.* **1996**, *8*, 744-750.

[30] Li, Y.; Tolley, H.D.; Lee, M.L. *J. Chromatogr. A* **2011**, *1218*, 1399-1408.

[31] Liu, K.; Tolley, H.D.; Lawson, J.S.; Lee, M.L. *J. Chromatogr. A* **2013**, *1321*, 80-87.

[32] Liu, K.; Tolley, H.D.; Lee, M.L. *J. Chromatogr. A* **2012**, *1227*, 96-104.

[33] Aggarwal, P.; Liu, K.; Sharma, S.; Tolley, H.D.; Lawson, J.S.; Lee, M.L. *Submitted*. **2014**.

[34] Aggarwal, P.; Tolley, H.D.; Lee, M.L. *Anal. Chem.* **2011**, *84*, 247-254.

[35] Svec, F.; Frechet, J.M. *Macromolecules* **1995**, *28*, 7580-7582.

[36] Courtois, J.; Byström, E.; Irgum, K. *Polymer* **2006**, *47*, 2603-2611.

[37] Okay, O. *Prog. Polym. Sci.* **2000**, *25*, 711-779.

[38] Li, J.; Litwinson, L.M.; Cantwell, F.F. *J. Chromatogr. A* **1996**, *726*, 25-36.

[39] Wilkins, D.K.; Grimshaw, S.B.; Receveur, V.; Dobson, C.M.; Jones, J.A.; Smith, L.J. *Biochem.* **1999**, *38*, 16424-16431.

# CHAPTER 6 FABRICATION OF HIGHLY EFFICIENT MONOLITHIC COLUMNS USING LIVING FREE-RADICAL POLYMERIZATION

## 6.1 Introduction

Monolithic (both silica and organic) columns were introduced as a low pressure alternative to particle packed columns for liquid chromatography (LC) separations in the early 1990s [1-5].The performance of silica monoliths improved significantly through understanding and optimizing the sol-gel synthesis method. As stated in the previous chapters, efforts have been made to optimize the fabrication process for organic monoliths. Organic monoliths have conventionally been fabricated using conventional free-radical polymerization (CFRP) [6]. The highest chromatographic efficiency obtained for an organic monolith is 186,000 plates/m for a non-retained analyte on a PEGDA column (Chapter 5) when corrected for dead volume (Chapter 4). Although this is the highest reported efficiency, it is still low when compared to particle packed columns.

This can be ascribed to the inherent structural heterogeneity associated with the CFRP fabrication process as indicated by 3D SEM characterization in Chapter 3. CFRP is difficult to control with regard to molecular weight of the growing polymer chain. During the course of polymerization, there occurs an abrupt increase in local degree of polymerization (i.e., spatially non-homogenous distribution of crosslinking points resulting from a wide distribution of molecular weight) because of the abrupt nature of the free radical system [7,8]. This heterogeneous crosslinking ultimately causes segregation of locally coherent domains from the solvent, leading to formation of microgels, known as the cauliflower-like structure of polymer monoliths [9-11]. This heterogeneous monolithic structure compromises the chromatographic performance. Also, due to poorly controlled polymerization reactions, the micropore and

mesopore volumes are not well regulated. Obviously, more homogeneous structures with well-defined skeletal and pore sizes are desirable for obtaining excellent chromatographic efficiencies.

Living free-radical polymerization (LFRP) has been explored as an alternative polymerization method to overcome this inherent heterogeneity associated with free-radical polymerization of monomers and to provide well-controlled molecular weight with low polydispersity [12]. In LFRP, there exists an equilibrium between the growing radical chain and dormant species, slightly favoring the dormant species [13,14]. This reversible equilibrium increases the time of chain propagation, giving it sufficient time to relax and distribute homogenously [15,16]. Moreover, the reversibility provides much better control over the molecular weight distribution of the growing radical chain and on the final monolith morphology. There have been several reports of using LFRP for controlling monolith morphology using different initiation systems. Yu et al. used atom transfer free-radical polymerization (ATRP) to prepare a poly(ethylene glycol dimethacrylate-co-ethylene glycol methyl ether methacrylate) (PEGDMA-co-PEGMEMA) monolith [17]. Nitroxide-mediated living radical polymerization (NMP) was used for fabricating a poly(styrene-co-divinylbenzene) (PS-DVB) monolith [18]. Reversible addition-fragmentation chain transfer polymerization (RAFT) was used to fabricate a molecularly imprinted poly(methacylic acid-co-ethylene glycol dimethacrylate) (MAA-co-EGDMA) monolith [19]. However, the complex reaction kinetics and difficulty in optimizing the reaction conditions in ATRP, the high temperatures required for NMP of styrene monomers, and limited applicability of RAFT to ring containing monomers [12] does not lend them to easy synthesis in capillary dimensions or to be widely applicable as fabrication methods.

Recently, organotellurium-mediated radical polymerization (TERP), a new branch of LFRP, was employed to fabricate monoliths from several different monomers such as styrene [20], glycidyl methacylate [21], and *N,N*-methylenebiacrylamide [22]. The reaction mechanism involved generation of carbon-centered radicals by thermolysis to initiate polymerization in the presence of a thermal initiator, azo-bis isobutyronitrile [23,24]. This polymerization method is applicable to a wide variety of functional monomers; takes place under mild polymerization conditions, and is relatively easy to optimize, thereby overcoming the limitations of ATRP, NMP and RAFT while still maintaining precise control over the monolith morphology. Therefore, there has been a growing interest in fabricating monolithic columns using TERP.

In this study, organic monolithic capillary columns were synthesized from a tri-functional monomer, pentaerythritol triacrylate (PETA) by TERP. One column gave an unprecedented column efficiency of 238,000 plates/m (corrected for dead volume) for a non-retained analyte, uracil. The fabricated columns were characterized using 3D SEM for structural parameters, and radial heterogeneity was found to be reduced significantly. The fabricated columns exhibited good mechanical stability.

## 6.2 Experimental

### 6.2.1 Chemicals and reagents

The reagents, 2,2-dimethoxy-2-phenyl-acetophenone (DMPA, 99%), 3-(trimethoxysilyl)propyl methacrylate (TPM, 98%) and penta erythritol triacrylate (PETA) were purchased from Sigma–Aldrich (St Louis, MO, USA). Ethyl-2-methyl-2-butyltellanyl propionate (BTEE) was kindly supplied by Dr. Takashi Kameshima, Otsuka Chemical Co. (Osaka, Japan). Since BTEE is oxygen sensitive, it was stored in vials that had been carefully cleaned and dried, and all transfers were conducted inside a nitrogen glove box. Water, 1,4-butanediol, and uracil

were obtained from Sigma–Aldrich. Acetonitrile, cyclohexanol and ethylene glycol were purchased from Mallinckrodt (Phillipsburg, NJ, USA).

### 6.2.2 Polymer monolith preparation

Monoliths were synthesized inside pre-treated UV transparent Teflon-coated capillaries (100 µm i.d.) functionalized using the procedure described in Section 2.2.2. Pre-polymer solutions were prepared in 1-dram (4 mL) glass vials by admixing initiator, monomer, and porogen solvents. The solution was vortexed and then degassed by sonicating for 2 min followed by purging with nitrogen gas for 5 min. The reaction promoter BTEE was added into the reaction solution using a 10 µL syringe. A section of the surface treated capillary was cut and filled with pre-polymer solution using nitrogen gas pressure. One end of the capillary was left empty for on-column UV detection. After introducing the reagent solution, the capillary was sealed with rubber septa at both ends and placed in an oil bath maintained at 60 °C. Monoliths obtained were flushed with methanol and then water until stable pressure readings were obtained. The fabricated columns were characterized using the 3D SEM technique described in Chapter 3.

### 6.2.3 Capillary liquid chromatography

The LC instrument and detector used for all chromatographic experiments in this chapter were the same as described in Section 5.2.3. The mobile phases was composed of acetonitrile and HPLC grade water.

## 6.3 Results and Discussion

The fabrication process of a monolithic column requires the occurrence of two processes, i.e., gelation and phase separation. To obtain a homogeneous monolithic column, both gelation and phase separation must take place at the appropriate time. If gelation occurs first, the resultant structure is a gel with no distinct macroporous structure. On the other hand, early or much

delayed precipitation of the growing polymer leads to monoliths with large globular morphology and increased structural heterogeneity. It is desirable for gelation and phase separation to take place at the same time to produce uniform skeletal and pore structures with small pores. Therefore, the polymerization conditions and the pre-polymer constituents must be investigated to obtain a highly efficient monolith.

### 6.3.1 Selection of porogens

The selection of organic solvent porogens is an important step in monolith fabrication. Solvent viscosity and solubility values used for porogen selection in Chapter 5 were again used as physical/chemical parameters to aid in porogen selection for this study. It was found that combination of a long chain aliphatic alcohol, such as dodecanol, and a polar solvent, such as DMF resulted in formation of a gel or a monolith with very low permeability. Monoliths fabricated using cyclohexanol as one of the porogens along with DMF gave monoliths with very high permeability; however, the chromatographic performance was very poor for these columns. Therefore, to fabricate a monolith with intermediate permeability and reasonable chromatographic performance, solvents such as 1,4-butanediol, ethylene glycol and polyethylene glycol (PEG) of different chain lengths were studied as co-porogens. Although PETA monoliths could be formed from various combinations of these porogens and cylcohexanol, those prepared from ethylene glycol and cyclohexanol gave better chromatographic performance at reasonable column back pressure. The use of longer chain di-hydroxy alcohols such as PEG 200, 400 and 600 was found to increase the heterogeneity of the system, and the resulting monoliths were found to have macroscopically non-homogenous structures. This could be explained by the increased viscosity of the pre-polymer system with longer chain alcohols, similar to the

observation in Section 5.3.1. Therefore, ethylene glycol and cyclohexanol were used as porogens for PETA monoliths (Table 6.1).

### 6.3.2 Optimization of polymerization conditions

As observed in the previous chapters, the weight proportion of pre-polymer constituents has an important influence on monolith morphology and its chromatographic efficiency. Therefore, the effect of percentage of monomer and the weight ratio of cyclohexanal to ethylene glycol was investigated. Uracil was used as a non-retained analyte in these efficiency tests.

Column performance was first found to improve with increase in percentage of monomer and then decrease, with 25% monomer being optimum for PETA monolithic columns (Table 6.1). This optimum performance corresponds to the optimum skeletal size. At higher percentage of monomer, the skeletal dimensions were thicker in the SEM images, increasing the resistance to mass transfer in the stationary phase. On the other hand, a lower percentage of monomer increased the average though-pore size, thereby increasing the resistance to mass transfer in the mobile phase.

The second parameter optimized was the porogen ratio, i.e., ratio of the amount of cylohexanol to ethylene glycol. The chromatographic performance was found to improve with a decrease in porogen ratio, with the plate count increasing from 40,000 plates/m to 168,000 plates/m. This increase in column performance with decrease in porogen ratio was accompanied with an increase in column back pressure, making ethylene glycol a good porogen. Therefore, an increase in amount of ethylene glycol can be associated with a delay in phase separation tendency of the polymerizing system, leading to improved monolith morphology and small through-pore size. These two changes in monolith morphology explain very well the

**Table 6.1.** Effect of different reagent compositions on chromatographic efficiency of PETA monoliths.

| Column | Reagent composition[a] | | | | | |
|---|---|---|---|---|---|---|
| | Monomer[b] | Cyclohexanol[c] | Ethylene glycol[c] | Percentage of monomer | Cyclohexanol/ ethylene glycol | Efficiency[d] |
| **Percentage of monomer** | | | | | | |
| 1 | 20.10 | 85.12 | 14.88 | 20 | 6.0 | 50,000 |
| 2 | 25.05 | 85.66 | 14.34 | 25 | 6.0 | 60000 |
| 3 | 29.07 | 85.71 | 14.29 | 30 | 6.0 | 18000 |
| **Cyclohexanol to ethylene glycol ratio** | | | | | | |
| 4 | 25.01 | 93.33 | 6.67 | 25 | 14 | 40,000 |
| 5 | 25.04 | 85.66 | 14.34 | 25 | 6.0 | 60,000 |
| 6 | 24.97 | 76.00 | 24.00 | 25 | 3.0 | 168,000 |

[a] All monoliths contained 1 wt % AIBN to monomer and 0.6 µL of BTEE.
[b] Percentage by weight.
[c] Percentage by weight for total amount of porogen.
[d] column efficiency (plates/m) measured using uracil as a non-retained analyte.

improvement in column performance. Any further decrease in porogen ratio resulted in monoliths with very high back pressure or formation of a gel. This could be associated with extensive delay in phase separation, resulting in early occurrence of gelation and formation of non-porous gels.

Several other parameters such as polymerization time, polymerization temperature, amount of initiator (AIBN) and amount of promoter (BTEE) were also analyzed. The polymerization time and temperature used for LFRP was 24 h and 60 °C, respectively. Since the reaction kinetics were slower for TERP, completion of polymerization required longer polymerization. The most commonly used polymerization temperature reported for thermal initiation is 60 °C. Therefore, the polymerization temperature was set at 60 °C. Moreover, polymerization was found to be too slow at 50 °C with AIBN as initiator, and a temperature above 60 °C resulted in a monolith with very low permeability when polymerized using TERP. The amount of AIBN in all reactions was 1 % (w/w) of monomer, and the amount of BTEE was 0.6 µL. Any increase in amount of BTEE was found to cause a rapid increase in reaction kinetics and the pre-polymer solution would polymerize even before filling the capillary.

### 6.3.3 Structural parameters using 3D SEM

The fabricated column with the highest efficiency was characterized using the 3D SEM technique described in Chapter 3. The measured morphological parameters were compared with the monoliths fabricated using CFRP, and the results are given in Table 6.2. Monoliths fabricated using TERP were found to have an average through-pore size of 2.77 µm in contrast to 5.23 µm for columns fabricated using CFRP. This reduction in through-pore size to almost half could be correlated to reduction in resistance to mass transfer and subsequent improvement in column performance. The porosities for the columns were found to be nearly the same, indicating an

**Table 6.2.** Morphological descriptors of monolith structure measured using 3D SEM.[a]

| Method of polymerization | Porosity | Pore diameter (μm) | Radial heterogeneity | Efficiency[b] |
|---|---|---|---|---|
| CFRP | 0.49 | 5.23 | 0.20 | 64,500 |
| TERP | 0.46 | 2.77 | 0.03 | 168,000 |

[a] Characterization method and terms described in Chapter 3.
[b] Column efficiency measured using uracil as a non-retained analyte.

increase in number of pores for the column fabricated by TERP. As a consequence of this increase in number of pores and decrease in pore size, the back pressure of the column was found to be low (6.90 MPa at 0.15 µL/min). Another structural parameter, i.e., radial heterogeneity, identified as a major factor for lower chromatographic performance of monolithic columns in Chapter 3,was also found to decrease significantly. This decrease in radial heterogeneity was a result of better control of the polymerization process provided by TERP as explained above.

### 6.3.4 Chromatographic efficiency

The PETA monolithic column (column 6 in Table 6.1) was used for collecting data for constructing a van-Deemter curve (Figure 6.1). The maximum theoretical plate number was 158,000 plates/m for uracil as a non-retained compound. As described in Chapter 4, the injection system often contributes significant extra-column volume, which adversely affects the measured column efficiencies for small-diameter columns. The extra-column volume of the injection valve for the capillary LC system used in this work was determined to be ~18 nL at a flow rate of 0.15 µL/min. Correcting for this extra-column contribution, the column performance was found to improve by ~ 50% (i.e., from 158,000 to 238,000 plate/m) for a non-retained compound (i.e., uracil). All efficiency values reported in this chapter represent the actual measured values (unless stated otherwise) and could be corrected to indicate the true column performance.

## 6.4 Conclusions

Monolithic columns fabricated using TERP showed a three-fold improvement in column performance for a non-retained compound without any significant rise in column back pressure. A plate count of 238,000 plates/m (corrected for dead volume) is the highest reported column efficiency for organic monoliths. This new polymerization method paves the way for fabricating

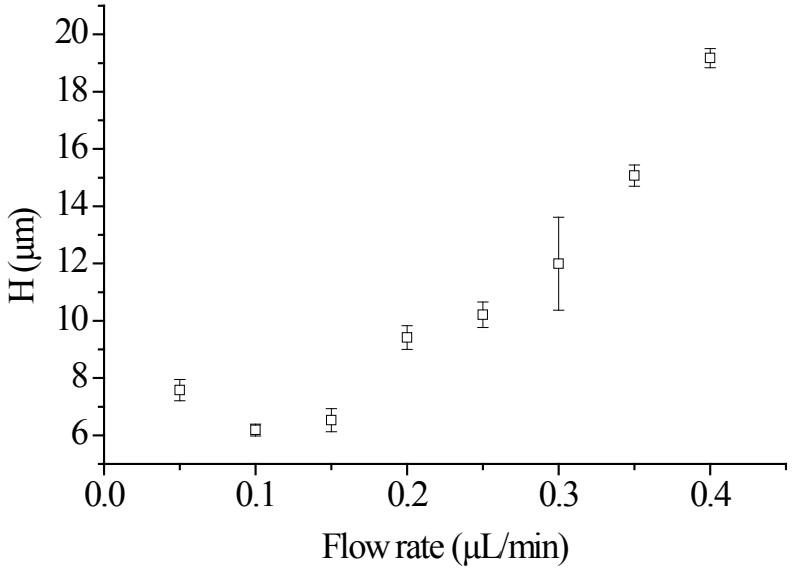


**Figure 6.1.** Plate height versus linear velocity for a PETA monolithic column using uracil as a non-retained analyte. Conditions: 15 cm x 100 µm i.d. column; 100% water as mobile phase; on-column UV detection at 214 nm.

highly efficient organic monoliths with high permeability. The chromatographic results were verified by structural characterization of the fabricated column. The 3D SEM characterization showed a significant reduction in average though-pore size and radial heterogeneity. This reduction in radial heterogeneity was a consequence of slower and better controlled reaction kinetics of LFRP, as proposed.

**6.5 References**


1. Hjertén, S.; Liao, J.-L.; Zhang, R. *J. Chromatogr. A* **1989**, *473*, 273-275.
2. Liao, J.-L.; Zhang, R.; Hjertén, S. *J. Chromatogr. A* **1991,** *586*, 21-26.
3. Tennikova, T. B.; Belenkii, B. G.; Svec, F. *J. Liq. Chromatogr.* **1990**, *13*, 63-70.
4. Tennikova, T. B.; Bleha, M.; Svec, F.; Almazova, T. V.; Belenkii, B. G. *J. Chromatogr.* **1991**, *555*, 97-107.
5. Svec, F.; Fréchet, J.M. *Anal. Chem.* **1992**, *64*, 820-822.
6. Svec, F. *J. Chromatogr. A* **2010**, *1217*, 902-924.
7. Hasegawa, J.; Kanamori, K.; Nakanishi, K.; Hanada, T.; Yamago, S. *Macromolecules* **2009**, *42*, 1270-1277.
8. Norisuye, T.; Morinaga, T.; Tran-Cong-Miyata, Q.; Goto, A.; Fukuda, T.; Shibayama, M. *Polymer* **2005**, *46*, 1982-1994.
9. Chiu, Y. Y.; Lee, L. J. *J. Polym. Sci. Part A: Polym. Chem.* **1995**, *33*, 257-267.
10. Chiu, Y. Y.; Lee, L. J. *J. Polym. Sci. Part A: Polym. Chem.* **1995**, *33*, 269-283.
11. Norisuye, T.; Kida, Y.; Masui, N.; Tran-Cong-Miyata, Q.; Maekawa, Y.; Yoshida, M.; Shibayama, M. *Macromolecules* **2003**, *36*, 6202-6212.
12. Kanamori, K.; Hasegawa, J.; Nakanishi, K.; Hanada, T. *Macromolecules* **2008**, *41*, 7186-7193.

13. Goto, A., Kwak, Y., Fukuda, T., Yamago, S., Iida, K., Nakajima, M., Yoshida, J., *J. Am. Chem. Soc.* **2003**, *125*, 8720-8721.

14. Yamago, S., *J. Polym. Sci., Part A* **2006**, *44*, 1-12.

15. Webster, O. W., *Science* **1991**, *251*, 887-893.

16. Odian, G., *Principles of Polymerization* 4th ed., John Wiley & Sons: Hoboken, New Jersey **2004.**

17. Yu, Q., Qin, Z., Li, J., Zhu, S., *Polym. Eng. Sci.* **2008**, *48*, 1254-1260.

18. Kanamori, K., Nakanishi, K., Hanada, T., *Adv. Mater.* **2006**, *18*, 2407-2411.

19. Turson, M.; Zhuang, X. L.; Liu, H. N; Jiang, P.; Dong, X. C. *Chinese Chem. Lett*. **2009**, *20.9*, 1136-1140.

20. Hasegawa, G., Kanamori, K., Ishizuka, N., Nakanishi, K., *ACS Appl. Mater. Interfaces* **2012**, *4*, 2343-2347.

21. Hasegawa, G., Kanamori, K., Ishizuka, N., Yamago, S., *Polymer* **2011**, *52*, 4644-4647.

22. Hasegawa, J., Kanamori, K., Nakanishi, K., Hanada, T., Yamogo, S., *Macromol. Rapid Commun.* 2009, *30*, 986-990.

23. Yamago, S., Iida, K., Yoshida, J., *J. Am. Che. Soc.* **2002**, *124*, 2874-2875.

24. Yamago, S., Iida, K., Yoshida, J., *J. Am. Che. Soc*. **2002**, *124*, 13666-13667.

# Chapter 7 FUTURE DIRECTIONS

## 7.1 Introduction

The results of my research clearly indicate that the chromatographic efficiency of organic monolith columns can be improved significantly by identifying and optimizing the factors governing monolith morphology. The developed characterization tools CFP, 3D SEM and conductivity measurements provide quantitative information about the structural parameters of monolith morphology such as through-pore size, radial heterogeneity, tortuosity and actual 3D reconstruction of the monolith under investigation. Characterizing different columns aided in identifying the factors (i.e., column dimensions, pre-polymer constituents and initiation method) governing monolith morphology and quantifying their effects. A statistical model was developed for optimizing the parameters governing monolith morphology, making the fabrication process more scientific. It also aided in identifying possible compositions that would result in highly efficient columns, which might be missed in normal experimental procedures. Now, all of this was conducted with one type of diacrylate monomer, i.e., PEGDA, and I believe that similar improvements are possible for other monolithic columns if the same principles are applied in their fabrication process. Moreover, I believe further improvements can be made for the diacrylate monoliths as well.

## 7.2 Further improvement in efficiency

The 3D reconstructions of monolithic columns can be applied for conducting computer simulations to understand the flow profiles of the mobile phase and diffusion of analytes with different molecular weights. These computational studies would help in establishing quantitative relationships between van Deemter coefficients and structural parameters of monolith morphology. Thereafter, the new information could be used for determining exact skeletal dimensions of monoliths capable of delivering high chromatographic efficiency. I believe the

ideal monolith morphology should have a through-pore size of 0.3 – 1.0 μm with skeletal thickness of 0.5 – 0.8 μm, and porosity > 0.4. This small skeletal thickness and small pore size would help in reducing the contribution of resistance to mass transfer, thereby providing faster kinetics and better column performance. Another important factor is the heterogeneity of the bed. These simulation studies would assist in determing the effect of different levels of heterogeneity on column performance with given skeletal dimensions. This computer simulation study should first be conducted for the PEGDA monolith and then for other monomer systems, such as pentaerythritol diacrylate monostearate (PDAM), 3-sulfopropyl methacrylate (SPMA) and phosphoric acid 2-hydroxyethyl methacrylate (PAHEMA), to verify the observed results.

In an effort to fabricate the exact optimum morphology identified by the computer simulation study, I suggest that the statistical model developed in Chapter 5 be applied for selection and optimization of the weight proportions of pre-polymer constituents based on their physical/chemical properties. A computer program could be developed using physical/chemical properties as input variables and calculating the weight proportion of the pre-polymer constituents as outputs, with parameters identified in Chapter 5 as bounding parameters. This computer program would assist in investigating unconventional porogens for other monomer systems besides PEGDA, which have not been used so far. The same program could be used for selecting the porogens and their weight proportions for monomers with different functionalities such as PDAM, SPMA, and PAHEMA. Over all, this study would aid in developing a scientific theory for the fabrication process and porogen selection, and lead to highly efficient organic monolith columns.

### 7.3 Optimizing pore-size distribution for size exclusion chromatography (SEC)

After optimizing the monolith morphology for optimum efficiency (i.e., optimizing the through-pore size distribution, skeletal thickness, radial heterogeneity and monolith tortuosity), the fraction of mesopores in the monolithic skeleton should be increased for improving the selectivity in SEC. Previously, the mesopore volume was increased for diacrylate monoliths (fabricated using two monomers) by using template porogens, mainly surfactants such as Brij, tween, and sodium dodecyl sulfate (SDS) [1]. A significant improvement was observed in chromatographic selectivity, corresponding to an increase in mesopore volume in the 7-17 nm range. Similar surfactants capable of forming micelles with different diameters can be employed to increase the mesopore volume in the PEGDA monolith. Since micelle formation is an important factor for mesopore formation, the selection of surfactant would be based on solubility in the porogens used for monolith formation. The surfactant selected should be able to form micelles in the porogen at low concentration without influencing the macro-morphology of the monolith. This would require a detailed investigation of different surfactants, their concentration and different porogens.

Other than surfactants, dendrimers or crown ethers could also be used as template porogens to increase the mesopore volume [2]. Dendrimers represent a class of macromolecule template, having a high degree of molecular uniformity, narrow molecular weight distribution, and specific shape and size. Moreover, dendrimers are available with different terminal functionalities, which could assist in making them soluble in any porogen of choice. For example, commercially available poly(propylene)imine dendrimer with a 1-4 diaminobutane core and having terminal amine functionalities could be a good candidate for template porogen for the PEGDA monolith. Crown ethers are macrocyclic oligomers of ethylene oxide units [3].

The combination of oxygen and ethylene units provides an appropriate choice of template porogen for PEGDA, which itself has repeating ethylene oxide units. The solubility values of the crown ethers are comparable to that of PEGDA and could, therefore, be used with the macro-porogens already investigated in the previous chapters of this dissertation. Moreover, their availability in different molecular sizes could prove useful in tuning the mesopore size distribution.

**7.4 Analysis of complex samples**

The developed PEGDA monolith columns showed good selectivity and efficiency for test compounds such as parabens, benzoic acids, and phenols (Chapter 5) under reversed-phase conditions. Their applicability has already been shown for hydrophobic interaction separations of protein samples. I believe these columns could be used for analyzing complex biological samples, pharmaceutical mixtures and real life samples such as water contaminated with pesticides and herbicides. These columns, being in capillary dimensions, offer several advantages such as low sample volume, easy coupling to mass spectrometry, and fast analysis. The high porosities of these column would enable analysis of biological samples with little to no sample preparation, similar to other organic monoliths already being used for complete cell analysis of microbes [4].

Moreover, the PEGDA monoliths with appropriate mesopore volume could be used for separation of a new class of anti-cancer drugs, i.e., antibody-drug conjugates (ADCs). These drug moeities are combinations of an antibody and a potent small molecule drug, linked to each other using a linker molecule [5]. PEGDA monoliths with already proven biocompatibility and improved mesopore fraction could prove to be useful stationary phases for SEC of these drugs.

## 7.5 References


1. Patterson, B. C. Surfactant micelles as templates in hydrogels, Ph.D. dissertation, Department of Chemistry, Florida State University, Tallahassee, FL, **2000**.
2. Larsen, G.; Lotera, E.; Marquez, M. *J. Mater. Res.* **2000**, *15*, 1842-1848.
3. Yost, T. L.; Fagan, B. C.; Allain, L. R.; Barnes, C. E.; Dai, S.; Sepaniak, M. J.; Xue, Z. *Anal. Chem.* **2000**, *72*, 5516-5519.
4. Ma, J.; Zhang, L.; Liang Z.; Zhang, W.; Zhang, Y. *J. Sep. Sci.* **2007**, *30*, 3050-3059.
5. Zolot, R. S.; Basu, S.; Milion, R. P. *Nat. Rev. Drug Discov.*, **2013**, *12*, 259-260.